NORTHWESTERN UNIVERSITY

An Offset ON-OFF Receptive Field is Created by Gap Junctions Between Distinct Types of Retinal Ganglion Cells

A DISSERTATION

SUBMITTED TO THE GRADUATE SCHOOL
IN PARTIAL FULFILLMENT OF THE REQUIREMENTS

for the degree

DOCTOR OF PHILOSOPHY

Field of Neuroscience

By

Sam Cooler

EVANSTON, ILLINOIS

March 2021

Abstract

In the vertebrate retina, neurons process visual signals, generating feature selectivity in their activity levels. We use computational models to understand these behaviors by interpreting them mathematically. One component of this analysis is the spatial selectivity or receptive field, a property found in all visual sensory neurons. The neurons found in the retina can be classified into cell types, which share many properties. Some retinal neurons are connected by gap junction synapses, which are small pores between their cytoplasms, which convey low-latency signals between them.

I have profiled two types of retinal ganglion cells (RGCs): the F-mini-ON and F-mini-OFF. I report the discovery of a systematic spatial offset between the ON and OFF receptive subfields in F-mini-ON. Surprisingly, this property does not come from spatially offset ON and OFF layer dendrites but instead arises from a network of electrical synapses via gap junctions to RGCs of a different type, the F-mini-OFF. I show that the asymmetric morphology and connectivity of these RGCs can explain their receptive field offset, and I use a multicell model to explore the effects of receptive field offset on the precision of edge-location representation in a population. This RGC network forms a new electrical channel combining the ON and OFF feedforward pathways within the output layer of the retina.

I also performed a survey of the ganglion cell types of the W3-Thy1 mouse line, aligned to complete typology datasets, as a reference for use by the retinal neuroscience community.

Acknowledgments

Seven years ago, I got the idea to try again for a doctorate, in a whole new field. Eyeballs! I have made it to the end of this stage. This has been a lot of work, and I have been supported throughout by my helpful and loving community and smart and passionate colleagues. I am proud of my accomplishments and attribute so much of it to those who have helped me in many ways.

I thank my parents and family for giving me a foundation for reaching for my goals, and helping me see myself as the person who earns this doctorate, and for ongoing care and thoughts. I thank my partners & close friends Jean, Olivia, Lily, Edie, Andrea, and many others, for caring about me and helping me stay emotionally aware and connected, for helping me to see the world as it is and to work hard and try things better. I thank my housemates, for everyday conversations, for excitement about my work, for taking care of and feeding me, for laughing and crying with me. I thank the local art community, for playing with me and connecting with my art along the way. I thank the members of the Schwartz Lab, and I could list a subset of them but I've learned from every one of them, for being my scientific community, for making me feel comfortable and part of such a good team. I thank my dissertation committee for reading this and guiding me, and the whole retinal neuroscience community for welcoming and funding me. I thank Greg Schwartz, my advisor and colleague. When we met years ago I knew quickly that I wanted to work with him. His great enthusiasm and excitement for and knowledge of science has rarely faltered. He has always been kind, thoughtful, and generous with his time. It has been an honor to work with him, and I will appreciate it forever. I hope people see some of him in me.

And finally, thanks to the leaf of my life, Eleanor the chameleon, for affection, for supervising my work, and always knowing just how to look to help me keep going okay.

Table of Contents

List of Figures

Introduction

My projects made contributions to several areas of retinal research: visual feature selectivity, receptive fields, and model building; ganglion cell typology; and understanding of gap junction roles and physiology.

Neural Responses to the Visual World

Feature Selectivity

Animals need to sense the world to navigate and interact with it. Sensory neurons take information into the nervous system about the world that is useful for behavior. The activity levels of sensory neurons represent the physical world as presented to it, signals that exist in a multi-dimensional feature space, such as frequency for auditory neurons, skin pressure for touch neurons, or edge contrast for visual neurons. We can stimulate a cell using parameterized stimuli varying along surfaces in these spaces and evaluate the way that our measurements of the output respond to changes in stimulus input using a model to estimate internal properties, to make observations otherwise impossible. Those models give us an understanding of the neuron's physiological relationship with the sensory input, which forms a spatial receptive field (RF) map and feature selectivity.

The way a visual neuron varies its response with a varying visual stimulus feature parameter is called "feature selectivity." The neuron firing more for a particular value of a visual input parameter is it *selecting* for that value. We assume that the brain has developed to be efficient, so to justify having a whole additional set of RGCs we assume that those RGCs must be providing some important information about the visual world that is not conveyed by other

types. When we can identify the feature selectivity of an RGC type we can develop an understanding of its role in visual computation. The core feature selectivity in the retina, shared by nearly all neurons, is localized change in light intensity over time. Cells responding to increases in intensity are ON, decreases are OFF, and responding to both are ON-OFF. A commonly explored feature selectivity is direction selectivity (DS), measured using a visual object moving in a parameterized direction (Fig 1A). In a subset of RGCs, the direction selective (DS) RGCs (ON-OFF DS Transient, ON DS Sustained), we find consistent across many stimulus parameters DS responses, so we use that property to identify and study these neurons (David I. Vaney, Sivyer, and Taylor 2012). The observation that the F-mini-ON separable from other RGCs by being DS, at low speeds (LSDS), motivated this study originally. Other features studied include approaching objects (Münch et al. 2009), object motion relative to the background (Baccus et al. 2008), and steady illumination (Jacoby et al. 2015).

Using Models to Analyze Retinal Neurons

The neurons in the retina work to encode the visual scene in a spike train, transmitted down the optic nerve. Sensory neurons have stimulus-to-response transformations that are stable and repeatable. With the visual stimulus and electrophysiology output described mathematically, the transformation from the former to the latter can similarly be described mathematically and solved and approximated using computers. Systems analysis techniques come to sensory neuroscience from physics via electrical engineering, which has applied them to analog electronics since the 1940s. These techniques use linear algebra, which can be applied to matrices of physical values, like contrast and spike rate, in the dimensions of space and time. By linking physical variables to estimated internal states, modeling provides a flexible toolset on

top of electrophysiology and visual stimulus in order to probe mechanisms deep within a neural circuit.

With the mathematical operations these neurons perform identified, we can use our understanding of the math to guide our investigation. Modeling gives researchers a framework for investigating neurons: by aiming to more accurately predict the responses of a neuron (a quantitative measure) we will also understand it better (a qualitative measure). When we find an aspect of the response that is not explained by our model, such as contrast adaptation or the omitted stimulus response, we are motivated to discover a new mechanistic component to explain it (G. Schwartz and Berry 2008). The model provides the ideal substrate in which to explore how that mechanism might function (Gao et al. 2009). Then, for example, we can search for an amacrine cell that performs that mechanism. A model with biophysically-approximate components lets us make internal measurements that are difficult in live tissue. A model can be evaluated in many copies to measure how many neurons might work in concert.

Fitting a model to the responses of a single real neuron yields a set of descriptive parameters for that neuron. We can look at those parameters to learn about a cell's properties in comparison to other types and among its type (Linsenmeier et al. 1982). The generalizability and applicability of the resulting model depend on the choice of stimulus and the quality of measured responses. The mechanisms that the model can estimate depend on the mathematical structure of the model.

Over time, visual neurons have been modeled using spatiotemporal filters and model structures of iteratively higher complexity. Early work used simple full-field stimulus, single linear filter steps, and a Poisson spiking threshold output nonlinearity (Baccus and Meister 2002). The next steps added gain control and feedback for adaptation, and an integrate-and-fire output

nonlinearity to accurately model spiking (Berry et al. 1999; Pillow et al. 2005). Recent work has collected around cascading LN models, having several layers each with gain and feedback (Herz et al. 2006). Models with this level of mechanistic complexity give us access to observations of activity levels in neurons (Fig 1B) (Real et al. 2017). Research has explored various more complex forms of signal mixing, showing that divisive or broadly parametric combination of inputs is more accurate than an additive combination (Cui et al. 2016). Very recently, artificial neural networks have been used to model RGCs with good accuracy, and this may represent the future of retinal electrophysiology modeling (McIntosh et al. 2016).

Receptive Fields of Ganglion Cells

That region of visual space in which a change in input changes the response is the receptive field (RF). The spatial receptive field is one form of feature selectivity which is present in all visual neurons. Measuring the RF is equivalent to building a very simple model, focused only on the spatial properties of the neuron.

Many methods have been used to measure the spatial receptive field of visual neurons, in the retina and elsewhere. Each of these methods has benefits and drawbacks, so researchers face the task of tool specification and design. Measurement of the RF should be one component of an overall model of the neuron to extract the RF map from other spatial integration and nonlinear output properties (Fig 1B).

One powerful method is to use a rapidly-changing random stimulus plus temporal averaging. A simple model is applied: a spike at a time is stimulated by the linear combination of the brief video clip preceding it. The stimulus regions that cause a particular cell to spike can be analyzed to generate a receptive field measurement. A checkerboard white noise stimulus uses a Gaussian distribution of contrast values to effect a broad, smooth distribution of

spatiotemporal frequencies. That enables the mean of those frames to be an unbiased measurement of the RF (Chichilnisky 2001). The noisy checkerboard stimulus can be as large as the projector's display, so RFs of many neurons can be measured simultaneously, an ability that makes it the gold standard for MEA recording. The resulting spike-triggered average (STA) gives a simple RF measurement for single polarity responding cells (Fig 1C) (Meister, Lagnado, and Baylor 1995). Cells with both ON and OFF polarity responses will not resolve using the STA technique because their pre-spike stimulus averages to zero, so the correlation of the stimulus regions can be analyzed to give an RF measurement (Fairhall et al. 2006; Katz, Viney, and Nikolic 2016; O. Schwartz et al. 2006).

The noisy checkerboard is not without drawbacks: it is overall low contrast, and many RGCs are strongly suppressed by contrast in their peripheral surrounds. Higher-contrast sparse or patterned noise, can be used with a more sophisticated analysis (Kühn and Gollisch 2019; G. W. Schwartz et al. 2012; Cao, Merwine, and Grzywacz 2011). Basic electrophysiology typology profiling of RGCs includes responses to circles of varying size and contrast. These profiles, analyzed with mixture-of-inputs models (typically concentric 1D or 2D Gaussians), give a simple measure of RF size (Jacoby and Schwartz 2017). Measurements of responses to drifting gratings of varying spatial frequency and offset gives a measure of RF size, inverted. A clever method is filtered back projection using short simple stimuli, adapted from CT scanning (Johnston et al. 2014). The RF mapping strategy used in this work is a rapidly-flashed small spots stimulus and current clamp recording mode, which works well on cells with strong spatial surrounds. This was the very first technique used to make RF maps, albeit at a much slower speed and lower spatial resolution (Kuffler 1953). More recently, it was used to map the subthreshold RFs of ON-OFF Direction Selective (OODS) RGCs (Fig 1D) (S. Trenholm et al.

2013). This strategy measures fine details of the receptive field map due to the high-resolution positioning of the stimulus spots and the subthreshold activation recording ability of the current clamp amplifier. An iterative model building process can find individual cones in the RF of primate and rodent RGCs, then closed-loop stimuli can measure the nonlinearity of input contribution combination (Fig 1E) (Freeman et al. 2015; Field et al. 2010). To make comparisons of the dendritic area and RF area, the stimulus projector and imaging microscope can be aligned (Fig 1F) (Brown, He, and Masland 2000).

Receptive Field Asymmetries and Irregularities

An RGC receives many types of input, of ON and OFF polarities, high and low frequency, via excitatory synapses, inhibitory synapses, and through gap junctions. A model that estimates the input from a pathway will be estimating input from one or two cell types. In the F-mini-ON, for example the ON input comes from ON bipolar cells. The ON pathway RF, then, is a combination of the RFs of those bipolar cells, which are themselves combinations of the RFs of the photoreceptors. At each stage, a smooth optimized relationship exists between the physical position of the cell and the receptive field. This generates an overall correspondence between cell location and RF location called the retinotopic map. In the retina, most RF maps are assumed to be well aligned between their various input types, because those are received through the dendrites, which have a fixed location in the retina (Brown, He, and Masland 2000).

Original work on estimating the RF of visual neurons assumed centered smooth Gaussian RF shapes, which remains a good first-order approximation of many cell types, such as the Midget ganglion cells in primate, where input is primarily from a single cone (Kolb and Dekorver 1991). Recent work, enabled by increased stimulus resolution, shows that some cells have atypical RF structures. The ON Delayed RGC has extra-dendritic excitation, that is, with an RF retinotopically

outside the area covered by its dendrites (Mani and Schwartz 2017). The PixON RGC has a missing surround from the center (Johnson, Zhao, and Kerschensteiner 2018). Smooth monostratified RGC RFs are irregularly shaped, with subregions of greater sensitivity, each having slightly varying spike waveforms (Fig 1) (Rhoades et al. 2019). In OODS RGCs, the inhibitory surround is offset to the null side, which acts as a mechanism for DS (Wei et al. 2011). Each RGC type aims to represent the visual field smoothly and completely, so spatial RFs of RGCs of the same type tile visual space (Fig 1G) (Wassle, Peichl, and Boycott 1981; Gauthier et al. 2009; D. I. Vaney 1994; Devries and Baylor 1997; Rhoades et al. 2019). At a sufficient stimulus and measurement quality, inhomogeneities will be apparent within the RFs of most RGCs, because they are composed of input from discrete spatially-separate upstream neurons (G. W. Schwartz et al. 2012; Freeman et al. 2015). My work reports on a specific case of asymmetric receptive fields in two types of mouse RGCs, and the effect of those RF properties on feature selectivity, using parametrically specified single and multi cell models.

In the visual cortex, simple cells are found which have multiple regions of their RF with different polarity. This spatially offset ON and OFF subfields result from input from ON and OFF LGN relay cells, which themselves receive input from ON and OFF RGCs. This RF effect is similar to that found in the F-mini RGCs, where the retinotopic locations of the input cells are offset. Responses to visual edges having contrast areas aligning with the offset RF subfields are increased, which creates an orientation and position selectivity for edges. This preference for a particular small edge is iteratively combined within the visual cortex to generate selectivity for textures, objects, depth, scenes, & c (Hubel and Wiesel 1959, 1962).

Figure 1: Neural Responses to the Visual World

A. Spiking responses (left) and direction selection polar plot (right) of spike count to a moving bar of varying direction angle, showing strong direction selectivity (Taylor et al. 2000). **B.** (left) Basic structure of the vertebrate retina with model components that capture their electrophysiological behavior. (center) A diagram of an advanced linear-nonlinear model with spatiotemporal filters, delays, feedback gain, and a nonlinear output. (right) RFs as measured by extracting spatial components of a model fit to the responses of an RGC. (Real et al. 2017). **C.** Simple RF measurements of neighboring RGCs using white noise flickering checkerboards and a spike-triggered analysis (Meister, Lagnado, and Baylor 1995). **D.** RF maps generated by subthreshold current clamp measurement of ON-OFF direction selective RGCs, comparing between similar gap junction coupled and uncoupled types (S. Trenholm et al. 2013). **E.** Very high resolution RF maps of four types of primate RGCs showing individual cone input RFs as highlight spots (Field et al. 2010). **F.** (left) Technique of microscopy alignment between stimulus and RGC morphology. (right) The RF that same RGC with the soma position marked in yellow (Brown, He, and Masland 2000). **G.** The RF maps of a complete population of primate RGCs in a small area showing smooth uniformity of RF coverage (Rhoades et al. 2019).

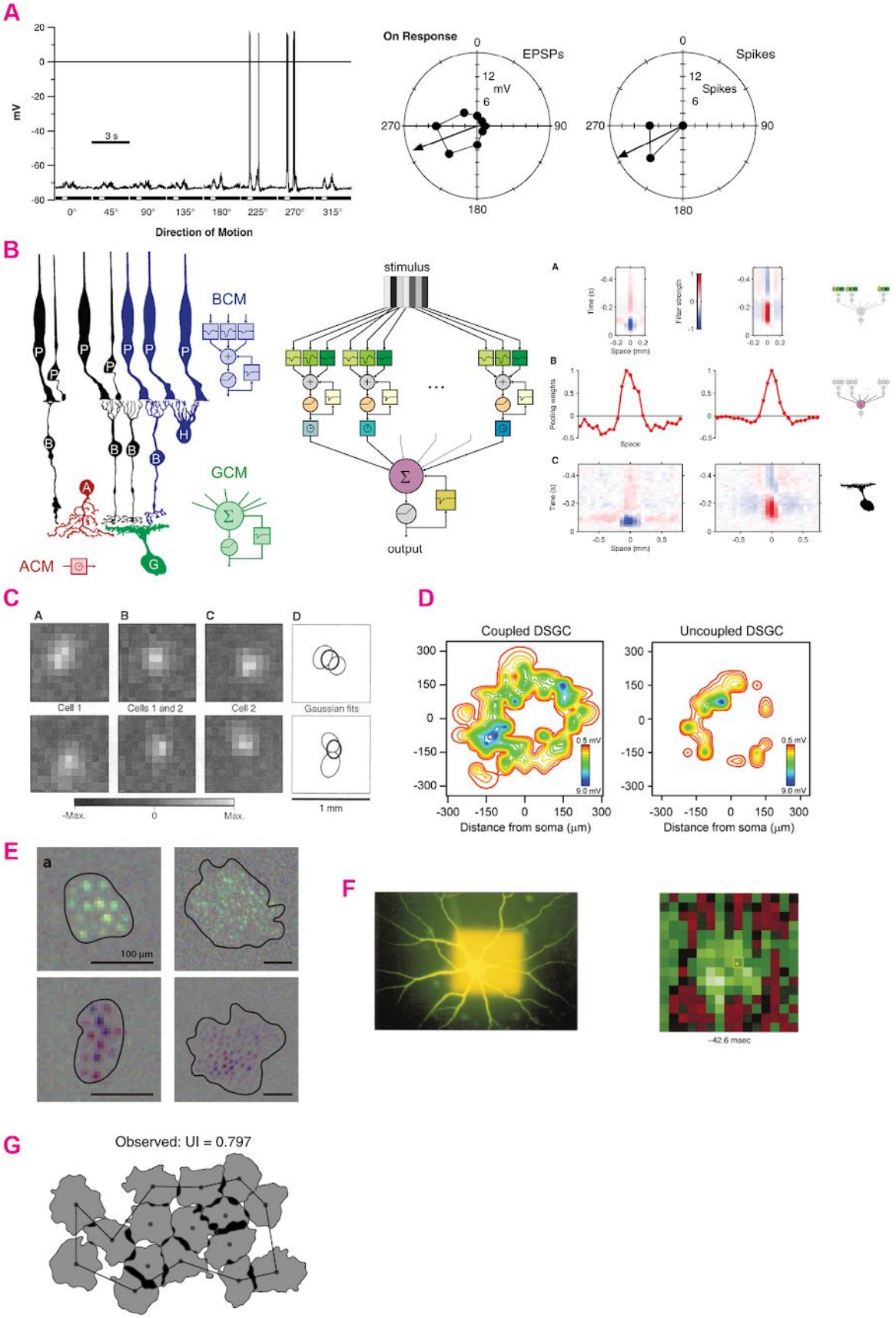
A
mV
3 s
Direction of Motion
On Response
EPSPs
Spikes
mV
Spikes
B
BCM
GCM
ACM
stimulus
output
C
Cell 1
Cells 1 and 2
Cell 2
Gaussian fits
1 mm
D
Coupled DSGC
Uncoupled DSGC
Distance from soma (μm)
E
100 μm
F
−42.6 msec
G
Observed: UI = 0.797

Retinal Cell Typology

Classifying retinal neurons into unique types

The retina aims to achieve consistent encoding of the visual world with eye movements and visual object motion, so it is mostly self-similar across its surface. To achieve this consistency, it consists of a fixed set of circuits that are repeated many times. That fixed circuitry gives rise to cell types, which are sets of neurons that develop the same way and function the same way in each iteration of the circuit across the retina. To understand the neural circuitry of the retina, we need to identify each unique cell type and its properties and role.

Research in the retina has led the process of identifying cell types and developing classification methods. This can be attributed to the particular characteristics of the tissue. The retina is small and separated from the rest of the central nervous system by a narrow information channel, which limits its circuitry in complexity. As early-order sensory neurons, retinal neurons have a clear light response encoding purpose, so their visual stimulus responses and sensory processing layer structure are informative for classification.

My work continues on this path of retinal type mapping by profiling two types of neurons with a fascinating connection property, and classifying the cell types found in a fluorescently-labeled subset of neurons determined by a neuronal promoter. I also aim to help others use this classification data to do better research. Access to specific cell typology makes observations of circuit measurement patterns clearer and more accurate.

Neurons in the retina fall into five major classes: photoreceptors (PR), horizontal cells (HC), bipolar cells (BC), amacrine cells (AC), and ganglion cells (GC). Within each larger class we find narrower cell *types*, serving similar roles with their microcircuits. The number of types within

each class varies moderately by species. In mice, we find: 2 types of PRs (Bowmaker, Loew, and Ott 2005; T. Baden and Osorio 2019), 1 HC (Peichl and González-Soriano 1994), ~15 BCs (Shekhar et al. 2016), ~50 ACs (Yan et al. 2020), ~45 GCs (Yan et al. 2020; Tran et al. 2019).

What we may call a unique type exhibits a narrow subset of properties across many forms of measurements. In parameterized form, we approximate it as normal using the law of large numbers. Consistent separation from other types when multiple measurement forms are used gives confidence in reaching unique type status. This increasing inventory of stable types enables work from many labs with independent sets of techniques to converge on the knowledge of unique types and develop circuit knowledge more effectively together. Regions with broadly type-intravarying classes like in the mammalian cortex probably have a correspondingly complex connectivity ruleset to interpret. The retina presents tractable circuit dissection problems, and the clear views we get help us develop our methods. Next stage advances in retinal measurement will give us the complete and confident set of unique types. We'll make more extensive studies looking at how various classes and their relationships vary over animals, then across species.

A variety of labs have aimed to categorize the complete set of RGC types in the retina, using various methods. Classifying visual neurons by their light stimulus responses is a long-standing method for typology in the retina. Some labs have used wide-field calcium imaging or single cell electrophysiology, plus light stimulus movies, to classify cells. A set of simple stimuli are presented (spots of multiple sizes, a frequency-sweep chirp, and a binary noise grid), and the neuronal responses are classified by eye and by machine learning classifiers (Fig 2A, B) (Tom Baden et al. 2016; Nath and Schwartz 2016; Jacoby and Schwartz 2017; Mani and Schwartz 2017; Farrow and Masland 2011). Morphology from electron microscopy volumetric data and

light responses via wide-field Ca^{2+} imaging in mice were used by the Seung Lab for RGC classification. That dataset was large enough to require a combined online team effort and customized computer algorithms. The resulting dataset is presented in the Eyewire Museum website, which I used in my work to measure stratification offsets (Fig 2C) (Bae et al. 2018). Electron microscopy volume data has the potent properties of complete sampling, connectomics, and multi-cell morphologies. Similar morphology work has also been performed with light microscopy images (Sümbül et al. 2014; Coombs et al. 2006). Or, simple soma size can be used to identify the alpha RGC types (Krieger et al. 2017). The Sanes lab has used primarily genetic methods to produce several large classifications of amacrine and ganglion cell types in the mouse (Fig 2D) (Yan et al. 2020; Tran et al. 2019; Badea and Nathans 2011). Together, these typology studies are converging onto a complete set of unique types.

Typology-Guided RGC Studies

With precise knowledge of the unique cell types, we can target them for investigation, looking to understand their physiology and connectivity. The task of identifying the types of RGCs in live tissue can be accomplished in several ways. The two most common methods are using an animal with a subset of neurons selectively labeled by gene expression and identifying neurons in wild-type retinas by light response electrophysiology.

The Cre/LoxP system is one of several ways to generate selective genetic fluorescent labeling of neurons. In a Cre/LoxP recombination mouse line, two components are brought together: the Cre protein and a specially encoded secondary protein, typically (for typology) a fluorescent reporter. Either the Cre or the secondary protein can be expressed selectively in a subset of cells. In only those cells carrying both the encoded protein DNA and the expressed Cre protein will there be expression of the reporter, which can be visualized in fluorescence microscopy.

This labeled subset of cells can be targeted selectively in experiments (Ivanova, Hwang, and Pan 2010). Several of these mouse lines have been used for retinal neuron typology and investigation. The Hb9 line labels a single type, the dorsal-motion encoding ON-OFF DS (Fig 2E) (S. Trenholm et al. 2013). The Grik4 line labels the PixON RGC type (Johnson, Zhao, and Kerschensteiner 2018). The PV line labels seven RGC types (Katz, Viney, and Nikolic 2016), and the W3 line approximately nine (see W3 chapter), which make these lines less straightforward to use for targeting. Research understanding the roles of amacrine cells in retinal circuits has been aided as well by these labeled lines, such as the ChAT, nNOS, TH, VG3, and CRH lines (Tahnbee Kim and Kerschensteiner 2017; Jacoby et al. 2018, 2015; Sethuramanujam et al. 2017).

Relying on the availability of Cre or other genetic lines hampers the experimenter's access to most RGC types. Identification for targeting of other RGC types in wild-type retina can be done with sufficient experimenter knowledge and skill. An interactive process of visual stimuli is used. Some RGC types can be identified quickly in cell-attached recordings: ON-OFF DS RGCs for example have vertically-centered spikes and return highly direction selective responses to moving bars, which is unlike any other type. This is not the case for many cell types, which appear to have similar light responses. The F-mini-ON was originally found to be a unique type when its low-speed DS properties were used to identify it in the Schwartz Lab. The physiology of the F-mini-ON and F-mini-OFF RGC types has only been described briefly; my work aims to create a more complete examination of these types and explore their particular behaviors.

Enabling this improved and straightforward WT typology strategy is excellent experimental repeatability and precision, as evidenced by the Schwartz lab, which has produced profiles of the HD1, HD2, and UHD (Fig 2F) (Jacoby and Schwartz 2017), ON and OFF OS (Nath and Schwartz 2016, 2017), Suppressed-by-Contrast (Jacoby et al. 2015), and ON Delayed RGCs

(Mani and Schwartz 2017). Within the Schwartz lab, light levels, stimulus shapes, cell conditions, electrical recording conditions, etc. are stable and controllable across yearly timescales. So, an observant experimenter can start to find patterns, which can be refined into true cell types by the careful splitting of combinations of light response measurements. This effort over several years to identify and record all cell types in WT retina using basic electrophysiology light responses has culminated in the release of the RGCTypes.org dataset and website.

Figure 2: Retinal Cell Typology

A. RGC types identified by morphology and electrophysiology presented for open use at the RGCTypes.org website. **B.** RGC classification using calcium imaging responses to light stimuli, clustered by a machine learning algorithm (Tom Baden et al. 2016). **C.** RGC classification using electron microscopy morphology, showing stratification density variations across types (Bae et al. 2018). **D.** A confusion matrix result showing amacrine cell classification based on selective genetic expression patterns (Yan et al. 2020)**. E.** The Hb9-eGFP mouse line labels a single RGC type: the dorsal-coding ON-OFF direction selective RGC (S. Trenholm et al. 2013)**. F.** RGC types identified by their specific patterns of varying responses to spots of multiple sizes (Jacoby and Schwartz 2017)

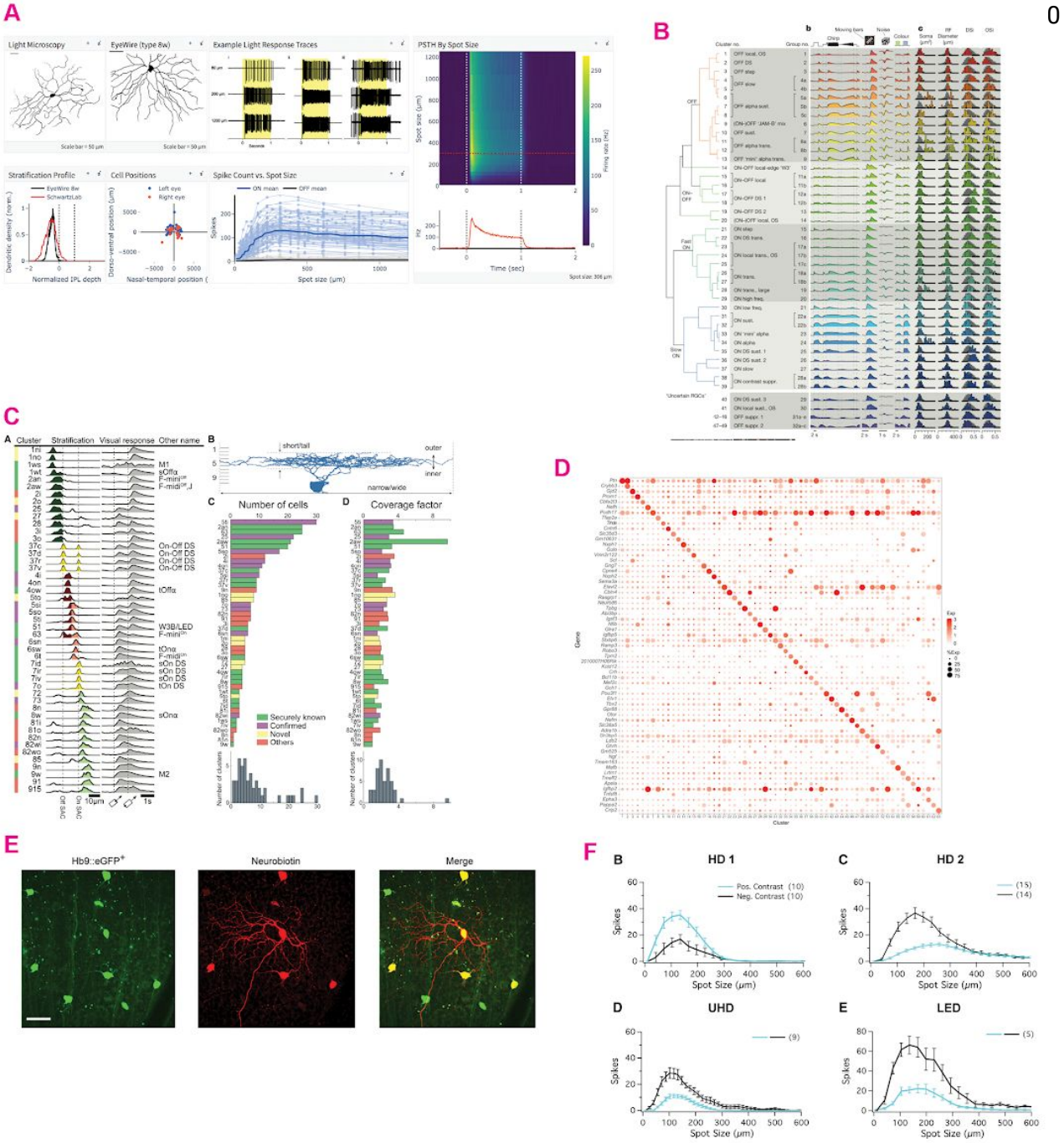
A
Light Microscopy
EyeWire (type 8w)
Example Light Response Traces
PSTH By Spot Size
Stratification Profile
Cell Positions
Spike Count vs. Spot Size
B
C
D
E
Hb9::eGFP+
Neurobiotin
Merge
F
HD 1
HD 2
UHD
LED
Spikes
Spot Size (μm)

Retinal Gap Junctions

A neural circuit is built of neurons communicating information to each other, performing computations individually and jointly through connections. There are a few ways that they make those connections, biophysically. One is the commonly-known closely-apposed chemical synapse, between opposed neurons, with a synaptic cleft and postsynaptic zone, between axon and dendrite. Another is diffusing carrier synapses, such as hormones and steroids, released systemically by glands. A third major type is gap junctions, proteins that create a narrow opening in a cell's membrane, which is secured to the same opening on another neuron. This aligned pore channel connects the cytoplasms of the two cells and allows for the flow of water, ions, and small molecules. Electrically, the diffusive flow of ionic charges acts to draw their membrane potentials closer with very low latency, which is a route by which sensory information is transmitted. Gap junctions (GJs) have been found and studied throughout the nervous system (Rohr 2004), and are also present in non-neuronal cell types (Willebrords et al. 2015). Neuroscientists measure GJs using electrophysiology (current injections, correlation analysis), light microscopy (GJ permeable dyes), and electron microscopy (identifying contact points). The physiological properties of GJs are determined in part by their particular composition. A single gap junction pore is composed of two opposing connexon hemichannels of the same or different type. Each of the two connexons is made of six connexin subunits and can be homomeric or heteromeric. The composition of all twelve components determines the electrical and physical properties of the channels (Weber et al. 2004). Neuronal gap junctions synapses in the retina are made of hundreds of such protein pores. Clusters of GJs can be visualized using immunohistochemistry (IHC) (Fig 3A).

Gap Junction Circuits in the Retina

GJs are prevalent among various combinations of cell classes in the vertebrate retina, where their fast kinetics are useful for visual processing and circuit regulation (Völgyi, Chheda, and Bloomfield 2009).

GJs provide visual signal input to retinal neurons, which can act to generate its feature selectivity. GJs have been found in alphas RGCs coupled via amacrine cells, where synchronous spikes signal the presence of a complete visual object (Völgyi et al. 2005). In ON DS RGCs coupled via amacrine cells, synchrony is decreased for null-direction stimulus (Ackert et al. 2006). AII amacrines are GJ coupled to ON cone BCs, forming one of the pathways for rod-based vision (Fig 3B) (Hartveit and Veruki 2012; Graydon et al. 2018). In bipolar cells, they can spread signals laterally, which effectively increases receptive field size (Kuo, Schwartz, and Rieke 2016; Sigulinsky et al. 2020). GJs couple cones in the fish and are dopamine-modulated (DeVries and Schwartz 1989). In dorsal-coding ON-OFF DS RGCs, they act to spread signals quickly ahead across the retina the first spikes of the response to a visual object, to compensate for delays between the outer and inner retina, a behavior called lag normalization (Fig 3C) (Stuart Trenholm et al. 2013). GJs were found in the recently-identified S3-Gbx2+ amacrine cells, which may be the only synapses on those neurons (Kerstein et al. 2020). Clearly, GJs are an important part of many retinal circuits.

Gap junctions between two RGCs have been identified among same-type RGCs, the ON-OFF DS dorsal-coding RGC found in the Hb9 mouse line, and between two types of ON RGCs, the ON Alpha and ON medium, in the guinea pig (Fig 3D) (Puller et al. 2020). Connectivity between the homologous types (ON alpha and a medium-sized ON RGC) in the mouse has not been found. In

my work, I identify and profile a new GJ connection between two RGC types having differing primary response polarity, which has not been found before in the mouse.

Many types of GJ compositions have been found in the mammalian retina (Söhl et al. 2000). The composition of gap junctions can be determined by immunohistochemistry with antibodies specific to each connexin. In particular, Cx36 has been found in RGCs (Pan et al. 2010) and between photoreceptors (Jin et al. 2020), Cx50 in HCs (J. J. O'Brien et al. 2006), Cx45 in nNOS-2 ACs (Jacoby et al. 2018), Cx36 and Cx30.2 in AII amacrine cells and ipRGCs (Meyer et al. 2016; Kothmann, Massey, and O'Brien 2009).

The retina has the task of quickly adjusting to varying light and scene structure conditions. One mechanism for adjustment is modulating gap junction conductance, which changes how visual signals are spread and combined in a network of neurons. Several examples of GJ modulation have been identified in the retina. Connectivity between alpha RGCs is greatly increased with increased light level (Hu et al. 2010). Connectivity between AII amacrine cells is increased by particular light levels, regulated by non-synaptic NMDA receptor activity (Fig 3E) (Bloomfield and Völgyi 2004; Kothmann et al. 2012). Coupling between nNOS-2 amacrine cells is modulated by nitric oxide (Jacoby et al. 2018). Gap junctions can be modulated by typical neural signaling mechanisms, such as dopamine via cAMP (Hampson, Vaney, and Weiler 1992; McMahon and Brown 1994; J. O'Brien 2014), and there are dopaminergic neurons in the retina which can produce it in response to light level changes (Contini et al. 2010).

Measurements of Gap Junctions

Gap junctions between neurons are most easily identified using dye coupling. Fluorescent molecules can move through gap junctions between cells. An injection of dye into one cell can result in the labeling of many surrounding neurons, which can then be investigated (Fig 3D) (Xin

and Bloomfield 1997; Völgyi, Chheda, and Bloomfield 2009). They could be found in EM datasets or using transcriptomics or IHC. The use of any of these requires strong experimental typology because they cannot be done pre-recording in vitro.

With a gap junction synapse identified between two neurons, we seek to measure its properties. Gap junctions between neurons act as electrical circuit resistors, so they can be easily measured using electrical techniques. Direct measurements include voltage pulses in current clamp mode (Fig 3F) (Jacoby et al. 2018), and current pulses in voltage clamp mode (Veruki and Hartveit 2009). The amount of dye passed through the GJ in a given amount of time can be a measure of conductance, and different size dye molecules can be used to determine the protein composition of the GJs (Weber et al. 2004). The heteromeric composition of a GJ can create an electrically rectified channel (Marder 2009). Pharmacological manipulations can be used to examine the role of gap junctions in retinal circuits. One commonly used drug is Meclofenamic Acid (MFA), which was shown to block GJs between AII and ON cone BCs (Fig 3G) (Veruki and Hartveit 2009) and between horizontal cells (Pan, Mills, and Massey 2007). Another chemical, quinine, blocks a subset of gap junctions when applied intracellularly (Srinivas, Hopperstad, and Spray 2001). With gap junctions blocked, the resulting changes in the light response properties show evidence of the function of the GJ in the circuit.

Gap junctions cause temporal correlation between membrane voltages of connected neurons. Correlation analysis is used to measure relationships between membrane voltages of GJ connected neurons over short time scales. At a short enough time scale (less than downstream integration time) these correlations are considered *synchrony*. Synchrony is easily read out as an informative signal within spike trains by downstream neurons with coincidence detection, that is, overall supralinear gain. We measure correlation by comparing time series data over

short time offsets using a sliding multiplication and integrating the two signals. Observations of correlation to measure GJ effects need to be carefully controlled to remove the effects of shared input signals, such as noise from photoreceptors (Ala-Laurila et al. 2011). In whole-cell mode, precise synchrony appears as a zero time lag peak in the cross-correlation analysis. Because spiking occurs after a small delay from input current change, correlations in spiking responses appear as a double peak around zero, that is, a spike in neuron A causes a spike in neuron B after a short delay, and vice versa (Fig 3H) (Hu and Bloomfield 2003; DeVries 1999). It has recently been shown that the order of those spikes can signal for precise object location due to the way current flows within the GJ microcircuit (Tong and Trenholm 2020). A zero-lag peak can also be caused by shared input, which varies with the proportion of shared input (Mastronarde 1989; Ala-Laurila et al. 2011). Correlations between RGCs have been identified as a way that they improve visual encoding performance (Cafaro and Rieke 2010).

Figure 3: Retinal Gap Junctions

A. Image of several dye-filled GJ coupled nNOS-2 amacrine cells, with IHC labeling of connexins found at cell intersection points (Jacoby et al. 2018). **B.** Diagram of the primary rod pathway showing gap junction synapses between AII amacrine cells and rod bipolar cells (Grimes et al. 2018). **C.** Illustration of the lag normalization behavior found in gap junction coupled ON-OFF direction selective RGCs, with spiking beginning before the moving visual object reaches the classical RF of the RGC (right) in comparison to the uncoupled RGC (left) (Stuart Trenholm et al. 2013). **D.** Microscopy image of a dye injection into an ON alpha RGC in the guinea pig showing illuminated somas of gap junction coupled cells (arrows) (Puller et al. 2020). **E.** Microscopy images of AII amacrine cells. In each, one cell was filled by injection with the GJ tracing dye Neurobiotin. The difference in GJ coupling by dye diffusion amount is visible in control (left) and NMDA-blocked (right) states (Kothmann et al. 2012). **F.** Diagram of voltage clamp technique for gap junction conductance measurement, showing input voltage pulses (left upper) and resulting current deflections (left lower), which are plotted together (right) (Veruki and Hartveit 2009). **G.** Effect of meclofenamic acid on the conductance of gap junctions between two cells as measured in F, showing a substantial decrease in coupling after drug application and a slow recovery with washout (Veruki and Hartveit 2009). **H.** Cross-correlation analysis of simultaneous spike responses of pairs of OFF RGCs in the rabbit, showing evidence of gap junction coupling as dual peaks around zero time offset (DeVries 1999).

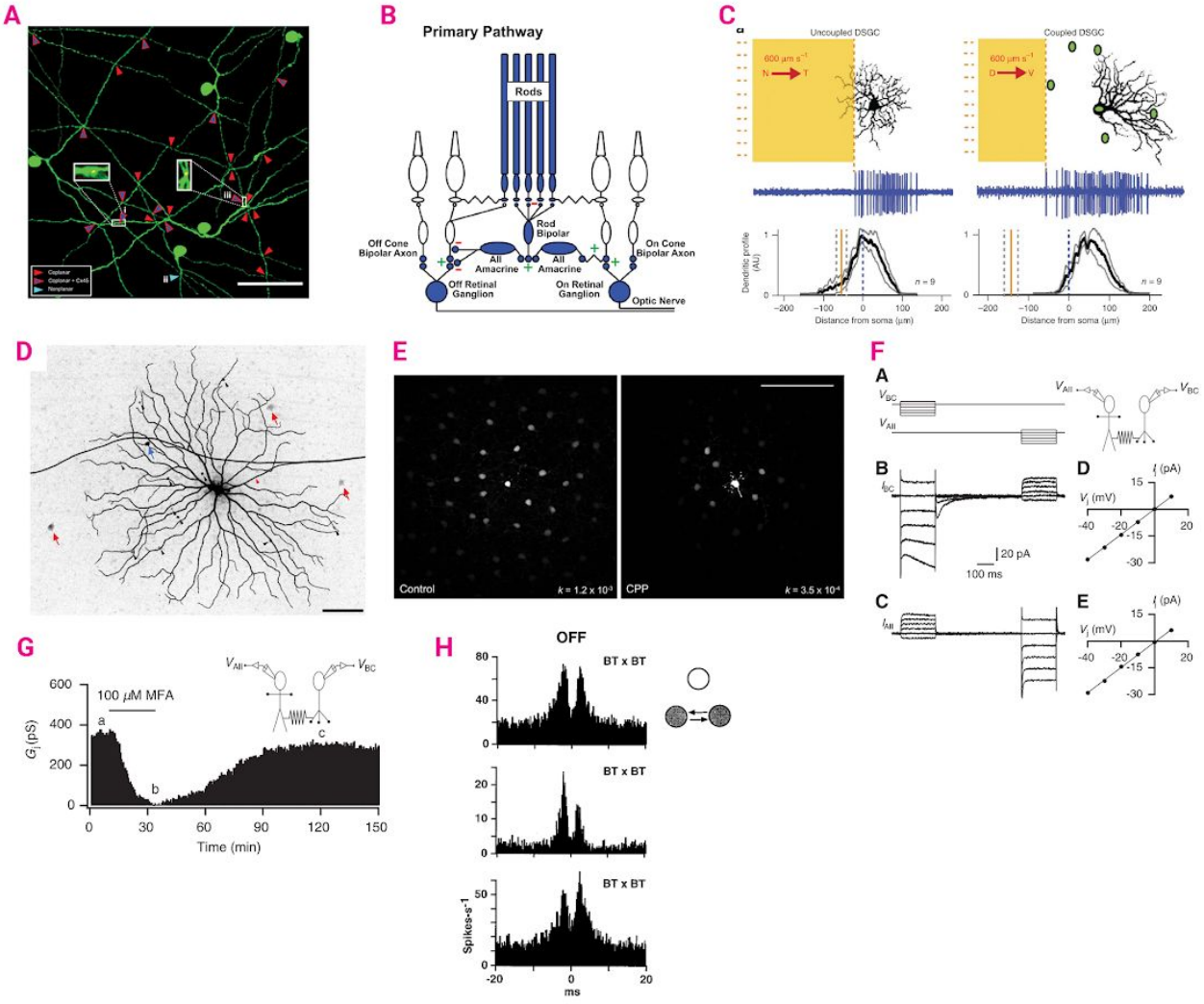
A
B
Primary Pathway
Rods
Rod Bipolar
Off Cone Bipolar Axon
On Cone Bipolar Axon
AII Amacrine
AII Amacrine
Off Retinal Ganglion
On Retinal Ganglion
Optic Nerve
C
Uncoupled DSGC
Coupled DSGC
600 μm s⁻¹
N → T
600 μm s⁻¹
D → V
Dendritic profile (AU)
n = 9
n = 9
Distance from soma (μm)
Distance from soma (μm)
D
E
Control
k = 1.2 x 10⁻³
CPP
k = 3.5 x 10⁻⁴
F
A
B
C
D
E
20 pA
100 ms
I (pA)
V_I (mV)
G
100 μM MFA
G_j (pS)
Time (min)
H
OFF
BT x BT
BT x BT
BT x BT
Spikes·s⁻¹
ms

Results & Discussions

An Offset ON-OFF Receptive Field is Created by Gap Junctions Between Distinct Types of Retinal Ganglion Cells

Status: Published in *Nature Neuroscience*, November 2020

Effort: I performed the majority of electrophysiology experiments, all IHC and microscopy, all modeling, all data collection and analysis, all figure creation. The experiment conception, text, and figure editing was a collaboration between Greg and me.

Included in Appendix A

A Survey of the Retinal Ganglion Cell Types of the W3 Mouse Line

Status: In draft status with a complete dataset, to be submitted for publishing in early 2021.

Effort: I performed the majority of electrophysiology experiments, all IHC and microscopy, all data collection and analysis, all figure creation, all text writing.

Included in Appendix B

Discussion

Parametric Models and Investigation of Apparent Feature Selectivity

I investigated the low-speed direction selectivity (LSDS) in the F-mini-ON RGC type. I used whole cell measurements and modeling to explore the mechanism underlying the LSDS. I measured asymmetries in receptive fields and their effects on visual feature response, using high-resolution receptive fields in the F-mini RGCs and several other types. I found that in the F-mini-ON and F-mini-OFF RGCs there is a spatial offset between ON and OFF RF input maps.

The single-cell model I created for response asymmetry investigation was a simple one-stage four-pathway LN model, with components created from parameterized versions of voltage-clamp whole-cell measurements of the ON and OFF pathways. I aimed to add the minimal elements necessary to replicate the low-speed selective direction selective (LSDS) behavior, in a way that allowed me to explore the possible results parametrically. I found that a simple spatial offset of excitation and inhibition, or ON and OFF, could generate LSDS. Exploring further by modifying RF shape eccentricity I was able to generate orientation selectivity (OS), and flexible combinations of DS and OS. This led to the understanding that small (relative to RF size) variations in the relationships between input pathway RFs can cause what appears to be feature selectivity. I extracted stratification offsets from the Eyewire Museum dataset (Bae et al. 2018), which can be used as a proxy for the amount of offset we might find in RGC RFs. This openly available morphology dataset proved to be very useful for quickly making observations in this fashion.

It is clear from electrophysiology and morphology studies in ON-OFF direction selective RGCs that many mechanisms, including varying excitation, varying inhibition, a spatial offset between

those two, and highly specific wiring patterns, contribute to robust direction selectivity across a wide variety of stimulus parameters (Taylor and Vaney 2002; Briggman, Helmstaedter, and Denk 2011). However, generating basic direction selectivity in a visual neuron has long been known to be simple. The Reichardt detector model, which has as components just two spatially and temporally offset receptive fields, generates direction selectivity. Furthermore, that DS is only significant at low object speeds. I replicated this behavior in my single-cell model, in which I used offsets and delays like those found in F-mini-ON RGCs. The bottom-up parameterized nature of that model allowed me to explore the way that offsets and delays can cause DS. I report on a subset of those findings in the supplement to the offset paper. Many biological mechanisms, such as electrical cable properties of asymmetric dendrites, could generate spatial or temporal offset, so we should expect that the presence of some LSDS in visual neurons is the default. A neuron would need some significant compensation mechanism to overcome a morphological asymmetry like that found in the dendrites of the F-mini RGCs. Future work may investigate this effect to explain the DS found in the asymmetric JAM-B RGCs (I.-J. Kim et al. 2008), and look for DS feature selectivity in the newly identified asymmetric S3-Gbx2+ AC (Kerstein et al. 2020).

Exploring Multi-cell Models for Populations

I combined many of the above single-cell RGC models into a multi-cell population model to evaluate the precision with which a population of RGCs could encode a visual edge location. In the future, we'll dive deeper into single-cell RFs and multi-cell RF populations. Multiple cells of the same type have RFs that interdigitate because the RFs are tied to dendrites that fill space with a consistent coverage factor (Gauthier et al. 2009). Building large complete sets of RF maps helps us solidify typology and study population feature encoding. Cells of opposing types

have RFs that might interleaf, which acts to reduce redundancy and improve information efficiency.

The multi-cell model is a first step in a larger project of investigating population encoding of medium-complexity stimuli. Future work will implement such a model with cell interaction terms, to estimate the effects of gap junctions among the RGCs. The decoder I used, the center of mass, is a very simplified version of the true downstream decoding mechanism, which eventually culminates in conscious experience. For the task of rapid simple object position localization, the COM may be moderately accurate in describing the superior colliculus, where cells receive direct input from groups of RGCs. However, it is vastly insufficient to describe the decoding of the LGN and visual cortex, each of which have their own complicated detection mechanisms. To continue this project, we would need a description of the way neural inputs are interpreted, which is research done in other brain areas that could be used. The retina sends a lot of information in its correlations and as whole populations (Ganmor, Segev, and Schneidman 2015). To improve on that we'll need to study large-scale correlations better and then build multi-cell models that aim to capture that behavior (Kühn and Gollisch 2019).

Current leading RGC response models are useful for retinal research, but they have various limitations. One limitation is the stimulus used: a white noise checkerboard does not have a spatial structure that will activate nonlinear mechanisms that might not be well captured by the model generated. Moving to modeling natural movie responses will improve this situation (Turner and Rieke 2016). Accurate models of light responses will be critical for restoring sight with prosthetics, however it has not yet been shown that current models replicate responses well enough to be useful for vision. They might perform well enough for an animal to identify a simple visual stimulus, which is experimentally useful in the development of these algorithms in

visual prosthetic research. For the purpose of replicating responses, an artificial neural network may be better than a biophysically accurate model (McIntosh et al. 2016).

The Important Role of Stimulus and Analysis in Retinal Neurophysiology

To investigate the mechanisms underlying LSDS in the F-mini RGCs, I needed to measure their receptive fields. I found that the F-mini RGCs did not respond well to white noise stimulus, since they are strongly suppressed for full-field stimulation. A different measurement stimulus was required. F-mini RGCs do respond well to flashed spots much smaller than their RF size, so I created a stimulus and analysis package which used that technique. This addition required an upgrade of the core of the rig software. I created a flexible analysis loop to perform sub-epoch stimulation, with online & offline analysis wrappers. This required learning the workings of the entire stimulus and recording and analysis system. The ability to modify this system to flexibly probe the retina is a powerful tool for many aspects of retinal neuroscience. In the near future, experimental rigs will include integrated live typology and optimized stimulus suggestions.

The stimulus we use and the models we make are intimately linked. The next steps in model building will require larger datasets with more complicated stimuli, to probe nonlinear effects that are mostly present at edge cases. Soon, models of rod and cone responses will be used to parameterize electrophysiology input to the retina at the PR output. With increasingly advanced knowledge of the biophysical mechanisms in the early retina embedded in models we are nearing the ability to identify specific individual neurons in the retina.

With a quickly fitted model, we can use interesting stimuli that use real-time feedback on the cells. Real-time response evaluation with machine learning evaluation enables online cell typology by unskilled researchers, which opens the field to more people. Iso-response, which varies inputs in a closed-loop fashion to ignore the effects of output nonlinearities, and methods

like cone clamp which varies inputs to counteract photoreceptor nonlinearities, can constrain signals within the outer retina (Gollisch and Herz 2012). Solving models online using methods like these will enable us to make fast measurements of circuits deep within the retina, to explore the variety of bipolar and amacrine cells and how they are combined. We could measure the spatial substrate of adaptation, trying to find amacrine cells through electrophysiology (Khani and Gollisch 2017).

Progress Towards Complete Typology

By examining in detail the F-mini-ON and F-mini-OFF RGC types, I have placed them confidently within the full set of mouse RGC types, which is part of an ongoing global effort to complete this knowledge.

The W3 line has been used by several labs with imprecise or unclear typology. Several labs have reported on the W3 or W3B as a single cell type, with or without using the genetic line. My typology work calls these results into question, especially where claims about connectivity between specific cell types is concerned. At least one other lab has used W3 as a single cell type without the use of the mouse line, so it is essential to clear this up before further misidentification occurs (T. Kim et al. 2020).

I also participated in creating the RGC atlas dataset, which contains electrophysiology measurements of several stimuli for all known unique RGC types. This dataset is distributed in data files and display figures at the RGCTypes.org website, enabling broad synchronization of efforts to understand the mouse retina. Open sharing of datasets will be how we as a scientific field make rapid iterative progress in understanding the retina’s circuitry with cell type specific knowledge.

In progress are several exciting projects on many species with complete typology datasets. The Schwartz/Sanes mouse RGC atlas will be released, creating a unified typology with electrophysiology, morphology, and single-cell genetics, which will describe the remaining third of ganglion cell types. As our typology datasets become more complete, we will be able to take the next steps in identifying circuit connectivity. With the F-mini RGCs, future work will situate them within their microcircuits by finding amacrine cell neighbors and bipolar cell input. From initial evaluation by eye on Eyewire Museum, the F-mini-ON receives ON input from BC5i, and the F-mini-OFF receives OFF input from BC2.

Gap Junctions Create Atypical Circuits in the Retina

I found a new gap junction connection between the F-mini-ON and F-mini-OFF RGCs in the mouse, made measurements of connected pairs using dual current clamp, and used MFA and ablation to manipulate the circuit to prove ON-OFF channel combination.

Gap junctions (GJs) are fascinating neural circuit components. Moving forward, knowledge of this circuit opens a wide field of questions, only a subset of which I investigated and answered in my projects. With a GJ connection identified, we can search for the protein composition of these channels. High resolution confocal images show puncta of GJ proteins at crossing points between cells. The next steps in protein identification can be done using immunohistochemistry and a library of primary antibodies. Our attempts at this for three of the most commonly found GJ proteins in the retina returned null results. Initial results using single-cell RNA transcriptomics data found no GJ encoding mRNA; this is not unexpected because GJs may have low turnover.

Modulation of GJ conductivity would enable the F-mini RGCs to vary their ON-OFF polarity balance as needed, an interesting behavior that may be relevant for natural vision. These GJs

may be modulated by dopamine or nitric oxide, which can be measured in-vitro. Gap junctions spread signals laterally in the network, so their effects are visible across a population of cells. In the future, we will measure these effects in large field recordings from many such cells. This atypical alternating RGC type connectivity pattern will align with an alternating pattern downstream. That pattern might match inhibitory and excitatory cell types, creating a mechanism in which each cell type acts as the surround for the other cell type, which could sharpen position readout.

Synchrony induced by gap junctions will be most visible over sets of many coupled neurons. This effect contributes to population coding, which is best explored using a multi-electrode array. Measurements using Ca^{2+} imaging are more often used in the mouse and may suffice for these investigations. Additionally, they could provide access to information about Ca^{2+} flow through gap junctions. However, this technique will struggle to measure noise correlations due to the inherently noisy readout using protein sensors. We can easily measure the flow through GJs of charged particles using electrophysiology, but GJs can also pass small molecules, which may act as signaling messengers. Future work may measure and model the flows of these other particles and show how these neurons communicate in additional ways.

For the restoration of vision using electrode arrays, GJ connectivity knowledge gives another lever on each cell's activity level. We can stimulate GJ-neighboring cells to lower a neuron's stimulation activation threshold, which I plan to exploit next. Development of the GJ connections will be interesting to study because it involves two RGC types developing in concert, which creates additional constraints on the process.

Overall Summary

I am excited to build on this understanding and to see how the field builds on it. The retina continues to give us strange patterns to investigate. My findings have generated new questions for us to answer in the course of understanding biology ever more completely.

References

Ackert, Jessica M., Synphen H. Wu, Jacob C. Lee, Joseph Abrams, Edward H. Hu, Ido Perlman, and Stewart A. Bloomfield. 2006. “Light-Induced Changes in Spike Synchronization between Coupled ON Direction Selective Ganglion Cells in the Mammalian Retina.” *The Journal of Neuroscience: The Official Journal of the Society for Neuroscience* 26 (16): 4206–15. https://doi.org/10.1523/JNEUROSCI.0496-06.2006.

Ala-Laurila, Petri, Martin Greschner, E. J. Chichilnisky, and Fred Rieke. 2011. “Cone Photoreceptor Contributions to Noise and Correlations in the Retinal Output.” *Nature Neuroscience* 14 (10): 1309–16. https://doi.org/10.1038/nn.2927.

Baccus, Stephen A., and Markus Meister. 2002. “Fast and Slow Contrast Adaptation in Retinal Circuitry.” *Neuron* 36 (5): 909–19. https://doi.org/10.1016/s0896-6273(02)01050-4.

Baccus, Stephen A., Bence P. Olveczky, Mihai Manu, and Markus Meister. 2008. “A Retinal Circuit That Computes Object Motion.” *The Journal of Neuroscience: The Official Journal of the Society for Neuroscience* 28 (27): 6807–17. https://doi.org/10.1523/JNEUROSCI.4206-07.2008.

Badea, Tudor Constantin, and Jeremy Nathans. 2011. “Morphologies of Mouse Retinal Ganglion Cells Expressing Transcription Factors Brn3a, Brn3b, and Brn3c: Analysis of Wild Type and Mutant Cells Using Genetically-Directed Sparse Labeling.” *Vision Research* 51 (2): 269–79. https://doi.org/10.1016/j.visres.2010.08.039.

Baden, Tom, Philipp Berens, Katrin Franke, Miroslav Román Rosón, Matthias Bethge, and Thomas Euler. 2016. “The Functional Diversity of Retinal Ganglion Cells in the Mouse.” *Nature* 529 (7586): 345–50. https://doi.org/10.1038/nature16468.

Baden, T., and D. Osorio. 2019. “The Retinal Basis of Vertebrate Color Vision.” *Annual Review of Vision Science* 5 (September): 177–200. https://doi.org/10.1146/annurev-vision-091718-014926.

Bae, J. Alexander, Shang Mu, Jinseop S. Kim, Nicholas L. Turner, Ignacio Tartavull, Nico Kemnitz, Chris S. Jordan, et al. 2018. “Digital Museum of Retinal Ganglion Cells with Dense Anatomy and Physiology.” *Cell* 173 (5): 1293–1306.e19. https://doi.org/10.1016/j.cell.2018.04.040.

Berry, M. J., 2nd, I. H. Brivanlou, T. A. Jordan, and M. Meister. 1999. “Anticipation of Moving Stimuli by the Retina.” *Nature* 398 (6725): 334–38. https://doi.org/10.1038/18678.

Bloomfield, Stewart A., and Béla Völgyi. 2004. “Function and Plasticity of Homologous Coupling between AII Amacrine Cells.” *Vision Research* 44 (28): 3297–3306. https://doi.org/10.1016/j.visres.2004.07.012.

Bowmaker, James K., Ellis R. Loew, and Matthias Ott. 2005. “The Cone Photoreceptors and Visual Pigments of Chameleons.” *Journal of Comparative Physiology. A, Neuroethology, Sensory, Neural, and Behavioral Physiology* 191 (10): 925–32. https://doi.org/10.1007/s00359-005-0014-4.

Briggman, Kevin L., Moritz Helmstaedter, and Winfried Denk. 2011. “Wiring Specificity in the Direction-Selectivity Circuit of the Retina.” *Nature* 471 (7337): 183–88. https://doi.org/10.1038/nature09818.

Brown, S. P., S. He, and R. H. Masland. 2000. “Receptive Field Microstructure and Dendritic

Geometry of Retinal Ganglion Cells." *Neuron* 27 (2): 371–83. https://doi.org/10.1016/s0896-6273(00)00044-1.
Cafaro, Jon, and Fred Rieke. 2010. "Noise Correlations Improve Response Fidelity and Stimulus Encoding." *Nature* 468 (7326): 964–67. https://doi.org/10.1038/nature09570.
Cao, Xiwu, David K. Merwine, and Norberto M. Grzywacz. 2011. "Dependence of the Retinal Ganglion Cell's Responses on Local Textures of Natural Scenes." *Journal of Vision* 11 (6). https://doi.org/10.1167/11.6.11.
Chichilnisky, E. J. 2001. "A Simple White Noise Analysis of Neuronal Light Responses." *Network* 12 (2): 199–213. https://www.ncbi.nlm.nih.gov/pubmed/11405422.
Contini, Massimo, Bin Lin, Kazuto Kobayashi, Hideyuki Okano, Richard H. Masland, and Elio Raviola. 2010. "Synaptic Input of ON-Bipolar Cells onto the Dopaminergic Neurons of the Mouse Retina." *The Journal of Comparative Neurology* 518 (11): 2035–50. https://doi.org/10.1002/cne.22320.
Coombs, J., D. van der List, G-Y Wang, and L. M. Chalupa. 2006. "Morphological Properties of Mouse Retinal Ganglion Cells." *Neuroscience*. https://doi.org/10.1016/j.neuroscience.2006.02.079.
Cui, Yuwei, Yanbin V. Wang, Silvia J. H. Park, Jonathan B. Demb, and Daniel A. Butts. 2016. "Divisive Suppression Explains High-Precision Firing and Contrast Adaptation in Retinal Ganglion Cells." *eLife* 5 (November). https://doi.org/10.7554/eLife.19460.
DeVries, S. H. 1999. "Correlated Firing in Rabbit Retinal Ganglion Cells." *Journal of Neurophysiology* 81 (2): 908–20. https://doi.org/10.1152/jn.1999.81.2.908.
Devries, S. H., and D. A. Baylor. 1997. "Mosaic Arrangement of Ganglion Cell Receptive Fields in Rabbit Retina." *Journal of Neurophysiology* 78 (4): 2048–60. https://doi.org/10.1152/jn.1997.78.4.2048.
DeVries, S. H., and E. A. Schwartz. 1989. "Modulation of an Electrical Synapse between Solitary Pairs of Catfish Horizontal Cells by Dopamine and Second Messengers." *The Journal of Physiology* 414 (July): 351–75. https://doi.org/10.1113/jphysiol.1989.sp017692.
Fairhall, Adrienne L., C. Andrew Burlingame, Ramesh Narasimhan, Robert A. Harris, Jason L. Puchalla, and Michael J. Berry 2nd. 2006. "Selectivity for Multiple Stimulus Features in Retinal Ganglion Cells." *Journal of Neurophysiology* 96 (5): 2724–38. https://doi.org/10.1152/jn.00995.2005.
Farrow, Karl, and Richard H. Masland. 2011. "Physiological Clustering of Visual Channels in the Mouse Retina." *Journal of Neurophysiology* 105 (4): 1516–30. https://doi.org/10.1152/jn.00331.2010.
Field, Greg D., Jeffrey L. Gauthier, Alexander Sher, Martin Greschner, Timothy A. Machado, Lauren H. Jepson, Jonathon Shlens, et al. 2010. "Functional Connectivity in the Retina at the Resolution of Photoreceptors." *Nature* 467 (7316): 673–77. https://doi.org/10.1038/nature09424.
Freeman, Jeremy, Greg D. Field, Peter H. Li, Martin Greschner, Deborah E. Gunning, Keith Mathieson, Alexander Sher, et al. 2015. "Mapping Nonlinear Receptive Field Structure in Primate Retina at Single Cone Resolution." *eLife* 4 (October). https://doi.org/10.7554/eLife.05241.
Ganmor, Elad, Ronen Segev, and Elad Schneidman. 2015. "A Thesaurus for a Neural Population Code." *eLife* 4 (September). https://doi.org/10.7554/eLife.06134.
Gao, Juan, Greg Schwartz, Michael J. Berry 2nd, and Philip Holmes. 2009. "An Oscillatory Circuit

Underlying the Detection of Disruptions in Temporally-Periodic Patterns." *Network* 20 (2): 106–35. https://doi.org/10.1080/09548980902991705.
Gauthier, Jeffrey L., Greg D. Field, Alexander Sher, Martin Greschner, Jonathon Shlens, Alan M. Litke, and E. J. Chichilnisky. 2009. "Receptive Fields in Primate Retina Are Coordinated to Sample Visual Space More Uniformly." Edited by Michael Robert DeWeese. *PLoS Biology* 7 (4): e63–e63. https://doi.org/10.1371/journal.pbio.1000063.
Gollisch, Tim, and Andreas V. M. Herz. 2012. "The Iso-Response Method: Measuring Neuronal Stimulus Integration with Closed-Loop Experiments." *Frontiers in Neural Circuits* 6 (December): 104. https://doi.org/10.3389/fncir.2012.00104.
Graydon, Cole W., Evan E. Lieberman, Nao Rho, Kevin L. Briggman, Joshua H. Singer, and Jeffrey S. Diamond. 2018. "Synaptic Transfer between Rod and Cone Pathways Mediated by AII Amacrine Cells in the Mouse Retina." *Current Biology: CB* 28 (17): 2739–51.e3. https://doi.org/10.1016/j.cub.2018.06.063.
Grimes, William N., Jacob Baudin, Anthony W. Azevedo, and Fred Rieke. 2018. "Range, Routing and Kinetics of Rod Signaling in Primate Retina." *eLife* 7 (October). https://doi.org/10.7554/eLife.38281.
Hampson, E. C., D. I. Vaney, and R. Weiler. 1992. "Dopaminergic Modulation of Gap Junction Permeability between Amacrine Cells in Mammalian Retina." *The Journal of Neuroscience: The Official Journal of the Society for Neuroscience* 12 (12): 4911–22. https://doi.org/10.1523/JNEUROSCI.12-12-04911.1992.
Hartveit, Espen, and Margaret Lin Veruki. 2012. "Electrical Synapses between AII Amacrine Cells in the Retina: Function and Modulation." *Brain Research* 1487 (December): 160–72. https://doi.org/10.1016/j.brainres.2012.05.060.
Herz, A. V. M., T. Gollisch, C. K. Machens, and D. Jaeger. 2006. "Modeling Single-Neuron Dynamics and Computations: A Balance of Detail and Abstraction." *Science*. https://doi.org/10.1126/science.1127240.
Hubel, D. H., and T. N. Wiesel. 1959. "Receptive Fields of Single Neurones in the Cat's Striate Cortex." *The Journal of Physiology*. https://doi.org/10.1113/jphysiol.1959.sp006308.
———. 1962. "Receptive Fields, Binocular Interaction and Functional Architecture in the Cat's Visual Cortex." *The Journal of Physiology*. https://doi.org/10.1113/jphysiol.1962.sp006837.
Hu, Edward H., and Stewart A. Bloomfield. 2003. "Gap Junctional Coupling Underlies the Short-Latency Spike Synchrony of Retinal Alpha Ganglion Cells." *The Journal of Neuroscience: The Official Journal of the Society for Neuroscience* 23 (17): 6768–77. https://www.ncbi.nlm.nih.gov/pubmed/12890770.
Hu, Edward H., Feng Pan, Béla Völgyi, and Stewart A. Bloomfield. 2010. "Light Increases the Gap Junctional Coupling of Retinal Ganglion Cells." *The Journal of Physiology* 588 (Pt 21): 4145–63. https://doi.org/10.1113/jphysiol.2010.193268.
Ivanova, E., G-S Hwang, and Z-H Pan. 2010. "Characterization of Transgenic Mouse Lines Expressing Cre Recombinase in the Retina." *Neuroscience* 165 (1): 233–43. https://doi.org/10.1016/j.neuroscience.2009.10.021.
Jacoby, Jason, Amurta Nath, Zachary F. Jessen, and Gregory W. Schwartz. 2018. "A Self-Regulating Gap Junction Network of Amacrine Cells Controls Nitric Oxide Release in the Retina." *Neuron* 100 (5): 1149–62.e5. https://doi.org/10.1016/j.neuron.2018.09.047.
Jacoby, Jason, and Gregory W. Schwartz. 2017. "Three Small-Receptive-Field Ganglion Cells in the Mouse Retina Are Distinctly Tuned to Size, Speed, and Object Motion." *The Journal of*

Neuroscience: The Official Journal of the Society for Neuroscience 37 (3): 610–25. https://doi.org/10.1523/JNEUROSCI.2804-16.2016.

Jacoby, Jason, Yongling Zhu, Steven H. DeVries, and Gregory W. Schwartz. 2015. "An Amacrine Cell Circuit for Signaling Steady Illumination in the Retina." *Cell Reports* 13 (12): 2663–70. https://doi.org/10.1016/j.celrep.2015.11.062.

Jin, Nange, Zhijing Zhang, Joyce Keung, Sean B. Youn, Munenori Ishibashi, Lian-Ming Tian, David W. Marshak, et al. 2020. "Molecular and Functional Architecture of the Mouse Photoreceptor Network." *Science Advances* 6 (28): eaba7232. https://doi.org/10.1126/sciadv.aba7232.

Johnson, Keith P., Lei Zhao, and Daniel Kerschensteiner. 2018. "A Pixel-Encoder Retinal Ganglion Cell with Spatially Offset Excitatory and Inhibitory Receptive Fields." *Cell Reports* 22 (6): 1462–72. https://doi.org/10.1016/j.celrep.2018.01.037.

Johnston, Jamie, Huayu Ding, Sofie H. Seibel, Federico Esposti, and Leon Lagnado. 2014. "Rapid Mapping of Visual Receptive Fields by Filtered Back Projection: Application to Multi-Neuronal Electrophysiology and Imaging." *The Journal of Physiology* 592 (22): 4839–54. https://doi.org/10.1113/jphysiol.2014.276642.

Katz, Matthew L., Tim J. Viney, and Konstantin Nikolic. 2016. "Receptive Field Vectors of Genetically-Identified Retinal Ganglion Cells Reveal Cell-Type-Dependent Visual Functions." *PLOS ONE*. https://doi.org/10.1371/journal.pone.0147738.

Kerstein, Patrick C., Joseph Leffler, Benjamin Sivyer, W. Rowland Taylor, and Kevin M. Wright. 2020. "Gbx2 Identifies Two Amacrine Cell Subtypes with Distinct Molecular, Morphological, and Physiological Properties." *Cell Reports* 33 (7): 108382. https://doi.org/10.1016/j.celrep.2020.108382.

Khani, Mohammad Hossein, and Tim Gollisch. 2017. "Diversity in Spatial Scope of Contrast Adaptation among Mouse Retinal Ganglion Cells." *Journal of Neurophysiology* 118 (6): 3024–43. https://doi.org/10.1152/jn.00529.2017.

Kim, In-Jung, Yifeng Zhang, Masahito Yamagata, Markus Meister, and Joshua R. Sanes. 2008. "Molecular Identification of a Retinal Cell Type That Responds to Upward Motion." *Nature* 452 (7186): 478–82. https://doi.org/10.1038/nature06739.

Kim, Tahnbee, and Daniel Kerschensteiner. 2017. "Inhibitory Control of Feature Selectivity in an Object Motion Sensitive Circuit of the Retina." *Cell Reports*. https://doi.org/10.1016/j.celrep.2017.04.060.

Kim, T., N. Shen, J-C Hsiang, K. P. Johnson, and D. Kerschensteiner. 2020. "Dendritic and Parallel Processing of Visual Threats in the Retina Control Defensive Responses." *Science Advances* 6 (47). https://doi.org/10.1126/sciadv.abc9920.

Kolb, H., and L. Dekorver. 1991. "Midget Ganglion Cells of the Parafovea of the Human Retina: A Study by Electron Microscopy and Serial Section Reconstructions." *The Journal of Comparative Neurology* 303 (4): 617–36. https://doi.org/10.1002/cne.903030408.

Kothmann, W. Wade, Stephen C. Massey, and John O'Brien. 2009. "Dopamine-Stimulated Dephosphorylation of Connexin 36 Mediates AII Amacrine Cell Uncoupling." *The Journal of Neuroscience: The Official Journal of the Society for Neuroscience* 29 (47): 14903–11. https://doi.org/10.1523/JNEUROSCI.3436-09.2009.

Kothmann, W. Wade, E. Brady Trexler, Christopher M. Whitaker, Wei Li, Stephen C. Massey, and John O'Brien. 2012. "Nonsynaptic NMDA Receptors Mediate Activity-Dependent Plasticity of Gap Junctional Coupling in the AII Amacrine Cell Network." *The Journal of Neuroscience:*

The Official Journal of the Society for Neuroscience 32 (20): 6747–59. https://doi.org/10.1523/JNEUROSCI.5087-11.2012.

Krieger, Brenna, Mu Qiao, David L. Rousso, Joshua R. Sanes, and Markus Meister. 2017. "Four Alpha Ganglion Cell Types in Mouse Retina: Function, Structure, and Molecular Signatures." *PloS One* 12 (7): e0180091. https://doi.org/10.1371/journal.pone.0180091.

Kuffler, S. W. 1953. "Discharge Patterns and Functional Organization of Mammalian Retina." *Journal of Neurophysiology* 16 (1): 37–68. https://doi.org/10.1152/jn.1953.16.1.37.

Kühn, Norma Krystyna, and Tim Gollisch. 2019. "Activity Correlations between Direction-Selective Retinal Ganglion Cells Synergistically Enhance Motion Decoding from Complex Visual Scenes." *Neuron* 101 (5): 963–76.e7. https://doi.org/10.1016/j.neuron.2019.01.003.

Kuo, Sidney P., Gregory W. Schwartz, and Fred Rieke. 2016. "Nonlinear Spatiotemporal Integration by Electrical and Chemical Synapses in the Retina." *Neuron* 90 (2): 320–32. https://doi.org/10.1016/j.neuron.2016.03.012.

Linsenmeier, R. A., L. J. Frishman, H. G. Jakiela, and C. Enroth-Cugell. 1982. "Receptive Field Properties of X and Y Cells in the Cat Retina Derived from Contrast Sensitivity Measurements." *Vision Research*. https://doi.org/10.1016/0042-6989(82)90082-7.

Mani, Adam, and Gregory W. Schwartz. 2017. "Circuit Mechanisms of a Retinal Ganglion Cell with Stimulus-Dependent Response Latency and Activation Beyond Its Dendrites." *Current Biology: CB* 27 (4): 471–82. https://doi.org/10.1016/j.cub.2016.12.033.

Marder, Eve. 2009. "Electrical Synapses: Rectification Demystified." *Current Biology: CB* 19 (1): R34–35. https://doi.org/10.1016/j.cub.2008.11.008.

Mastronarde, David N. 1989. "Correlated Firing of Retinal Ganglion Cells." *Trends in Neurosciences* 12 (2): 75–80. https://doi.org/10.1016/0166-2236(89)90140-9.

McIntosh, Lane T., Niru Maheswaranathan, Aran Nayebi, Surya Ganguli, and Stephen A. Baccus. 2016. "Deep Learning Models of the Retinal Response to Natural Scenes." *Advances in Neural Information Processing Systems* 29: 1369–77. https://www.ncbi.nlm.nih.gov/pubmed/28729779.

McMahon, D. G., and D. R. Brown. 1994. "Modulation of Gap-Junction Channel Gating at Zebrafish Retinal Electrical Synapses." *Journal of Neurophysiology* 72 (5): 2257–68. https://doi.org/10.1152/jn.1994.72.5.2257.

Meister, M., L. Lagnado, and D. A. Baylor. 1995. "Concerted Signaling by Retinal Ganglion Cells." *Science*. https://doi.org/10.1126/science.270.5239.1207.

Meyer, Arndt, Stephan Tetenborg, Helena Greb, Jasmin Segelken, Birthe Dorgau, Reto Weiler, Sheriar G. Hormuzdi, Ulrike Janssen-Bienhold, and Karin Dedek. 2016. "Connexin30.2: In Vitro Interaction with Connexin36 in HeLa Cells and Expression in AII Amacrine Cells and Intrinsically Photosensitive Ganglion Cells in the Mouse Retina." *Frontiers in Molecular Neuroscience* 9 (May): 36. https://doi.org/10.3389/fnmol.2016.00036.

Münch, Thomas A., Rava Azeredo da Silveira, Sandra Siegert, Tim James Viney, Gautam B. Awatramani, and Botond Roska. 2009. "Approach Sensitivity in the Retina Processed by a Multifunctional Neural Circuit." *Nature Neuroscience* 12 (10): 1308–16. https://doi.org/10.1038/nn.2389.

Nath, Amurta, and Gregory W. Schwartz. 2016. "Cardinal Orientation Selectivity Is Represented by Two Distinct Ganglion Cell Types in Mouse Retina." *The Journal of Neuroscience: The Official Journal of the Society for Neuroscience* 36 (11): 3208–21.

https://doi.org/10.1523/JNEUROSCI.4554-15.2016.
———. 2017. “Electrical Synapses Convey Orientation Selectivity in the Mouse Retina.” *Nature Communications* 8 (1): 2025. https://doi.org/10.1038/s41467-017-01980-9.
O’Brien, Jennifer J., Wei Li, Feng Pan, Joyce Keung, John O’Brien, and Stephen C. Massey. 2006. “Coupling between A-Type Horizontal Cells Is Mediated by Connexin 50 Gap Junctions in the Rabbit Retina.” *The Journal of Neuroscience: The Official Journal of the Society for Neuroscience* 26 (45): 11624–36. https://doi.org/10.1523/JNEUROSCI.2296-06.2006.
O’Brien, John. 2014. “The Ever-Changing Electrical Synapse.” *Current Opinion in Neurobiology* 29 (December): 64–72. https://doi.org/10.1016/j.conb.2014.05.011.
Pan, Feng, Stephen L. Mills, and Stephen C. Massey. 2007. “Screening of Gap Junction Antagonists on Dye Coupling in the Rabbit Retina.” *Visual Neuroscience* 24 (4): 609–18. https://doi.org/10.1017/S0952523807070472.
Pan, Feng, David L. Paul, Stewart A. Bloomfield, and Béla Völgyi. 2010. “Connexin36 Is Required for Gap Junctional Coupling of Most Ganglion Cell Subtypes in the Mouse Retina.” *The Journal of Comparative Neurology*. https://doi.org/10.1002/cne.22254.
Peichl, L., and J. González-Soriano. 1994. “Morphological Types of Horizontal Cell in Rodent Retinae: A Comparison of Rat, Mouse, Gerbil, and Guinea Pig.” *Visual Neuroscience* 11 (3): 501–17. https://doi.org/10.1017/s095252380000242x.
Pillow, Jonathan W., Liam Paninski, Valerie J. Uzzell, Eero P. Simoncelli, and E. J. Chichilnisky. 2005. “Prediction and Decoding of Retinal Ganglion Cell Responses with a Probabilistic Spiking Model.” *The Journal of Neuroscience: The Official Journal of the Society for Neuroscience* 25 (47): 11003–13. https://doi.org/10.1523/JNEUROSCI.3305-05.2005.
Puller, Christian, Sabrina Duda, Elaheh Lotfi, Yousef Arzhangnia, Christoph T. Block, Malte T. Ahlers, and Martin Greschner. 2020. “Electrical Coupling of Heterotypic Ganglion Cells in the Mammalian Retina.” *The Journal of Neuroscience: The Official Journal of the Society for Neuroscience* 40 (6): 1302–10. https://doi.org/10.1523/JNEUROSCI.1374-19.2019.
Real, Esteban, Hiroki Asari, Tim Gollisch, and Markus Meister. 2017. “Neural Circuit Inference from Function to Structure.” *Current Biology: CB* 27 (2): 189–98. https://doi.org/10.1016/j.cub.2016.11.040.
Rhoades, Colleen E., Nishal P. Shah, Michael B. Manookin, Nora Brackbill, Alexandra Kling, Georges Goetz, Alexander Sher, Alan M. Litke, and E. J. Chichilnisky. 2019. “Unusual Physiological Properties of Smooth Monostratified Ganglion Cell Types in Primate Retina.” *Neuron* 103 (4): 658–72.e6. https://doi.org/10.1016/j.neuron.2019.05.036.
Rohr, S. 2004. “Role of Gap Junctions in the Propagation of the Cardiac Action Potential.” *Cardiovascular Research*. https://doi.org/10.1016/j.cardiores.2003.11.035.
Schwartz, Greg, and Michael J. Berry 2nd. 2008. “Sophisticated Temporal Pattern Recognition in Retinal Ganglion Cells.” *Journal of Neurophysiology* 99 (4): 1787–98. https://doi.org/10.1152/jn.01025.2007.
Schwartz, Gregory W., Haruhisa Okawa, Felice A. Dunn, Josh L. Morgan, Daniel Kerschensteiner, Rachel O. Wong, and Fred Rieke. 2012. “The Spatial Structure of a Nonlinear Receptive Field.” *Nature Neuroscience* 15 (11): 1572–80. https://doi.org/10.1038/nn.3225.
Schwartz, Odelia, Jonathan W. Pillow, Nicole C. Rust, and Eero P. Simoncelli. 2006. “Spike-Triggered Neural Characterization.” *Journal of Vision* 6 (4): 484–507. https://doi.org/10.1167/6.4.13.
Sethuramanujam, Santhosh, Xiaoyang Yao, Geoff deRosenroll, Kevin L. Briggman, Greg D. Field,

and Gautam B. Awatramani. 2017. "'Silent' NMDA Synapses Enhance Motion Sensitivity in a Mature Retinal Circuit." *Neuron*. https://doi.org/10.1016/j.neuron.2017.09.058.

Shekhar, Karthik, Sylvain W. Lapan, Irene E. Whitney, Nicholas M. Tran, Evan Z. Macosko, Monika Kowalczyk, Xian Adiconis, et al. 2016. "Comprehensive Classification of Retinal Bipolar Neurons by Single-Cell Transcriptomics." *Cell* 166 (5): 1308–23.e30. https://doi.org/10.1016/j.cell.2016.07.054.

Sigulinsky, Crystal L., James R. Anderson, Ethan Kerzner, Christopher N. Rapp, Rebecca L. Pfeiffer, Taryn M. Rodman, Daniel P. Emrich, et al. 2020. "Network Architecture of Gap Junctional Coupling among Parallel Processing Channels in the Mammalian Retina." *The Journal of Neuroscience: The Official Journal of the Society for Neuroscience* 40 (23): 4483–4511. https://doi.org/10.1523/JNEUROSCI.1810-19.2020.

Söhl, Goran, Martin Güldenagel, Otto Traub, and Klaus Willecke. 2000. "Connexin Expression in the Retina." *Brain Research Reviews* 32 (1): 138–45. https://doi.org/10.1016/S0165-0173(99)00074-0.

Srinivas, M., M. G. Hopperstad, and D. C. Spray. 2001. "Quinine Blocks Specific Gap Junction Channel Subtypes." *Proceedings of the National Academy of Sciences of the United States of America* 98 (19): 10942–47. https://doi.org/10.1073/pnas.191206198.

Sümbül, Uygar, Sen Song, Kyle McCulloch, Michael Becker, Bin Lin, Joshua R. Sanes, Richard H. Masland, and H. Sebastian Seung. 2014. "A Genetic and Computational Approach to Structurally Classify Neuronal Types." *Nature Communications* 5 (March): 3512. https://doi.org/10.1038/ncomms4512.

Taylor, W. Rowland, S. He, W. R. Levick, and David Vaney. 2000. "Dendritic Computation of Direction Selectivity by Retinal Ganglion Cells." *Science* 289 (5488): 2347–50. https://doi.org/10.1126/science.289.5488.2347.

Taylor, W. Rowland, and David I. Vaney. 2002. "Diverse Synaptic Mechanisms Generate Direction Selectivity in the Rabbit Retina." *The Journal of Neuroscience: The Official Journal of the Society for Neuroscience* 22 (17): 7712–20. https://www.ncbi.nlm.nih.gov/pubmed/12196594.

Tong, Rudi, and Stuart Trenholm. 2020. "High Resolution Visual Information via a Gap Junction-Mediated Spike Order Code." *Neuroscience*. bioRxiv.

Tran, Nicholas M., Karthik Shekhar, Irene E. Whitney, Anne Jacobi, Inbal Benhar, Guosong Hong, Wenjun Yan, et al. 2019. "Single-Cell Profiles of Retinal Ganglion Cells Differing in Resilience to Injury Reveal Neuroprotective Genes." *Neuron* 104 (6): 1039–55.e12. https://doi.org/10.1016/j.neuron.2019.11.006.

Trenholm, S., A. J. McLaughlin, D. J. Schwab, and G. B. Awatramani. 2013. "Dynamic Tuning of Electrical and Chemical Synaptic Transmission in a Network of Motion Coding Retinal Neurons." *Journal of Neuroscience*. https://doi.org/10.1523/jneurosci.0808-13.2013.

Trenholm, Stuart, David J. Schwab, Vijay Balasubramanian, and Gautam B. Awatramani. 2013. "Lag Normalization in an Electrically Coupled Neural Network." *Nature Neuroscience* 16 (2): 154–56. https://doi.org/10.1038/nn.3308.

Turner, Maxwell H., and Fred Rieke. 2016. "Synaptic Rectification Controls Nonlinear Spatial Integration of Natural Visual Inputs." *Neuron* 90 (6): 1257–71. https://doi.org/10.1016/j.neuron.2016.05.006.

Vaney, David I., Benjamin Sivyer, and W. Rowland Taylor. 2012. "Direction Selectivity in the Retina: Symmetry and Asymmetry in Structure and Function." *Nature Reviews. Neuroscience*

13 (3): 194–208. https://doi.org/10.1038/nrn3165.
Vaney, D. I. 1994. “Territorial Organization of Direction-Selective Ganglion Cells in Rabbit Retina.” *The Journal of Neuroscience: The Official Journal of the Society for Neuroscience* 14 (11 Pt 1): 6301–16. https://www.ncbi.nlm.nih.gov/pubmed/7965037.
Veruki, Margaret Lin, and Espen Hartveit. 2009. “Meclofenamic Acid Blocks Electrical Synapses of Retinal AII Amacrine and on-Cone Bipolar Cells.” *Journal of Neurophysiology* 101 (5): 2339–47. https://doi.org/10.1152/jn.00112.2009.
Völgyi, Béla, Joseph Abrams, David L. Paul, and Stewart A. Bloomfield. 2005. “Morphology and Tracer Coupling Pattern of Alpha Ganglion Cells in the Mouse Retina.” *The Journal of Comparative Neurology* 492 (1): 66–77. https://doi.org/10.1002/cne.20700.
Völgyi, Béla, Samir Chheda, and Stewart A. Bloomfield. 2009. “Tracer Coupling Patterns of the Ganglion Cell Subtypes in the Mouse Retina.” *The Journal of Comparative Neurology* 512 (5): 664–87. https://doi.org/10.1002/cne.21912.
Wassle, H., L. Peichl, and B. B. Boycott. 1981. “Dendritic Territories of Cat Retinal Ganglion Cells.” *Nature* 292 (5821): 344–45. http://www.nature.com/doifinder/10.1038/292344a0.
Weber, Paul A., Hou-Chien Chang, Kris E. Spaeth, Johannes M. Nitsche, and Bruce J. Nicholson. 2004. “The Permeability of Gap Junction Channels to Probes of Different Size Is Dependent on Connexin Composition and Permeant-Pore Affinities.” *Biophysical Journal* 87 (2): 958–73. https://doi.org/10.1529/biophysj.103.036350.
Wei, Wei, Aaron M. Hamby, Kaili Zhou, and Marla B. Feller. 2011. “Development of Asymmetric Inhibition Underlying Direction Selectivity in the Retina.” *Nature* 469 (7330): 402–6. https://doi.org/10.1038/nature09600.
Willebrords, Joost, Sara Crespo Yanguas, Michaël Maes, Elke Decrock, Nan Wang, Luc Leybaert, Tereza Cristina da Silva, et al. 2015. “Structure, Regulation and Function of Gap Junctions in Liver.” *Cell Communication & Adhesion* 22 (2-6): 29–37. https://doi.org/10.3109/15419061.2016.1151875.
Xin, D., and S. A. Bloomfield. 1997. “Tracer Coupling Pattern of Amacrine and Ganglion Cells in the Rabbit Retina.” *The Journal of Comparative Neurology* 383 (4): 512–28. https://doi.org/3.0.co;2-5">10.1002/(sici)1096-9861(19970714)383:4<512::aid-cne8>3.0.co;2-5.
Yan, Wenjun, Mallory A. Laboulaye, Nicholas M. Tran, Irene E. Whitney, Inbal Benhar, and Joshua R. Sanes. 2020. “Mouse Retinal Cell Atlas: Molecular Identification of over Sixty Amacrine Cell Types.” *The Journal of Neuroscience: The Official Journal of the Society for Neuroscience* 40 (27): 5177–95. https://doi.org/10.1523/JNEUROSCI.0471-20.2020.

Appendix A:

An Offset ON-OFF Receptive Field is Created by Gap Junctions Between Distinct Types of Retinal Ganglion Cells

Nature Neuroscience, November 2020

nature neuroscience

ARTICLES

https://doi.org/10.1038/s41593-020-00747-8

An offset ON–OFF receptive field is created by gap junctions between distinct types of retinal ganglion cells

Sam Cooler[1,2] and Gregory W. Schwartz[2,3] ✉

In the vertebrate retina, the location of a neuron's receptive field in visual space closely corresponds to the physical location of synaptic input onto its dendrites, a relationship called the retinotopic map. We report the discovery of a systematic spatial offset between the ON and OFF receptive subfields in F-mini-ON retinal ganglion cells (RGCs). Surprisingly, this property does not come from spatially offset ON and OFF layer dendrites, but instead arises from a network of electrical synapses via gap junctions to RGCs of a different type, the F-mini-OFF. We show that the asymmetric morphology and connectivity of these RGCs can explain their receptive field offset, and we use a multicell model to explore the effects of receptive field offset on the precision of edge-location representation in a population. This RGC network forms a new electrical channel combining the ON and OFF feedforward pathways within the output layer of the retina.

Receptive fields (RFs) are a foundational concept in sensory neuroscience. The RF of a sensory neuron is shaped by the properties of its synaptic inputs from connected neurons. In the early visual system, retinotopic maps define a strict correspondence between the location of a cell's dendrites and its RF location in visual space[1]. RGCs, the output cells of the retina, form dendritic mosaics that tile retinal space and have corresponding RF mosaics that tile visual space[2,3].

Superimposed on the mosaic organization of retinal neurons is the division into ON and OFF channels, which respond to light increments and decrements, respectively. The ON and OFF pathways diverge at the first synapse in the visual system, the output of the photoreceptors, and they reconverge in multiple locations, including in ON–OFF RGCs that increase their firing for both increments and decrements. In the mouse, where they are best characterized, RGCs comprise greater than 40 functionally, morphologically and transcriptomically distinct types[4–9]. All previously identified ON–OFF RGC types have aligned ON and OFF RFs[10–13], and they all receive excitatory synaptic inputs from both ON and OFF bipolar cells. Inputs from ON and OFF bipolar cells are formed either at two distinct dendritic strata in the inner plexiform layer[13] or at a single stratum in the middle of the inner plexiform layer where ON and OFF bipolar cell terminals overlap[14].

We report on an RGC type that breaks both of these conventions. These RGCs have a systematic spatial offset between their ON and OFF RF subfields. The RGCs do not receive ON and OFF input from bipolar cells on spatially offset dendrites. Instead, the RF offset arises from a new circuit composed of gap junctions with several RGCs of a single, different functional type. While RFs with offset ON and OFF subfields result in a modest amount of direction selectivity and orientation selectivity for certain stimuli at the level of single RGCs, modeling demonstrates a large enhancement in the encoding of edge position within a population of RGCs. Our multicell model reveals that offset ON and OFF RF subfields could help a population of RGCs encode edge position with precision down to 0.6 degrees of visual angle, less than 12% of the RF diameter of a single RGC.

Results

F-mini RGCs have both ON and OFF responses. F-mini RGCs were recently identified as two different cell types, F-mini-ON and F-mini-OFF, based on their expression patterns of several transcription factors, their unique morphologies and their light responses[15]. F-mini RGCs are the second and third most numerous RGC types in the mouse retina, together constituting 13% of RGCs[8]. We recorded light responses from functionally identified F-mini RGCs in dark-adapted mouse retina (Methods) and later confirmed their identity by morphological analysis (Fig. 1a–c) and immunohistochemistry (IHC) (Extended Data Fig. 1). Unlike in the initial reports, we found that both F-mini RGC types responded to both light increments (ON) and decrements (OFF) for small spots and moving bars (Fig. 1d–k and Discussion). We focused primarily on F-mini-ON RGCs in search of a circuit mechanism for the ON–OFF responses.

To explore the robustness of the ON–OFF responses in F-mini-ON RGCs, we adapted the retina to different mean luminances across the range from scotopic to photopic. We found robust ON and OFF responses across this range (Fig. 1j). We also measured the contrast response functions of F-mini-ON RGCs on a photopic background and found similar contrast sensitivity for the ON and OFF responses (Fig. 1k).

The ON and OFF RFs of F-mini-ON RGCs are systematically displaced despite aligned dendritic strata. We mapped ON and OFF RFs in F-mini and other RGCs using a stimulus consisting of small spots of positive and negative contrast[12]. We identified a consistent spatial offset between the ON and OFF RF subfields in F-mini-ON RGCs (Fig. 2). F-mini-ON RGCs had an ON–OFF offset of $38 \pm 14\,\mu m$ ($n = 9$ cells; Fig. 2d), greater than that of control RGCs, which had an offset of $25 \pm 15\,\mu m$ ($n = 14$ cells; $P = 0.047$).

[1]Northwestern University Interdepartmental Neuroscience Graduate Program, Chicago, IL, USA. [2]Departments of Ophthalmology and Physiology, Feinberg School of Medicine, Northwestern University, Chicago, IL, USA. [3]Department of Neurobiology, Weinberg School of Arts and Sciences, Northwestern University, Chicago, IL, USA. ✉e-mail: greg.schwartz@northwestern.edu

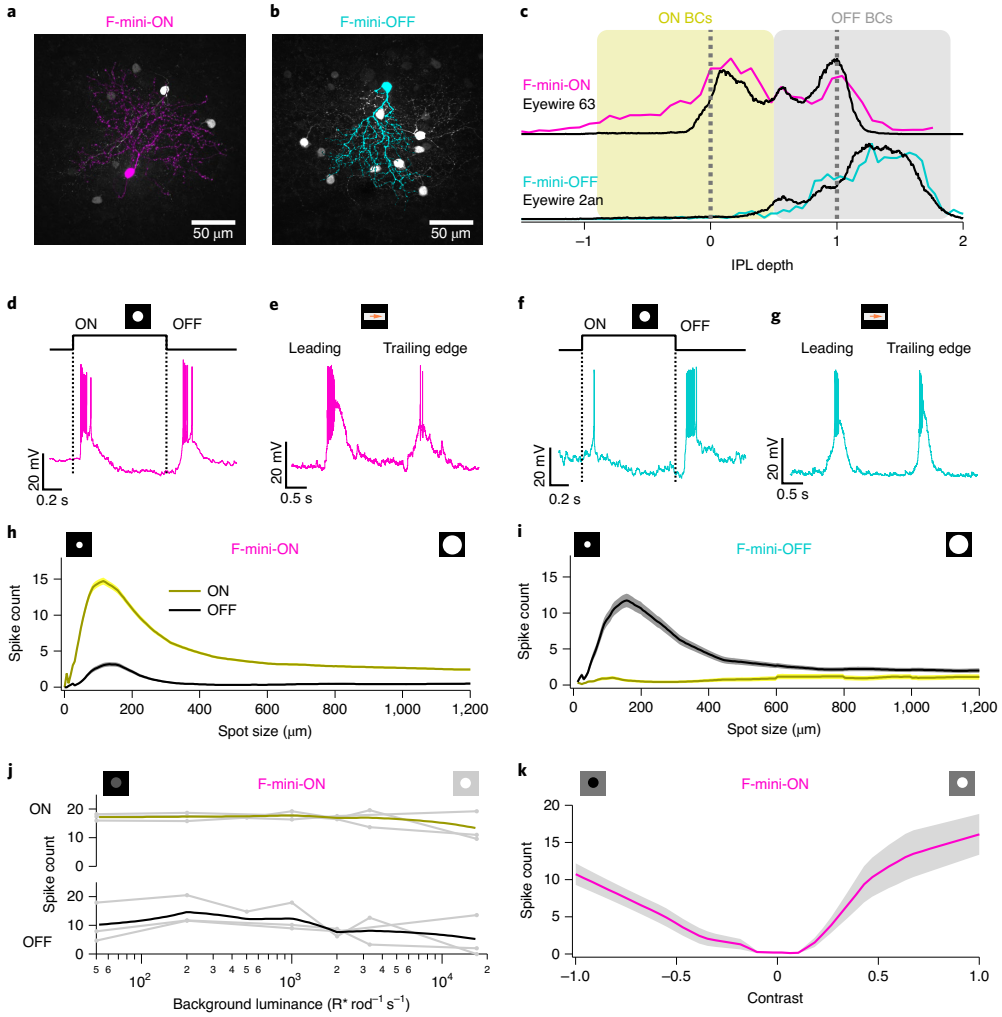

Fig. 1 | F-mini-ON and F-mini-OFF RGCs have both ON and OFF light responses. a,**b**, Images of F-mini-ON (magenta) and F-mini-OFF (cyan) RGCs from fixed tissue. All cell images are shown with the dorsal direction on the retina toward the top. Targeted RGCs were traced and colored, overlaid on gray. Morphology was consistent in all images ($n=40$; 20 cells) **c**, Stratification profiles of an F-mini-ON and an F-mini-OFF RGC from our cell fills (colored lines) and from the data in the Eyewire museum (black lines). Dashed lines indicate ON and OFF choline acetyltransferase bands. Shading shows the stratification regions of ON (yellow) and OFF (gray) bipolar cells (BCs) in the inner plexiform layer (IPL). **d**, F-mini-ON RGC in current-clamp recording responding to the onset and offset of a positive contrast spot from darkness to 200 rhodopsin isomerizations per rod per second (R* rod^{-1} s^{-1}). **e**, F-mini-ON RGC responding to the leading and trailing edge of a positive contrast moving bar (140 µm × 500 µm, 1,000 µm s^{-1}, 200 R* rod^{-1} s^{-1}). **f**,**g**, Same as **d** and **e** for an F-mini-OFF RGC. **h**, Spike counts in F-mini-ON RGCs responding to positive contrast spots of varying diameters. Mean onset responses are in yellow; mean offset responses are in black. The shaded region is the s.e.m. ($n=172$ cells). **i**, Same as **h** for F-mini-OFF RGCs ($n=85$ cells). **j**, Spiking responses of F-mini-ON RGCs to a flashed spot at varying mean luminance, showing the variations in ON and OFF responses to light level ($n=3$ cells; spot diameter: 130 µm). **k**, Spiking responses of F-mini-ON RGCs to onset of flashed spots of varying contrast from the background luminance. Data are the mean ± s.d. (shaded area) across cells ($n=8$).

We found a significant asymmetry in the offset of the F-mini-ON RGCs but not control RGCs (all mean ± standard deviation (s.d.); one-sample two-tailed *t*-test). The vertical component of the offset in F-mini-ON RGCs was always ventralward (OFF ventral to ON; -30 ± 13 µm, $P=9.2\times10^{-5}$; Fig. 2e), with a horizontal component not significantly distributed to one side (-7.5 ± 24 µm, $P=0.37$). Control ON–OFF RGCs lacked a systematic vertical or horizontal displacement (vertical: -4.0 ± 18 µm, $P=0.42$; horizontal: -3.7 ± 23 µm, $P=0.56$). The distribution of offset directions was uniform for control ON–OFF RGCs ($P=0.93$; Rayleigh test) and highly non-uniform for F-mini-ON RGCs ($P<0.001$, Fig. 2e). We also quantified the fractional overlap (intersection area / union area) between the ON and OFF RFs and found it to be lower in F-mini-ON RGCs than in other ON–OFF RGCs ($n=9$ and 14

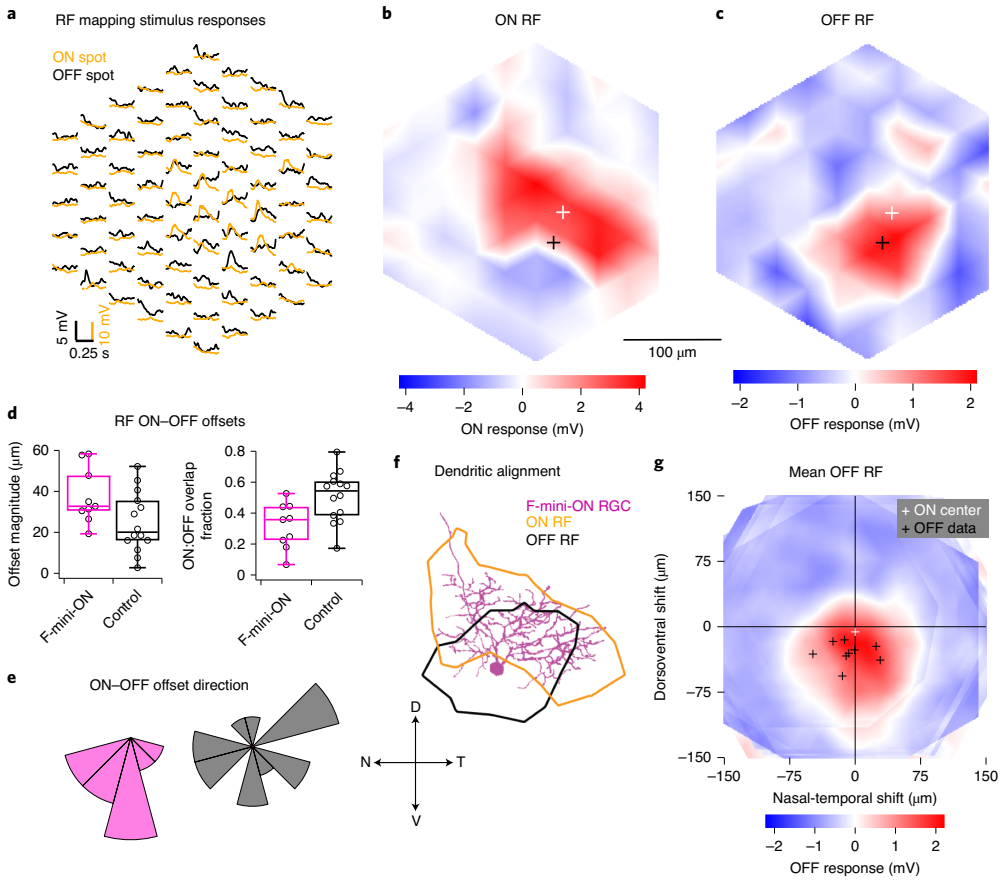

Fig. 2 | RF ON and OFF subfields measured by flashed spots are spatially offset. a, Average responses of an F-mini-ON RGC to 30-µm spots of positive (orange) or negative (black) contrast at the indicated positions. **b**,**c**, Interpolated ON and OFF spatial RFs from the data in **a**. White and black crosses mark the ON and OFF centers of mass, respectively. **d**, Population data showing the fractional overlap of the OFF RF relative to the ON RF for F-mini-ON RGCs (magenta; $n = 9$) and other ON–OFF RGCs (black; $n = 14$; Methods). **e**, Polar histograms showing the offset angle between the ON RF center of mass and the OFF RF center of mass for F-mini-ON RGCs (magenta) and other ON–OFF RGCs (gray). The vertical component of the offset in F-mini-ON RGCs is ventralward (OFF ventral to ON). **f**, Image of the cell from **a**–**c** overlaid with its ON and OFF RF contours. **g**, Average OFF RF for F-mini-ON RGCs aligned to the center of mass of each ON RF at the origin. Crosses are the centers of mass for individual cells ($n = 9$). Scale bar is the same in **a**–**c**, **f** and **g**. Box plots in **d** show the maximum, 75th percentile, median, 25th percentile and minimum values.

cells; $P < 0.01$, two-sample t-test; Fig. 2d,e). A smaller sample of F-mini-OFF RFs also showed diffuse ON and ventrally displaced OFF subfields (Extended Data Fig. 2).

We sought to determine whether the RF offset might be explained by an offset within the dendritic area of an F-mini-ON RGC. RF locations in visual space are derived from bipolar cell and amacrine cell inputs arriving at the dendrites of the RGC. So, a spatial offset in the dendritic area could create a spatial offset in the RF[2,3,16]. We used the Eyewire museum electron microscopy reconstruction RGC dataset[8] and measured the center of mass of the dendrites within ON and OFF bipolar cell layers for all bistratified RGC types. The population of F-mini-ON RGCs showed well-aligned dendritic strata, similar to other bistratified RGCs (Fig. 3 and Extended Data Fig. 3). Thus, F-mini-ON RGCs have RFs with spatially offset ON and OFF subfields, with the OFF subfield consistently ventral of the ON subfield, and this result is not simply explained by displacement of their dendritic strata.

F-mini-ON and F-mini-OFF RGCs are directly coupled through gap junctions. Many RGCs make gap junctions with other RGCs of the same type or with amacrine cells[17], and these electrical synapses can affect RF properties[18,19]. Since dendritic morphology alone could not explain the ON–OFF RF offset in F-mini-ON RGCs, we sought to test whether gap junctions contributed to this unusual RF property. We filled individual F-mini-ON RGCs with the gap-junction permeable tracer Neurobiotin, delivered during whole-cell patch-clamp recordings. In addition to the patched cell, Neurobiotin labeled several surrounding cells in the ganglion cell layer with a distinct morphology. We confirmed that the coupled cells were RGCs by the presence of an axon extending toward the optic nerve, and we confirmed their identity as F-mini-OFF RGCs by their light stimulus responses, their morphology and the presence of both of the transcription factors Forkhead box protein P1 and P2 (FOXP1 and FOXP2; Figs. 1 and 4 and Extended Data Fig. 1).

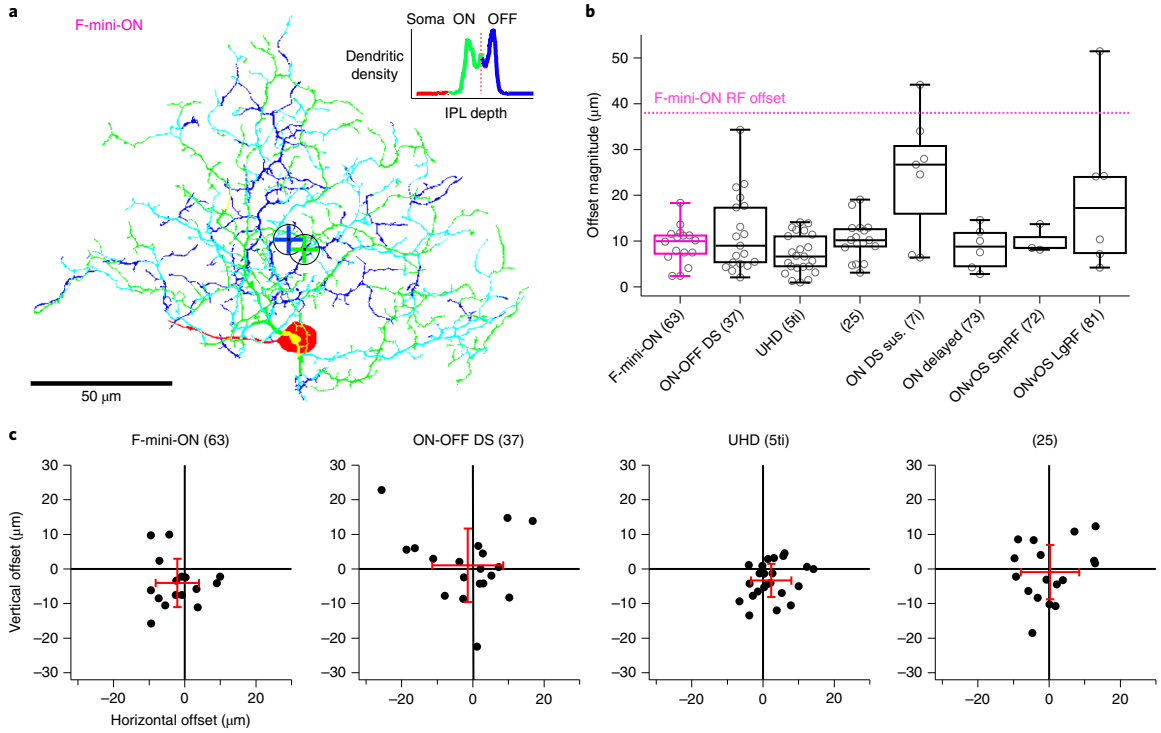

Fig. 3 | Alignment between ON and OFF strata of bistratified RGCs. a, Example projection image of an F-mini-ON RGC from Eyewire[8]. Dendrites are colored by stratification: green, proximal/inner/ON; blue, distal/outer/OFF; cyan, between ON and OFF; red, soma and axon. Centers of mass of inner and outer strata are marked by circled crosses. **b**, Box plots showing dendritic offset distance by cell type. Data are the mean ± s.d. of $n = 16$, 19, 23, 17, 7, 6, 3 and 6 cells. RGC type names are followed by Eyewire anatomical types in parentheses. The magenta line denotes 38 µm, the mean RF offset found in F-mini-ON RGCs. **c**, Offset values in micrometers from four small bistratified RGC types in Eyewire. Red crosses show the mean ± s.d. of offsets. Spatial data from the remaining four bistratified types are available in Extended Data Fig. 3. Box plots in **b** show the maximum, 75th percentile, median, 25th percentile and minimum values. ON-OFF DS, ON-OFF direction-selective; UHD, ultra-high-definition; ON DS sus, ON direction-selective sustained; ONvOS SmRF, ON vertical-orientation-selective small RF; ONvOS SmRF, ON vertical-orientation-selective large RF. All RGC type names are also found at http://rgctypes.org/.

Gap junctions between F-mini RGCs were not only bidirectionally permeable to Neurobiotin (Figs. 1a,b and 4) but also to the larger fluorescent molecule Alexa Fluor 488 (Fig. 5a). This dye allowed us to identify coupled cells in live tissue by two-photon (2P) excitation[20] and record their light responses sequentially or simultaneously (Fig. 5b). F-mini-ON RGCs were coupled to 3.85 ± 1.3 RGCs ($n = 13$ cells) and F-mini-OFF RGCs to 4.0 ± 3 RGCs ($n = 3$ cells; Fig. 5c). In every case where we attempted to classify a cell directly coupled to an F-mini RGC, it was an F-mini RGC of the 'other' type. For F-mini-ON RGC injections, all coupled cells tested by IHC were FOXP1$^+$FOXP2$^+$, the molecular identity of F-mini-OFF RGCs ($n = 19$ cells). All coupled cells measured in live retina had the morphological signature (ventrally directed, compact and OFF-stratifying dendrites) and/or the physiological signature (primarily transient OFF response and strong surround suppression) of F-mini-OFF RGCs[15] ($n = 54$ cells). Similar experiments in F-mini-OFF RGCs revealed F-mini-ON RGCs verified by IHC as FOXP1$^-$FOXP2$^+$ ($n = 14$ cells) or by physiology and morphology ($n = 24$ cells). Regions of dendritic contact between F-mini-ON and F-mini-OFF RGCs did not show immunoreactivity for antibodies against three connexin proteins known to exist in the inner retina, Cx36, Cx45 and Cx30.2 (Extended Data Fig. 4), so the identity of the connexin at these gap junctions remains an open question.

Having found a dense network formed by heterotypic coupling of RGCs, we sought to test for functional connectivity. We performed paired whole-cell current-clamp recordings aided by 2P visualization of Alexa Fluor 488. Both depolarizing and hyperpolarizing current injections were transmitted between the coupled cells, and the resulting voltage transfer was symmetric, the hallmarks of a non-rectifying electrical synapse[21] (Fig. 5d–f; $P > 0.19$ for both hyperpolarizing versus depolarizing currents, and injections into F-mini-ON versus F-mini-OFF RGCs). A coupling coefficient expresses the fraction of the voltage change in one cell that is transmitted to the coupled cell. We measured a coupling coefficient of 0.14 ± 0.08 (range 0.05–0.31, $n = 11$ cell pairs) between F-mini-ON and F-mini-OFF RGCs (Fig. 5f), comparable to the strongest coupling coefficients reported in the inner retina, between amacrine cells[22] (0.25) or between RGCs of the same type[12] (0.14). Pharmacological block of gap junctions with meclofenamic acid (MFA)[23] decreased the coupling coefficient to 0.04 ± 0.03 ($n = 4$ cell pairs; $P = 0.0056$, paired-sample one-tailed t-test; Fig. 5f,g) and also reduced noise correlations ($P = 0.0068$, paired-sample one-tailed t-test; Extended Data Fig. 5). While the reduction in noise correlations in MFA could, in principle, be due to a number of factors, including indirect coupling[18], multiple lines of evidence (dye coupling with no intervening amacrine cells, paired recordings and additional experiments described below) support the claim that

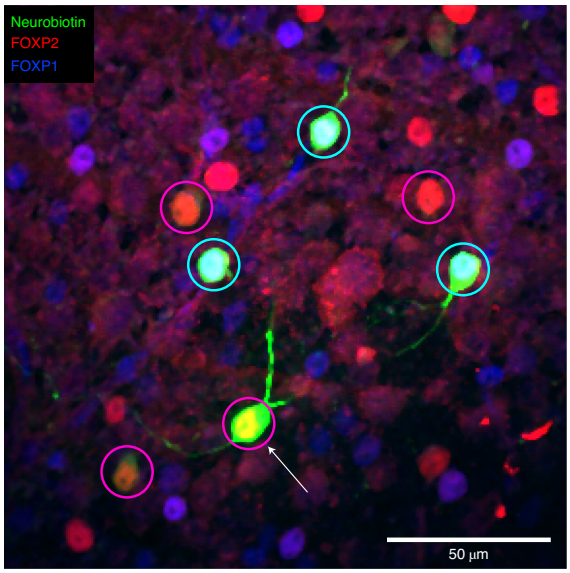

Fig. 4 | Heterotypic gap junctions among F-mini RGCs are confirmed by immunohistochemistry. Image of the ganglion cell layer in a patch of retina in which a single F-mini-ON RGC was filled with Neurobiotin (arrow). RGC somas labeled by the dye are circled: cyan, F-mini-OFF (first-degree connections); magenta, F-mini-ON (filled RGC and second-degree connections). FOXP2 is found in all F-mini RGCs; FOXP1 is found in F-mini-OFF RGCs. Results were consistent over several images ($n=5$ filled networks on four retinas).

heterotypic coupling between F-mini RGCs is direct. Thus, F-mini-ON and F-mini-OFF RGCs are not only dye coupled, but they are also capable of passing substantial amounts of current through their gap junctions, which could potentially mix ON and OFF pathways directly at the level of the RGCs.

OFF responses in F-mini-ON RGCs arise from coupled F-mini-OFF RGCs. To determine how gap junctions with F-mini-OFF RGCs affect the light responses in F-mini-ON RGCs, we sought to measure light responses from the same F-mini-ON RGCs with and without coupling. We used two different manipulations to uncouple F-mini-ON RGCs from their electrical network: pharmacological gap-junction block with MFA and physical ablation of coupled RGCs.

Our first strategy to isolate F-mini-ON RGCs from their coupled network used MFA, which decreases gap-junction coupling (Fig. 6f,g). We recorded from F-mini-ON RGCs in current-clamp mode and stimulated the retina with positive contrast spots and moving bars (Fig. 6a,b). MFA was bath applied, and we observed that the OFF responses were selectively decreased (all mean ± s.d.; $n=6$ cells, paired-sample one-tailed t-tests). We compared the OFF:ON ratio in these RGCs and found that MFA selectively decreased OFF responses. The OFF:ON spiking ratio decreased from 0.22 ± 0.24 to 0.00 ± 0.00 ($P=0.034$; Fig. 6c). The OFF:ON subthreshold peak response ratio decreased from 0.70 ± 0.27 to 0.02 ± 0.15 ($P=0.0011$; Fig. 6d). To evaluate the effect of MFA on the ON pathway, we compared ON responses before and after MFA. The ON spiking decreased from 10.0 ± 1.73 to 5.29 ± 2.23 spikes ($P=0.0074$; Fig. 6c), whereas the ON subthreshold peak responses did not (25.2 ± 3.69 to 24.0 ± 2.52; $P=0.28$; Fig. 6d). The reduction in ON spike count despite an unchanged light-evoked depolarization can be attributed to a hyperpolarizing baseline shift (from -61 ± 2.37 mV in control to -66.2 ± 5.64 mV in MFA; $P=0.011$), likely caused by nonspecific effects of MFA[24,25]. Non-F-mini RGCs showed a moderate reduction of spiking in MFA, consistent with reduced contrast sensitivity[24], but the ON and OFF pathways were affected similarly ($n=3$; $P>0.05$ in all cases; Extended Data Fig. 6).

Our second strategy to isolate F-mini-ON RGCs from their coupled network used physical ablation[26], which had the advantage of increased specificity. Using Alexa Fluor 488 fluorescence under 2P illumination, we were able to visualize the F-mini-OFF RGCs coupled to a targeted F-mini-ON RGC. In the ablation procedure, we recorded responses to positive contrast spots and moving bars in F-mini-ON RGCs (Fig. 6g,h) in current-clamp mode before and after destroying the coupled cells by membrane rupture with sharp microelectrodes (Fig. 6e,f shows partial ablation; in general, all connected cells were ablated). We compared the OFF:ON ratio in these RGCs and found that ablation selectively decreased OFF responses (all data show the mean ± s.d. from $n=6$ cells; paired-sample one-tailed t-tests). The OFF:ON spiking ratio decreased from 0.53 ± 0.20 to 0.00 ± 0.00 ($P=0.00062$; Fig. 6i). The OFF:ON subthreshold peak response ratio decreased from 0.92 ± 0.11 to 0.18 ± 0.12 ($P=0.000013$; Fig. 6j). To evaluate the effect of ablation on the ON pathway, we compared ON responses before and after ablation. The ON spiking decreased slightly from 11.1 ± 2.35 to 8.87 ± 3.15 ($P=0.06$; Fig. 6i). The ON subthreshold peak responses decreased slightly from 26.1 ± 5.53 to 22.5 ± 5.12 ($P=0.043$; Fig. 6j). The reduction in ON responses is significant but small, and might be caused by a decrease in second-order connectivity, that is, input current from F-mini-ON RGCs connected through neighboring F-mini-OFF RGCs.

Results from both approaches demonstrated that F-mini-ON RGCs receive ON input through canonical chemical synaptic pathways and receive OFF input through a noncanonical pathway involving gap junctions with F-mini-OFF RGCs.

The spatial arrangement of coupled F-mini RGCs and their dendritic fields can account for the ON–OFF RF offset in F-mini-ON RGCs. With this knowledge of the different circuits responsible for the ON and OFF components of the RFs of F-mini-ON RGCs, we returned to our observation of the spatial offset between the ON and OFF RF subfields in search of a mechanism. The distinctive asymmetric morphology and connection pattern of F-mini RGCs offered an important clue. In the ventral and central retina, where we performed our measurements, F-mini-ON RGCs have dorsally directed dendrites, and F-mini-OFF RGCs have ventrally directed dendrites, relative to their somas[15]. We also observed in F-mini-ON RGCs that coupled soma positions were located dorsally to the filled soma. Using confocal microscopy images of dye-filled F-mini-ON RGCs, we observed that their dendrites generally lie dorsally to the dendrites of coupled F-mini-OFF RGCs (Fig. 7a). A measurement of this offset could explain the offset RF position. However, the dendritic tips of coupled cells are generally not well filled by intracellular dye, so single-cell fills are not well suited for this measurement, and complete fills by manual dye filling is experimentally prohibitive. So, we sought to model this combined dendritic offset using accessible imaging morphology datasets (Fig. 7).

To construct this model, we created two datasets. For each dye-filled F-mini-ON RGC, we measured the positions of neighboring brightly labeled (first-order) connected somas (Fig. 7d; $n=50$ coupled soma positions from 13 injected F-mini-ON RGCs). Next, for both F-mini-ON and F-mini-OFF RGCs, we measured a polygon around the dendrites within their ON and OFF layer stratifications, respectively (Fig. 7e; $n=38$, 12 cells). With the knowledge that the neighboring somas were F-mini-OFF RGCs, we could combine these datasets. We randomly generated combinations of measured soma offsets, F-mini-ON polygons and F-mini-OFF polygons

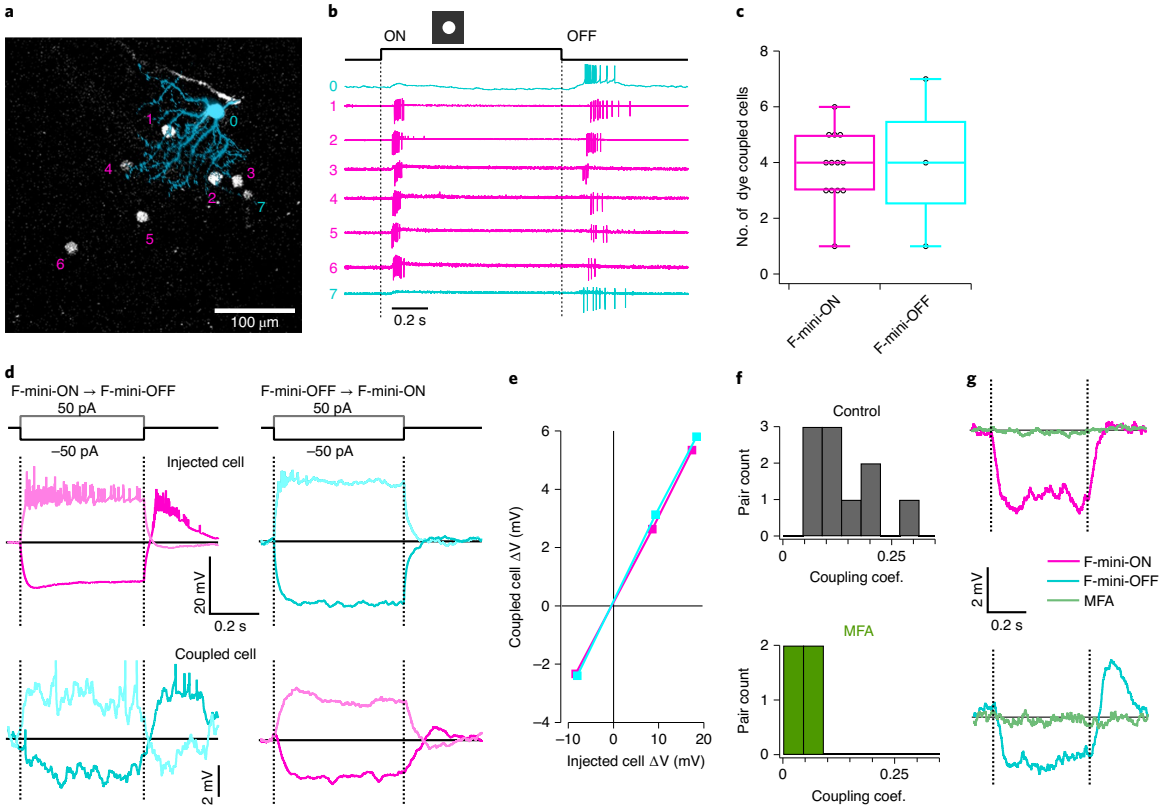

Fig. 5 | F-mini-ON and F-mini-OFF RGCs are electrically coupled to each other by gap junctions. a, An example illustrating heterotypic network connectivity. The F-mini-OFF RGC labeled '0' was filled with Alexa Fluor 488 (cyan), revealing seven coupled somas (white). **b**, Cell-attached recordings from each of the labeled somas shown in **a**. Cells 1–6 show clear signs of being neighboring F-mini-ON RGCs. The soma of cell 7 is dimmer and is likely a second-order connected F-mini-OFF RGC. **c**, Distribution of the number of dye-coupled cells observed in Neurobiotin and Alexa Fluor 488 cell fills of F-mini-ON and F-mini-OFF RGCs; $n = 13$ and 3 cells. **d**, Average voltage traces from an RGC pair in which one F-mini RGC was injected with current (top row) and the coupled F-mini RGC of the opposite type (bottom row) showed a response. Current injections were +50 pA (lighter traces) and −50 pA (darker traces). **e**, Voltage change relationship across the electrical synapse in both directions for the pair in **d**. **f**, Distribution of the coupling coefficient (slope of line in **e**) for all recorded pairs, in control conditions (top) and in the presence of MFA (bottom). **g**, Example of MFA abolishing voltage deflection, showing voltage in F-mini RGCs (for −50 pA injection in coupled cell) in control conditions and in the presence of MFA (green). Image in **a** is a composite of a maximum projection image of the F-mini-OFF dendrites in cyan with a maximum projection image of the ganglion cell layer in white. Cell '0' in **b** was recorded in current-clamp mode. Box plots in **c** show the maximum, 75th percentile, median, 25th percentile and minimum values.

(Fig. 7c). The resulting ON–OFF RF subfield center-of-mass offset was on average 26-µm long ventrally (Fig. 7f), similar to the dorsoventral offset we measured in F-mini-ON RGCs (Fig. 2g; -30 ± 13 µm). This result demonstrates that the spatial structure of the F-mini RGC network is sufficient to account for the ON–OFF RF offset we observed in F-mini-ON RGCs.

The RF structure of F-mini-ON RGCs can account for their weak direction and orientation selectivity. What visual features are represented by an RF structure with offset ON and OFF subregions? We first tried to answer this question at the level of single RGCs using a model that captured both the spatial structure of the ON–OFF RF center of F-mini-ON RGCs and suppression by their RF surround (Extended Data Fig. 7a,b and Methods). The search for a component of visual stimulus space that is encoded by an RGC type has many avenues. Direction selectivity, which is an asymmetry in the response spike count or rate with visual motion direction, has been reported in F-mini-ON RGCs[15]. We also measured mild direction selectivity in F-mini-ON RGCs only for slowly moving stimuli, a behavior the model replicated (Extended Data Fig. 7c,d). Direction preference was broadly distributed with no apparent relationship to retinal position (Extended Data Fig. 7g). We also found mild orientation selectivity in F-mini-ON RGCs with the presentation of drifting gratings (Extended Data Fig. 7e). In a version of our single-cell model that matched the axis of elongation of the F-mini-ON RFs, we were able to predict a similar degree of orientation selectivity to our measurements (Extended Data Fig. 7f). However, neither of these properties provides a satisfying explanation for this unique RF structure, since other specialized RGCs encode movement direction[27] and orientation[28,29] with much greater specificity and robustness over parameters like speed (Extended Data Fig. 7c,e).

A multicell model of F-mini-ON RGCs demonstrates that systematic ON–OFF offset RFs can aid in the encoding of edge position.

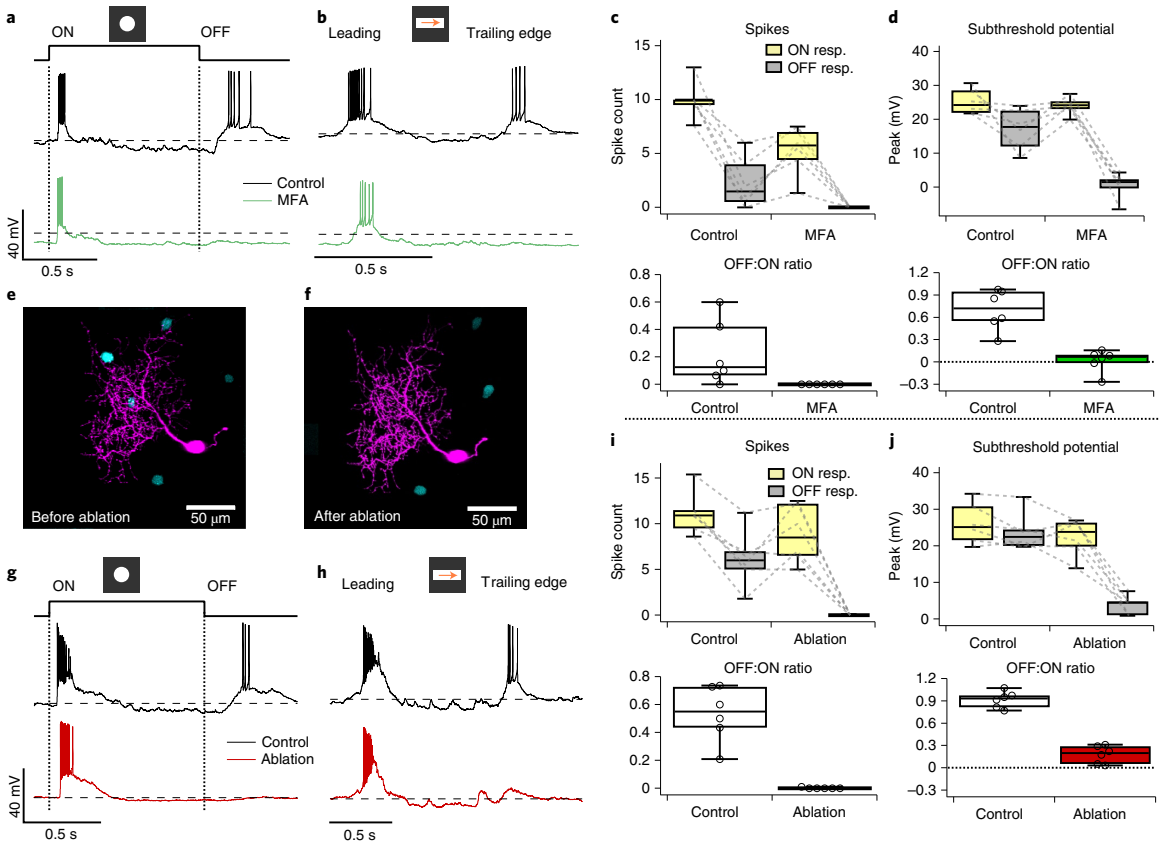

Fig. 6 | F-mini-ON RGCs receive ON input from chemical synapses and OFF input from electrical synapses. a, Response of an F-mini-ON RGC to an ON 120-µm spot before (black) and after (green) MFA application. Dashed line is −60 mV. **b**, Responses of the cell in **a** to a moving positive contrast bar before and after MFA application. **c**, Top: population data for F-mini-ON RGC spike responses to flashed spots as in **a** ($n = 6$ cells). Points connected by dashed lines are individual cells. Bottom: OFF:ON ratio in control and MFA conditions. **d**, Same as **c** for peaks of subthreshold voltage responses ($n = 6$ cells). **e**,**f**, Images of a recorded F-mini-ON RGC (magenta) before and after ablation of three of the coupled somas (cyan). **g**, Responses of an F-mini-ON RGC to an ON 120-µm spot at 2,000 R* rod^{-1} s^{-1} before and after ablation of coupled somas. Dashed line is −60 mV. **h**, Responses of a different cell to a moving ON bar at 700 R* rod^{-1} s^{-1} before and after ablation. **i**, Top: population data for F-mini-ON RGC spike responses to flashed spots as in **c** ($n = 6$ cells). Bottom: OFF:ON ratio in control and ablation conditions. **j**, Same as **i** for subthreshold membrane voltage ($n = 6$ cells). Box plots in **c**, **d**, **i** and **j** show the maximum, 75th percentile, median, 25th percentile and minimum values.

Next, we constructed a multicell model to explore whether offset ON–OFF RFs could provide an encoding benefit in the population that is less apparent at the single-cell level. Specifically, we tested whether a population of RGCs with consistently offset ON–OFF RFs is more precise in representing the position of a dark–light edge than a population of RGCs with either overlapping ON–OFF RFs or randomly offset RFs (Fig. 8). Our model used (1) overlapped ON and OFF RFs, (2) larger RFs resulting from offsetting the same ON and OFF subfields or (3) RFs with the same overall size but with offset ON and OFF subfields, as measured in F-mini-ON RGCs (Fig. 8a). The two offset models used either a consistent ventral offset between ON and OFF subfields or a random distribution of offset directions, consistent with our measurements from F-mini-ON and control ON–OFF RGCs, respectively (Fig. 2d,e). All other aspects of the five models were identical. We presented our five RF models with edge stimuli at various orientations and spatial locations to generate a response lookup table for each.

To generate a population of RGC responses, we simulated many of the above RGCs simultaneously. Cell positions were generated as a noisy hexagonal grid based on the measured density of F-mini-ON RGCs[8] (250 cells in an area of 1 mm^2). Gaussian noise with a magnitude consistent with our spike data from F-mini-ON RGCs was added to each response. In each instantiation of the multicell model, the random seeds that defined position jitter and response noise were varied. To evaluate performance, we created a simple position decoder on the output responses of the model cell population (Methods). We computed the decoded position as the center of mass of the RFs from model RGCs responding over a cutoff threshold (8 ± 1.5 cells, mean ± s.d.) with each RGC weighted by its response strength. Error was measured as the distance between decoded position and the true stimulus center.

RGC models having offset ON–OFF RFs with consistent direction had lower error than those with overlapped or randomly offset RFs in representing the position of an edge stimulus (Fig. 8d–f). Along the vertical axis of separation of the RF subfields, F-mini-ON

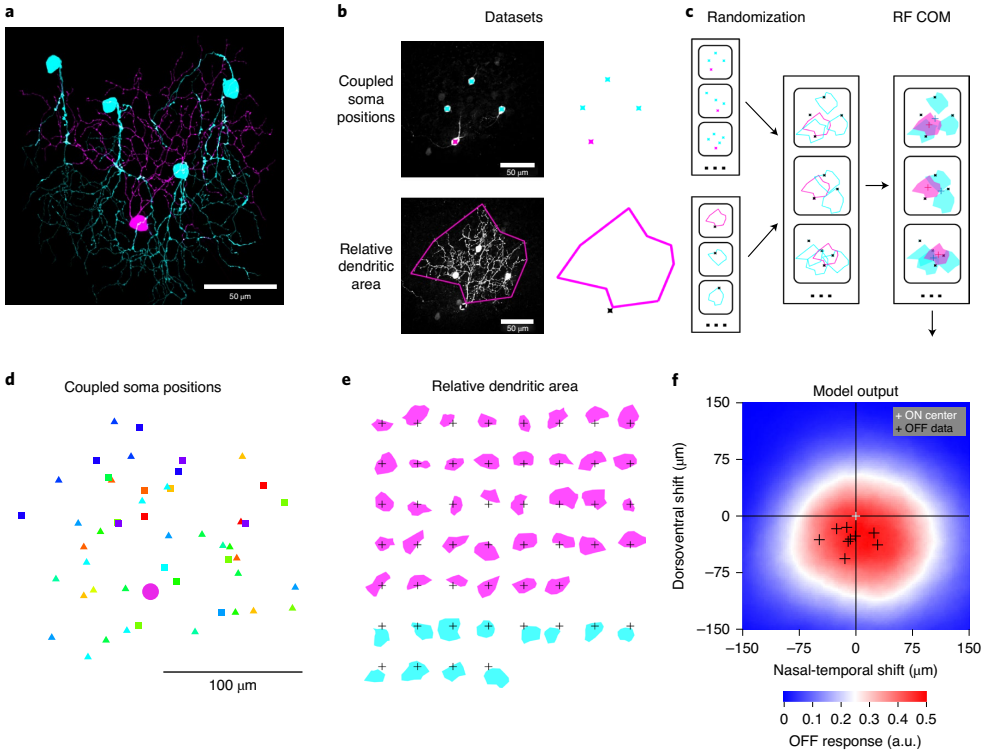

Fig. 7 | F-mini-ON RGCs RF offset is captured by a morphological model. a, Traced microscope image from an experiment in which a single F-mini-ON RGC (magenta) was filled with Neurobiotin. Four coupled F-mini-OFF RGCs are in cyan. A spatial offset is apparent in the dendritic arbors of the two cell types relative to the soma of the F-mini-ON. **b**, Diagram of the imaging datasets used in the morphological model, described in **d** and **e**. **c**, RF model diagram (Methods). Measurements of F-mini-ON coupled soma positions in **d** were randomly combined with convex polygon fits to the dendrites of F-mini-ON and F-mini-OFF RGCs in **e** to create a purely anatomical prediction of the center-of-mass (COM) offset of ON and OFF RFs (red and blue crosses, respectively). **d**, Locations of labeled somas relative to the injected F-mini-ON RGCs (magenta circle) included both confirmed F-mini-OFF RGCs (squares) and RGC somas that were not further characterized (triangles; $n = 50$ somas and 13 injected cells, colored by injected cell). Each point represents the position of a gap-junction-labeled soma relative to the position of the filled F-mini-ON RGC. Results above suggest that all coupled cells were in fact F-mini-OFF RGCs, but only some of them (squares) were confirmed by electrophysiology or IHC. **e**, Area of dendrites relative to soma position for the measured population of F-mini-ON and F-mini-OFF RGCs ($n = 38$; 12 cells). Soma locations are marked by 50-µm crosses. **f**, Result from the model. Colored surface is the mean OFF RF relative to the centered ON RF. True F-mini-ON RF offset data (black crosses) and format are from Fig. 2g. A.u., arbitrary units.

RGC model was 40% better than the overlapped RF model at representing the position of horizontal edges (Fig. 8d), particularly the vertical component perpendicular to the edge (Fig. 8e). This improvement came with no decrease in horizontal position decoding performance (Fig. 8f), but with a trade-off in performance for edges having a contrast offset perpendicular or opposed to the RF offset. The F-mini-ON RGC population model was able to represent the position of an edge with precision down to 0.6 degrees of visual angle (Fig. 8f), less than 12% of the RF diameter (2σ) of a single F-mini-ON RGC. The improvement of the offset models relative to the overlapped RF model was robust across a broad range of cell densities, RF sizes and noise amplitudes (Extended Data Fig. 8).

Discussion

Collectively, our results demonstrate that the F-mini-ON RGC mixes a canonical ON input via chemical synapses with a noncanonical OFF input via gap junctions with F-mini-OFF RGCs to create an RF with spatially offset ON and OFF subfields. The offset is consistent with the asymmetric morphology and connectivity of F-mini RGCs (Fig. 7). Our multicell model shows that the ON–OFF RF offset can improve the precision with which F-mini-ON RGC populations represent the position of an edge (Fig. 8). A causal link between this proposed role in encoding edge location and a specific behavior will require selective genetic access to F-mini RGCs. With advances in molecular profiling of RGCs[9], the tools for such a study are on the horizon.

This report follows on from the work of several groups investigating both of these RGC types in the mouse. Descriptions of their electrophysiological responses to visual stimuli have varied in approach and findings. In the Eyewire dataset, Bae et al. found both ON and OFF calcium responses in F-mini-ON RGCs to a moving bar[8]. The F-mini-OFF is labeled in the PV^{Cre} mouse line (type PV7)[30]. Using that line, Farrow et al. found both ON and OFF responses to small spots in F-mini-OFF RGCs[31]. Working with a $Fox2^{Cre}$ mouse line, Rousso et al. identified only primary polarity responses in F-mini RGCs[15]. Although we found the ON–OFF responses to be robust across a range of light levels and contrasts (Fig. 1j,k), differences in light adaptation state or other recording conditions may have caused this discrepancy.

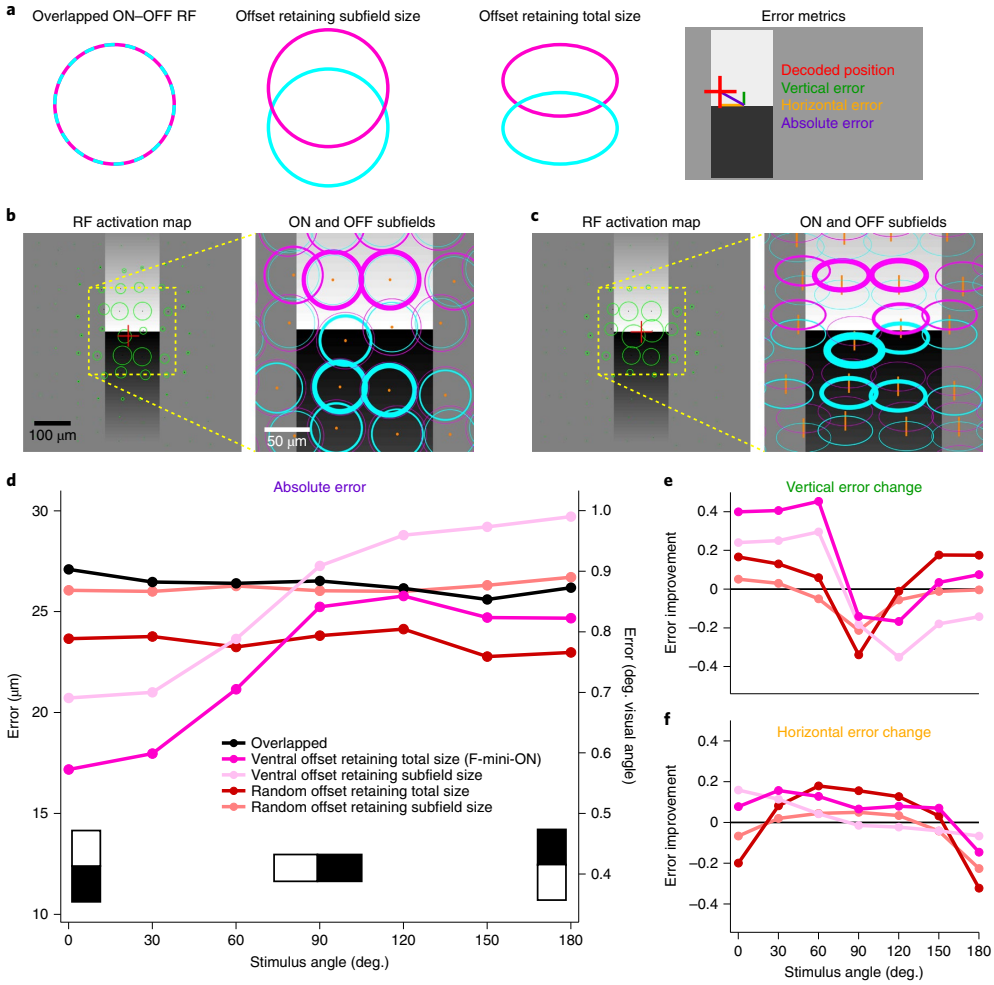

Fig. 8 | Multicell model of object localization shows an advantage of offset ON–OFF RFs. a, Schematics of the different RF structures and error metrics. ON and OFF RFs are in magenta and cyan. **b**, RF activation map (left) for a single instantiation of the overlapped RF model. The stimulus is the black–white edge. Green circles show the positions of each RGC with the radius of the circle proportional to its response. The red cross indicates the center of mass of the RGC responses. Magnified portion (right) shows the ON and OFF subfields of each RF. Line thickness is proportional to activation of each subfield. **c**, RF activation map for the same positions and stimulus as in **b**, but for the offset RF model retaining total size. Orange lines in the magnified view (right) connect ON and OFF subfields from the same RGC. **d**, Absolute error in decoded edge position for each model. Points are the means of 500 iterations of each model with different RGC and stimulus positions. Error bars for the s.e.m. are obscured by symbols; s.d. values were similar for each point with a mean of 0.42 µm. **e**, Vertical component of the error in **d** shown as a change ratio relative to the overlapped RF result. **f**, Same as **e** for the horizontal component.

Heterotypic RGC coupling was also recently identified in the guinea pig using multielectrode array recordings and morphological tracing with Neurobiotin[32]. The coupled RGCs in the guinea pig study were both ON sustained cells—one of them was the ON alpha—so heterotypic coupling in that system does not mix ON and OFF signals. Nonetheless, the discovery of heterotypic RGC coupling in two different circuits in two different species suggests that it might be a conserved motif in the mammalian retina, augmenting our understanding of the organization of information in RGC populations.

Notably, F-mini-ON RGCs are bistratified even though we found no evidence of OFF bipolar cell input. Perhaps the OFF dendritic stratum is used primarily for making gap junctions with F-mini-OFF RGCs or chemical synapses with amacrine cells. This adds to a growing list of RGC types with dendrites in the outer half of the inner plexiform layer with no apparent OFF bipolar cell input: sustained suppressed-by-contrast[26], ON delayed[33], ON orientation selective (both horizontal and vertical)[28], OFF orientation selective (horizontal and vertical)[29] and M1 intrinsically photosensitive RGCs[34]. The size of this list suggests a reevaluation of the dogma that the stratification of an RGC alone is sufficient to predict the polarity of its bipolar cell inputs.

Recent work has shown that mice use vision to capture small, quickly moving prey objects, like crickets[35,36], so perhaps precise edge localization with F-mini-ON RGCs plays a role in this behavior. While our multicell model used flashed stimuli, a

similar mechanism could, in principle, aid in the precise localization of moving objects by the joint firing of coupled F-mini RGCs. It has long been known that direct electrical coupling between RGCs is important for synchronizing spikes on the timescale of several milliseconds[37–39], and tight spike synchrony has been shown to enhance transmission at retino-geniculate synapses[40]. Synchronous firing among RGCs has been proposed as a mechanism for improving the fidelity of the population code for direction selectivity[41] and binding visual objects across space[18]. Precise timing between the spikes of coupled RGCs has recently been proposed as a mechanism for object localization with resolution much higher than predicted by the RF size of a single RGC[42]. Estimating the position of a moving object is, of course, a more complex computation because neural lag can be conflated with object speed. A subset of direction-selective RGCs uses homotypic gap junctions to help normalize this lag[12,19]. Simultaneous recordings from larger populations of F-mini RGCs could test our model for the localization of static edges (Fig. 8) and reveal whether this network could play a role in the localization of moving objects.

Since the RF offset in F-mini-ON RGCs is along the vertical axis, our model showed enhanced object localization preferentially along this axis (Fig. 8). It will be interesting to see whether future behavioral experiments reveal that mice show more precise object localization along the vertical axis than along the horizontal axis of the visual field. Since rodents use compensatory eye movements to maintain the orientation of their eyes relative to the horizon[43], a potential advantage of precise localization along the vertical axis is that it would provide information about changes in distance: approaching objects have increasing space between their dorsal and ventral edges with time, while receding objects have decreasing space. The direction of the ON–OFF asymmetry is also interesting as it relates to rodent visual ethology. Dark-below-light edges in retinal space were represented best by our model F-mini-ON RGC population (Fig. 8d). This corresponds to dark-above-light edges in visual space, consistent with the special behavioral relevance of 'looming' dark objects in the upper visual field[44].

The dynamics of the F-mini RGC network are another target for future studies. The strength of gap junctions in the retina, including those between RGCs, can be altered by neuromodulators[17,20,45]. If the F-mini RGC network is modulated, this could change its function with sensory or behavioral context. Finally, comparisons with other species will provide information about the evolution and function of this particular heterotypic RGC circuit. FOXP2 is also found in a subset of RGCs in the ferret[46] and macaque retinas[15], so it is possible that the F-mini RGC circuit has a homolog in humans.

Online content

Any methods, additional references, Nature Research reporting summaries, source data, extended data, supplementary information, acknowledgements, peer review information; details of author contributions and competing interests; and statements of data and code availability are available at https://doi.org/10.1038/s41593-020-00747-8.

Received: 14 July 2020; Accepted: 23 October 2020;
Published online: 23 November 2020

References

1. Schwartz, G. W. et al. The spatial structure of a nonlinear receptive field. *Nat. Neurosci.* **15**, 1572–1580 (2012).
2. Wassle, H., Peichl, L. & Boycott, B. B. Dendritic territories of cat retinal ganglion cells. *Nature* **292**, 344–345 (1981).
3. Gauthier, J. L. et al. Receptive fields in primate retina are coordinated to sample visual space more uniformly. *PLoS Biol.* **7**, e1000063 (2009).
4. Roska, B. & Werblin, F. Vertical interactions across ten parallel, stacked representations in the mammalian retina. *Nature* **410**, 583–587 (2001).
5. Masland, R. H. The fundamental plan of the retina. *Nat. Neurosci.* **4**, 877–886 (2001).
6. Baden, T. et al. The functional diversity of retinal ganglion cells in the mouse. *Nature* **529**, 345–350 (2016).
7. Sanes, J. R. & Masland, R. H. The types of retinal ganglion cells: current status and implications for neuronal classification. *Annu. Rev. Neurosci.* **38**, 221–246 (2015).
8. Bae, J. A. et al. Digital museum of retinal ganglion cells with dense anatomy and physiology. *Cell* **173**, 1293–1306 (2018).
9. Tran, N. M. et al. Single-cell profiles of retinal ganglion cells differing in resilience to injury reveal neuroprotective genes. *Neuron* **104**, 1039–1055 (2019).
10. Sivyer, B., Venkataramani, S., Taylor, W. R. & Vaney, D. I. A novel type of complex ganglion cell in rabbit retina. *J. Comp. Neurol.* **519**, 3128–3138 (2011).
11. Puller, C., Manookin, M. B., Neitz, J., Rieke, F. & Neitz, M. Broad thorny ganglion cells: a candidate for visual pursuit error signaling in the primate retina. *J. Neurosci.* **35**, 5397–5408 (2015).
12. Trenholm, S., McLaughlin, A. J., Schwab, D. J. & Awatramani, G. B. Dynamic tuning of electrical and chemical synaptic transmission in a network of motion coding retinal neurons. *J. Neurosci.* **33**, 14927–14938 (2013).
13. Field, G. D. et al. Spatial properties and functional organization of small bistratified ganglion cells in primate retina. *J. Neurosci.* **27**, 13261–13272 (2007).
14. Marvin, J. S. et al. An optimized fluorescent probe for visualizing glutamate neurotransmission. *Nat. Methods* **10**, 162–170 (2013).
15. Rousso, D. L. et al. Two pairs of ON and OFF retinal ganglion cells are defined by intersectional patterns of transcription factor expression. *Cell Rep.* **15**, 1930–1944 (2016).
16. Brown, S. P., He, S. & Masland, R. H. Receptive field microstructure and dendritic geometry of retinal ganglion cells. *Neuron* **27**, 371–383 (2000).
17. Bloomfield, S. A. & Völgyi, B. The diverse functional roles and regulation of neuronal gap junctions in the retina. *Nat. Rev. Neurosci.* **10**, 495–506 (2009).
18. Roy, K., Kumar, S. & Bloomfield, S. A. Gap junctional coupling between retinal amacrine and ganglion cells underlies coherent activity integral to global object perception. *Proc. Natl Acad. Sci. USA* **114**, E10484–E10493 (2017).
19. Trenholm, S., Schwab, D. J., Balasubramanian, V. & Awatramani, G. B. Lag normalization in an electrically coupled neural network. *Nat. Neurosci.* **16**, 154–156 (2013).
20. Jacoby, J., Nath, A., Jessen, Z. F. & Schwartz, G. W. A self-regulating gap junction network of amacrine cells controls nitric oxide release in the retina. *Neuron* **100**, 1149–1162 (2018).
21. Phelan, P. et al. Molecular mechanism of rectification at identified electrical synapses in the *Drosophila* giant fiber system. *Curr. Biol.* **18**, 1955–1960 (2008).
22. Elgueta, C., Leroy, F., Vielma, A. H., Schmachtenberg, O. & Palacios, A. G. Electrical coupling between A17 cells enhances reciprocal inhibitory feedback to rod bipolar cells. *Sci. Rep.* **8**, 3123 (2018).
23. Pan, F., Mills, S. L. & Massey, S. C. Screening of gap junction antagonists on dye coupling in the rabbit retina. *Vis. Neurosci.* **24**, 609–618 (2007).
24. Kuo, S. P., Schwartz, G. W. & Rieke, F. Nonlinear spatiotemporal integration by electrical and chemical synapses in the retina. *Neuron* **90**, 320–332 (2016).
25. Peretz, A. et al. Meclofenamic acid and diclofenac, novel templates of KCNQ2/Q3 potassium channel openers, depress cortical neuron activity and exhibit anticonvulsant properties. *Mol. Pharmacol.* **67**, 1053–1066 (2005).
26. Jacoby, J., Zhu, Y., DeVries, S. H. & Schwartz, G. W. An amacrine cell circuit for signaling steady illumination in the retina. *Cell Rep.* **13**, 2663–2670 (2015).
27. Vaney, D. I., Sivyer, B. & Taylor, W. R. Direction selectivity in the retina: symmetry and asymmetry in structure and function. *Nat. Rev. Neurosci.* **13**, 194–208 (2012).
28. Nath, A. & Schwartz, G. W. Cardinal orientation selectivity is represented by two distinct ganglion cell types in mouse retina. *J. Neurosci.* **36**, 3208–3221 (2016).
29. Nath, A. & Schwartz, G. W. Electrical synapses convey orientation selectivity in the mouse retina. *Nat. Commun.* **8**, 2025 (2017).
30. Katz, M. L., Viney, T. J. & Nikolic, K. Receptive field vectors of genetically-identified retinal ganglion cells reveal cell-type-dependent visual functions. *PLoS ONE* **11**, e0147738 (2016).
31. Farrow, K. et al. Ambient illumination toggles a neuronal circuit switch in the retina and visual perception at cone threshold. *Neuron* **78**, 325–338 (2013).
32. Puller, C. et al. Electrical coupling of heterotypic ganglion cells in the mammalian retina. *J. Neurosci.* **40**, 1302–1310 (2020).
33. Mani, A. & Schwartz, G. W. Circuit mechanisms of a retinal ganglion cell with stimulus-dependent response latency and activation beyond its dendrites. *Curr. Biol.* **27**, 471–482 (2017).
34. Lauritzen, J. S. et al. ON cone bipolar cell axonal synapses in the OFF inner plexiform layer of the rabbit retina. *J. Comp. Neurol.* **521**, 977–1000 (2013).
35. Hoy, J. L., Yavorska, I., Wehr, M. & Niell, C. M. Vision drives accurate approach behavior during prey capture in laboratory mice. *Curr. Biol.* **26**, 3046–3052 (2016).
36. Hoy, J. L., Bishop, H. I. & Niell, C. M. Defined cell types in superior colliculus make distinct contributions to prey capture behavior in the mouse. *Curr. Biol.* **29**, 4130–4138.e5 (2019).

37. Shlens, J., Rieke, F. & Chichilnisky, E. J. Synchronized firing in the retina. *Curr. Opin. Neurobiol.* **18**, 396–402 (2008).
38. DeVries, S. H. Correlated firing in rabbit retinal ganglion cells. *J. Neurophysiol.* **81**, 908–920 (1999).
39. Mastronarde, D. N. Correlated firing of retinal ganglion cells. *Trends Neurosci.* **12**, 75–80 (1989).
40. Rathbun, D. L., Warland, D. K. & Usrey, W. M. Spike timing and information transmission at retinogeniculate synapses. *J. Neurosci.* **30**, 13558–13566 (2010).
41. Zylberberg, J., Cafaro, J., Turner, M. H., Shea-Brown, E. & Rieke, F. Direction-selective circuits shape noise to ensure a precise population code. *Neuron* **89**, 369–383 (2016).
42. Tong, R. & Trenholm, S. High-resolution visual information via a gap junction-mediated spike order code. Preprint at *bioRxiv* https://doi.org/10.1101/2020.08.14.250910 (2020).
43. Wallace, D. J. et al. Rats maintain an overhead binocular field at the expense of constant fusion. *Nature* **498**, 65–69 (2013).
44. Yilmaz, M. & Meister, M. Rapid innate defensive responses of mice to looming visual stimuli. *Curr. Biol.* **23**, 2011–2015 (2013).
45. Mills, S. L. & Massey, S. C. Differential properties of two gap junctional pathways made by AII amacrine cells. *Nature* **377**, 734–737 (1995).
46. Sato, C., Iwai-Takekoshi, L., Ichikawa, Y. & Kawasaki, H. Cell-type-specific expression of FoxP2 in the ferret and mouse retina. *Neurosci. Res.* **117**, 1–13 (2017).

Methods

Animals and electrophysiology. The retinas of wild-type mice (C57BL/6J, The Jackson Laboratory) were used for all experiments. The mice were dark adapted overnight and killed by cervical dislocation in accordance with all animal care standards provided by Northwestern University's Institutional Animal Care and Use Committee. Lighting in animal facilities was kept on a 14/10-h cycle, with lights on at 06:00. Typical retina in vitro times were 12:00 through 19:00. For all experiments, mice of either sex (approximately 69% male) and of ages postnatal day (P) 30–90 were used; no differences in results were observed with sex or age. Eyes were dissected in oxygenated Ames' medium at 32 °C. Dissections were performed in complete darkness using infrared (900 nm) illumination and photo converters. In the experimental rig, retinas were mounted in a shallow dish, below a microscope objective and above a digital projector, in oxygenated Ames' medium from Sigma-Aldrich (A1420) at 32 °C at a flow rate of 10 ml min^{-1}. Two glass electrodes on head-stage amplifiers were mounted on micromanipulators on either side. Cell-attached and current-clamp experiments were performed as previously described[26].

Microscopy. Two microscopes were used to visualize cell morphology. The in vitro microscope, a Scientifica SliceScope Pro 6000, used 980-nm illumination from a SpectraPhysics MaiTai Laser steered by a Galvo scanner for 2P excitation and infrared visualization. The software used was SciScan version 1.3 by Scientifica in LabVIEW by National Instruments. Dyes for 2P visualization were Alexa Fluor 488 and 568 hydrazides from Invitrogen (A10436 and A10437), the latter of which was found to be not gap-junction permeable and was used for single-cell image isolation. Microscopy was continued on fixed retinas, which were stained with antibodies and fluorescent dyes for IHC. The fixed-tissue microscope was a Nikon A1R confocal microscope with a 1.0 NA ×40 oil immersion objective at the Northwestern Center for Advanced Microscopy. In Figs. 1 a–c and 7a, neurons were traced using Simple Neurite Tracer[47] in ImageJ/Fiji. Stratification analysis in Fig. 1c used choline acetyltransferase layers to computationally flatten traced neural morphology. In Fig. 4, individual image channels from confocal microscopy were contrast adjusted and de-speckled with a 3×3 median filter to improve clarity, then projected at maximum intensity through 7 µm of depth.

Light stimulation. Spatiotemporal light patterns were focused on the photoreceptors of the in vitro retina. The light patterns were generated by a computerized digital display, DLP Lightcrafter 4500 from Texas Instruments, illuminated by a blue LED at 457 nm (peak wavelength after optics), integrated by EKB Technologies. This input supported a resolution of 1,140×912 pixels, operating at 60 Hz, with frames modulated to an 8-bit intensity depth. Overall light intensity was modulated using neutral density filters (Thorlabs) and calibrated regularly. Measured intensity values were converted to R* rod^{-1} s^{-1}. Light stimuli were generated by MATLAB software packages: Schwartz Lab protocols (https://github.com/Schwartz-AlaLaurila-Labs/sa-labs-extension) interfacing with the Symphony 2 Data Acquisition System (https://symphony-das.github.io) drawing via Stage (http://stage-vss.github.io) and OpenGL to the screen. The condenser of the microscope allowed the projected image to focus on the photoreceptor outer segments at a scale of 1.38 µm per pixel. Stimuli included circles (30–1,200 µm in diameter) flashed with positive or negative contrast for 1.0 s, moving bars (140–1,200 µm width × 600–1,200 µm length, at 250–2,000 µm s^{-1}), and small spots for RF mapping (see below). The stimulus for the light stimulation cross-correlation analysis was a randomly moving light spot of 80 µm diameter for 30 s in duration. The random motion path was a zero-centered two-dimensional (2D) Gaussian noise signal, low-pass filtered at a 3-Hz cutoff frequency. Light stimuli were presented from darkness (<2 R* rod^{-1} s^{-1}) to a level of 200 R* rod^{-1} s^{-1} unless otherwise noted, to preserve the sensitivity of the retina.

Receptive field mapping. Current-clamp recordings allowed us to measure subthreshold voltage responses with small spots to obtain high-resolution RF maps. Visual stimulus spots were circles of positive and negative 100% contrast on a background of 1,000 R* rod^{-1} s^{-1}, with a diameter of 40 µm. A triangular grid of 30-µm spacing was used for F-mini RGCs. Larger spacing and spot sizes of up to 80 µm were used for RGCs with larger RFs and lower sensitivity to small spots. Voltage responses to individual spots were separated, and peak values were averaged to generate a value for each position. These values were displayed on the grid locations to create a 2D RF strength map. The center of mass of the map area above the 80–85th percentile of response strength was used to generate offset vectors for comparison to the model. The RF overlap index (Fig. 1k) uses the proportion of overlap relative to the total of the RF area within the 80th percentile of response strength. Control ON–OFF RGCs were of types UHD, HD2 and ON–OFF DS, which exhibit similar ON–OFF transient responses to small spots.

Cell identification. Somas in the ganglion cell layer were surveyed in cell-attached mode using a set of basic light stimuli: flashing contrast steps in 160-µm spots, spots of varying sizes and moving bars. F-mini RGCs could be identified by their characteristic responses to these stimuli. Once an F-mini RGC was identified, it was dye filled and recorded to verify type and collect data. Pairs were generally identified sequentially as follows: (1) identify F-mini-ON/OFF RGC by its light response, (2) fill with Alexa Fluor 488, confirming typology by morphology, (3) use dye to find coupled F-mini-OFF/ON RGCs and (4) patch and record original and dye-filled cells. Sequential filling of coupled F-mini RGCs with Alexa Fluor 488 allowed for identification of large networks of >10 cells. Neurobiotin in a single F-mini RGC labels second-order connected cells more dimly than first-order ones, in fixed tissue, allowing for similarly large network identification.

Pharmacology. MFA (Sigma-Aldrich, M4531) was bath applied at 100 µM to block gap junctions[23] (Figs. 2 and 3 and Extended Data Figs. 5 and 6). Electrophysiology results in MFA conditions were 5–45 min during application. MFA washed out incompletely, so no data after application was reported.

Ablation. Neighbor ablation is a physical technique for neuronal inactivation where a micropipette is used to rupture the cellular and nuclear membranes of the dye-illuminated somas[26]. This causes the membrane of the entire cell to dissociate, and stops it from having a membrane potential or transmitting and receiving signals within the dendrites. Neuron death was confirmed by lack of Alexa Fluor 488 in 2P imaging. Some responses continued for one stimulus epoch before being silenced. Where incomplete network ablation occurred, changes to response properties were partial. These data were not used further.

Immunohistochemistry. Target neurons were filled with Neurobiotin (Vector Laboratories, SP-1150) at 3% wt/vol and 280 mOsm in our standard potassium aspartate internal solution[26]. For whole-mount IHC, retinas were fixed after the in vitro period in 4% paraformaldehyde for 15 min, then rinsed in phosphate buffer. Primary antibodies for cell typology were FOXP1 to guinea pig (1:10,000) from B. Novich[48] and FOXP2 to rabbit (1:200) from Millipore (ABE73)[49]. Primary antibodies and their dilutions for connexin typology were Cx30.2 to rabbit (1:50) from Invitrogen (40–7400)[50], Cx36 to rabbit (1:250) from Invitrogen (51–6200)[51] and Cx45 to mouse (1:200) from Invitrogen (41–5800)[52]. Retinas were soaked with primary antibodies in normal donkey serum + Triton X-100 from Sigma-Aldrich (T8787) for 3 d at 4 °C. Secondary antibodies/fluorophores were (for typology) donkey anti-rabbit Alexa Fluor 568 (1:500) from Life Technologies (A10042), goat anti-guinea pig Alexa Fluor 647 (1:400) from Abcam (ab150187); and (for connexins) donkey anti-rabbit Alexa Fluor 568 (1:500) from Abcam (ab175470), donkey anti-rabbit Alexa Fluor 647 (1:500) from Jackson ImmunoResearch (711-605-152), donkey anti-mouse Cyanine Cy3 (1:500) from Jackson ImmunoResearch (715-165-150); and (for both) Streptavidin DyLight Conjugate 488 (1:500) from Thermo Science (21832). Retinas were soaked in secondary antibodies in normal donkey serum + Triton X-100 for 1 d at 4 °C. Retinas were mounted on glass slides in Fluoromount Aqueous mounting medium from Sigma-Aldrich (F4680) and stored at −20 °C.

Stratification offset analysis. Offsets are measured as a vector from proximal/inner center of mass to distal/outer center of mass, which, in most RGCs, is ON to OFF dendrites. The mean and s.d. are shown by red crosses. All figure data is from the Eyewire dataset[8], exported via the Eyewire museum mesh tool. Meshes were flattened and offset by eye.

Morphological receptive field model. Two types of datasets were used. RFs relative to soma location of F-mini-ON and F-mini-OFF RGCs were estimated using the area between the tips of the dendritic fields ($n = 38$ F-mini-ON cells; $n = 12$ F-mini-OFF cells). These were outlined manually using 2P or confocal image stacks. Locations of F-mini RGCs in coupled networks were traced from images of dye-filled somas to create maps of soma locations ($n = 11$ networks). Random combinations of network soma locations, F-mini-ON dendrite offsets and F-mini-OFF dendrite offsets were generated 5,000 times and averaged to generate a mean OFF RF relative to ON RF (Fig. 7f). The model ignores any possible interdependence of F-mini-ON and F-mini-OFF RGC dendritic fields (meta-mosaics) and assumes that F-mini-OFF RGCs receive OFF input via bipolar cells at their dendritic tips.

Single-cell RF model. A computational model (Extended Data Fig. 7a) was used to generate single-cell responses to an edge, moving bar and drifting grating stimulus. The model simulated four pathways of input to a single RGC: ON and OFF, excitation and inhibition for each. Excitation was modeled as a small 2D Gaussian function of direct excitation with a larger 2D gaussian function subtracted to model presynaptic inhibition. Direct inhibition was modeled as a larger 2D gaussian function. The visual stimulus was multiplied by the spatial RFs, then those signals were integrated across space and temporally filtered by convolution. Temporal filter kernels were parameterized curves with values extracted from typical F-mini-ON voltage-clamp light-step responses, over a 3.0 s simulation time. A semi-rectifying nonlinearity was applied to each ON and OFF subfield, then the responses were summed. The OFF delay relative to the ON delay was estimated from spike latencies. RF sizes and surround strength were adjusted manually to match F-mini-ON responses to spots of multiple sizes. This model is meant to explore RF map concepts analytically over many variables and is not meant to precisely emulate recorded RGCs.

Multicell decoding model. The multicell model composed responses from many single-cell RF instances and decoded them using their center of mass. Gaussian noise was added to each of the modeled cellular responses. The decoded location of the stimulus was compared to the true location to generate an error value. Trials of randomly placed cells and stimulus were used, with 500 trials for each parameter configuration. Cellular RF centers were laid out on an equilateral triangular grid with a Gaussian jitter of $\sigma = 10\,\mu m$. RF strengths were integral normalized across shape parameters. Comparisons across parameters used a density of 250 RGCs per mm^2, a noise of 2 (arbitrary units, but similar to spiking output) and a stimulus angle of 0 (horizontal, ON upper). RGC responses fell to baseline outside of the model region, which had an area of $0.36\,mm^2$ with a 600-µm side length. The stimulus was placed, uniformly at random, within the central $300 \times 300\,\mu m$ square region. The edge stimulus was a 150-µm long edge of positive and negative 100% contrast, falling off in a linear gradient above and below the edge for 150 µm. Rousso et al[15] found a range of densities of between 100 and 350 RGCs per mm^2 for F-mini-ON RGCs. Eyewire museum's patch of retina, the E2198 dataset[8], has a density for F-mini-ON RGCs (anatomical type 63) of approximately 240 RGCs per mm^2. Decoder input cell activity threshold was 0.3 times the highest response, resulting in 8.5 ± 1.5 s.d. RGCs at the default parameters.

Analysis and statistics. Analysis was performed with a custom MATLAB software package. Figures were generated in Igor 8.0 from WaveMetrics. All data are reported as the mean ± s.d. unless otherwise noted. No statistical methods were used to predetermine sample sizes, but our sample sizes are similar to those reported in previous publications[1,15,19,20]. In general, data distribution was assumed to be normal but this was not formally tested; data points are shown on the figures. Data collection was not randomized due to the nature of the experiments. Data collection and analysis were not performed blind to the conditions of the experiments. Cells were excluded from analysis if confidence in typology was insufficient. All data points shown are individual RGCs or cell pairs presented as the mean of three or more repeated stimulus presentations. Box plots in figures show the maximum, 75th percentile, median, 25th percentile and minimum values. Comparisons for statistical significance were performed with a paired or unpaired Student's *t*-test, as appropriate, unless otherwise noted. Direction and orientation selectivity indices were calculated as the normalized magnitude of the vector sum of the responses across directions or orientations. For measurements of connexin overlap, RGCs were traced using Simple Neurite Tracer in Fiji software. RF ellipticity was measured using the 80th percentile response contour, finding the longest line contained within that (a), then the longest such line perpendicular to that line (b). The ellipticity is then lengths $(a - b)/a$. Subthreshold membrane potential measurements (RF maps and Fig. 6d,j) were normalized to a pre-stimulus baseline mean value and used a spike-removal low-pass filter of a 100-Hz cutoff frequency.

Reporting Summary. Further information on research design is available in the Nature Research Reporting Summary linked to this article.

Data availability

Data for ganglion cell typology in the mouse is available at http://RGCTypes.org/. A subset of the datasets that support the findings of this study are available at https://github.com/SchwartzNU/ProjectData_Fmini. The remainder of the datasets are available from the corresponding author upon reasonable request.

Code availability

Software code for the analyses supporting the findings of this work is available at https://github.com/SchwartzNU/ProjectData_Fmini. Visual and electrical stimulus code is available at https://github.com/Schwartz-AlaLaurila-Labs/sa-labs-extension and https://symphony-das.github.io.

References

47. Longair, M. H., Baker, D. A. & Armstrong, J. D. Simple neurite tracer: open-source software for reconstruction, visualization and analysis of neuronal processes. *Bioinformatics* **27**, 2453–2454 (2011).
48. Rousso, D. L., Gaber, Z. B., Wellik, D., Morrisey, E. E. & Novitch, B. G. Coordinated actions of the forkhead protein Foxp1 and Hox proteins in the columnar organization of spinal motor neurons. *Neuron* **59**, 226–240 (2008).
49. Lu, M. M., Li, S., Yang, H. & Morrisey, E. E. Foxp4: a novel member of the *Foxp* subfamily of winged-helix genes co-expressed with Foxp1 and Foxp2 in pulmonary and gut tissues. *Mech. Dev.* **119**, S197–S202 (2002).
50. Bhattacharyya, S. et al. Using Gjd3-CreEGFP mice to examine atrioventricular node morphology and composition. *Sci. Rep.* **9**, 2106 (2019).
51. Han, Y. & Massey, S. C. Electrical synapses in retinal ON cone bipolar cells: subtype-specific expression of connexins. *Proc. Natl Acad. Sci. USA* **102**, 13313–13318 (2005).
52. de Andrade, G. B., Kunzelman, L., Merrill, M. M. & Fuerst, P. G. Developmentally dynamic colocalization patterns of DSCAM with adhesion and synaptic proteins in the mouse retina. *Mol. Vis.* **20**, 1422–1433 (2014).

Acknowledgements

We thank the entire Schwartz Laboratory group for discussions, advice and support. We thank B. Novich for generously providing the FOXP1 antibody. Imaging work was performed at the Northwestern University Center for Advanced Microscopy, generously supported by a National Cancer Institute cancer center support grant (P30 CA060553) awarded to the Robert H. Lurie Comprehensive Cancer Center. Multiphoton microscopy was performed on a Nikon A1R multiphoton microscope, acquired through the support of the National Institutes of Health (NIH; 1S10OD010398-01). This work was supported by grants from the NIH National Eye Institute (F31 EY029593 and T32 EY025202) and an NIH Director's New Innovator (DP2) award (EY026770).

Author contributions

S.C. and G.W.S performed the experiments. S.C. analyzed data and constructed models. S.C. and G.W.S. designed research and wrote the paper.

Competing interests

The authors declare no competing interests.

Additional information

Extended data is available for this paper at https://doi.org/10.1038/s41593-020-00747-8.

Supplementary information is available for this paper at https://doi.org/10.1038/s41593-020-00747-8.

Correspondence and requests for materials should be addressed to G.W.S.

Peer review information *Nature Neuroscience* thanks Bart Borghuis, Stuart Trenholm, and the other, anonymous, reviewer(s) for their contribution to the peer review of this work.

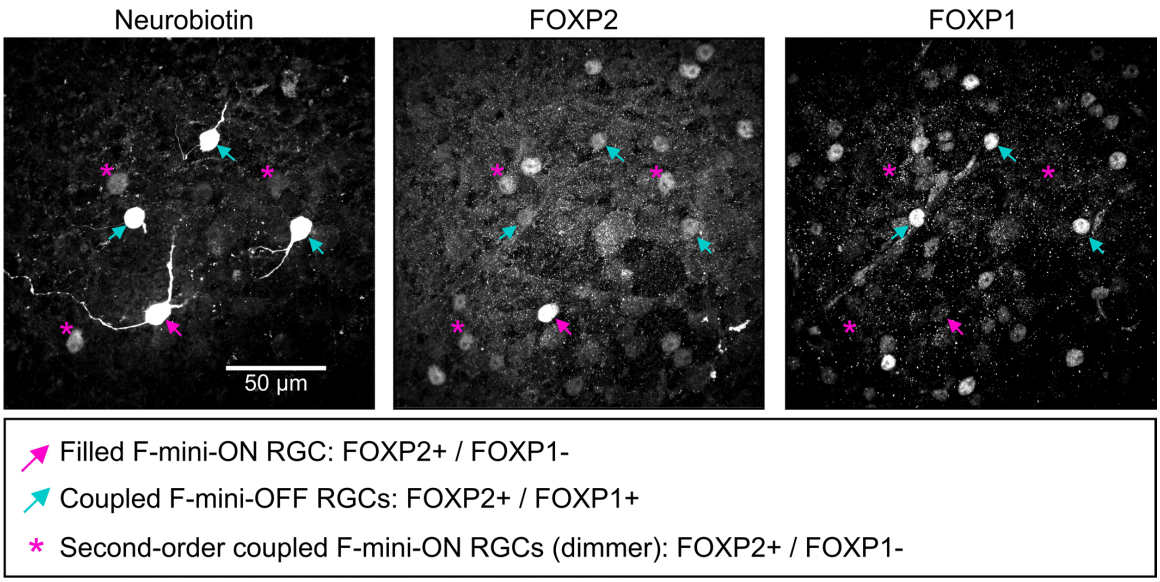

Extended Data Fig. 1 | Coupled cells are immunoreactive for F-mini RGC markers. Images of the ganglion cell layer in a patch of retina in which a single F-mini-ON RGC was filled with Neurobiotin (magenta arrowhead). Left panel shows the Neurobiotin channel, with three brightly labelled coupled cells (white arrowheads) and three dimly labelled cells that likely represent second-order connections (magenta asterisks). Middle panel shows the same region with immunoreactivity for FOXP1, which labels F-mini-OFF RGCs, but does not label F-mini-ON RGCs[15]. Right panel shows immunoreactivity for FOXP2, which labels both F-mini RGC types. This experiment was performed on five F-mini RGC networks in four retinas: four F-mini-ON RGCs and one F-mini-OFF RGC injected. Three networks were stained for FOXP2 and FOXP1; two networks for FoOXP2 only. Neurobiotin labeled 9.0 ± 6.4 somas per retina, and was found in varying amounts in neurons; indicating first and second order connectivity. FOXP2 was present in 43 of 45 RGCs that were labeled with Neurobiotin. Coupled cells from these networks that could be morphologically identified by using the visible primary dendrites, and all showed the expected patterns of FoxP1 expression. 8/8 F-mini-ON RGCs were FOXP1 negative and 14/14 F-mini-OFF RGCs were FOXP1 positive.

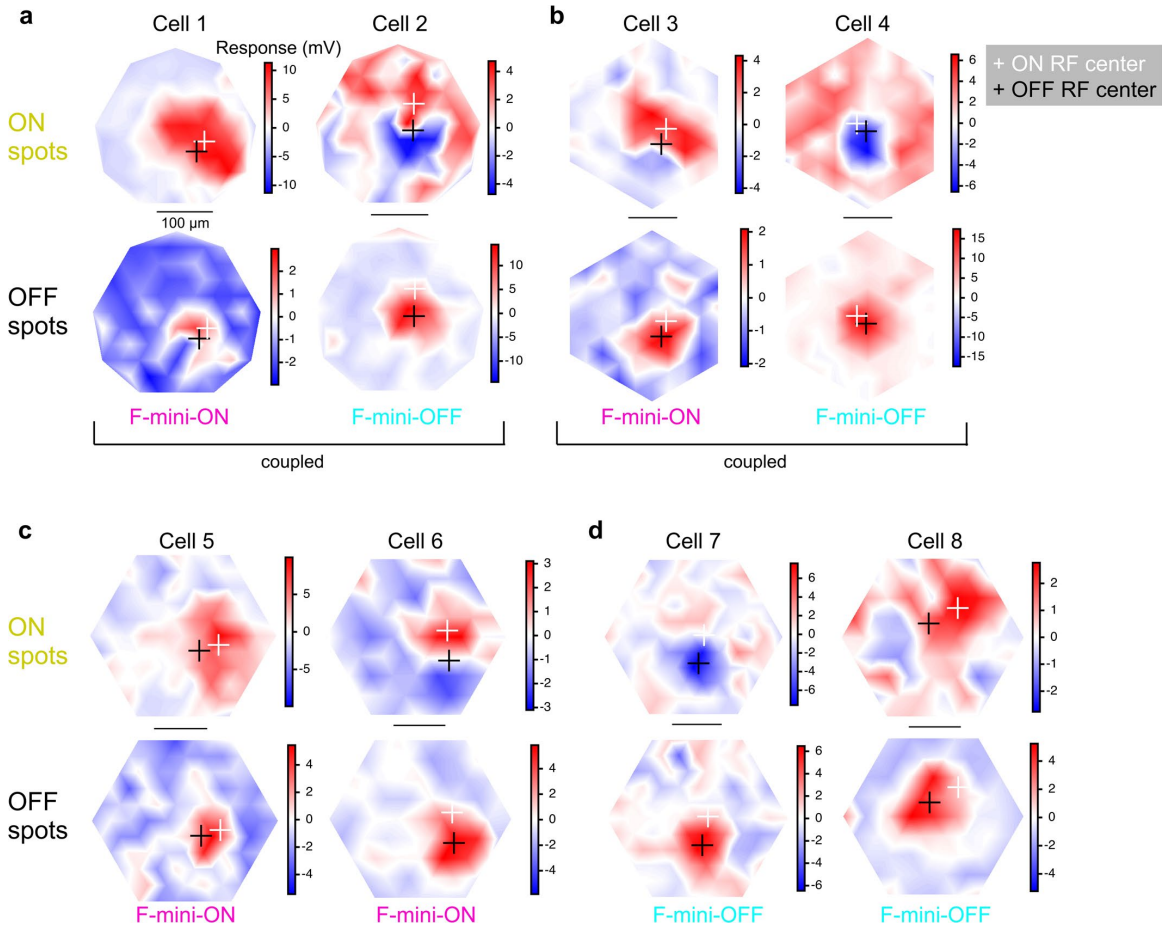

Extended Data Fig. 2 | Example RF maps from F-mini-ON and F-mini-OFF RGCs. Receptive field maps of peak response to 40 µm flashed spots over the RF area, averaged over 2 or 3 repeats. **a**, A GJ coupled F-mini-ON and F-mini-OFF recorded simultaneously. **b**, Another such RGC pair. **c**, Two unconnected F-mini-ON RGCs. **d**, Two unconnected F-mini-OFF RGCs. On all plots, the cross markers are at the center of mass of responses over the 80th percentile (ON, white; OFF, black). Color scale is in mV change from baseline. All scale bars are 100 µm.

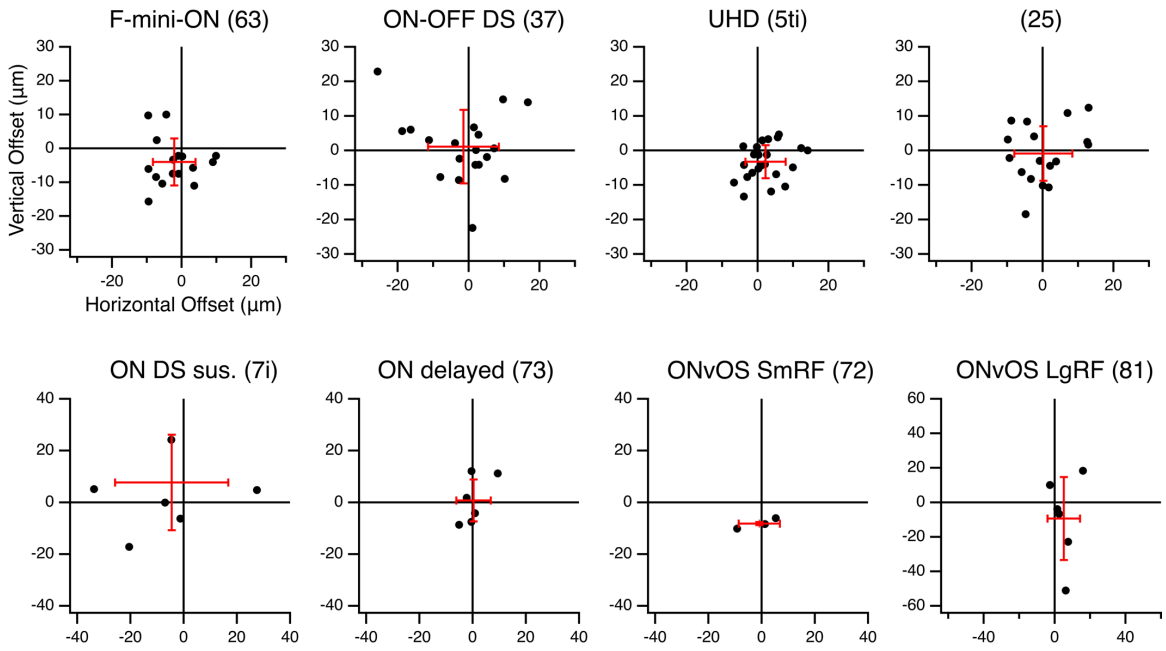

Extended Data Fig. 3 | Alignment between ON and OFF strata of bistratified RGCs. Offset values in µm from each bistratified RGC in Eyewire by type, followed by Eyewire anatomical type name in parentheses. Offsets are measured as a vector from proximal/inner COM to distal/outer COM, which in most RGCs is ON to OFF dendrites. Mean and SD of offsets are shown by red crosses. All figure data is from the Eyewire dataset[8], exported via the Eyewire Museum mesh tool. Meshes were flattened and offset computationally with parameters fit by eye to maximize flatness.

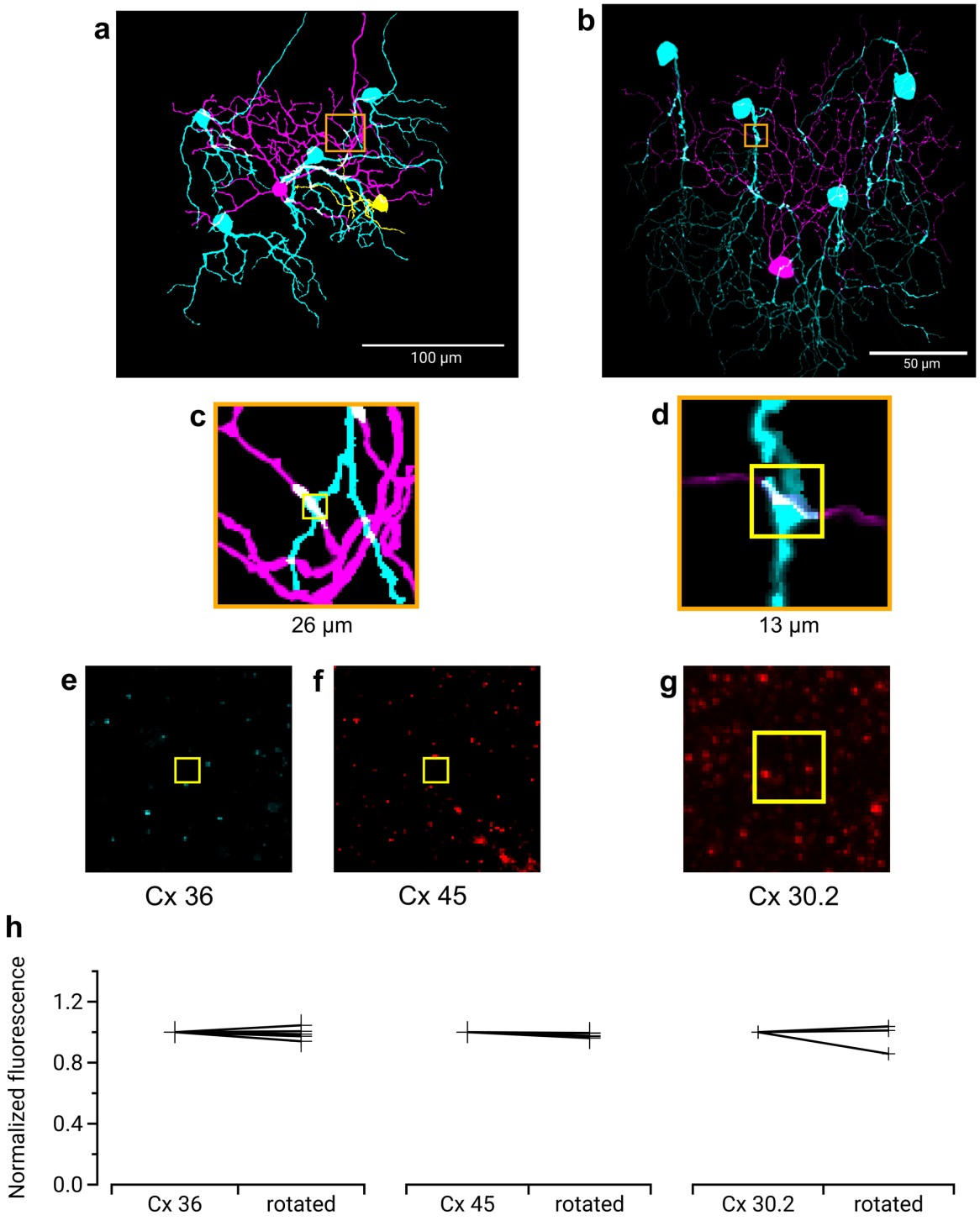

Extended Data Fig. 4 | See next page for caption.

Extended Data Fig. 4 | Immunohistochemistry for three types of Connexin at RGC contact points shows negative results. Three connexins were evaluated for presence at the regions of contact between an F-mini-ON and multiple F-mini-OFF RGCs, $n=1$ of each experiment. **a**,**b**, Full depth maximum intensity projection images of a Neurobiotin-filled F-mini-ON RGC (magenta),the connected F-mini-OFF RGCs (cyan), and a cell of unclassified type due to insufficiently filled dendrites (yellow). Tracing, segmentation, and masking were performed manually. Image brightness was scaled separately by cell type for illustration here but not for analysis. **c,d** Thin projection images of regions in orange squares in **a**,**b** showing an example RGC crossing point with yellow square for spatial reference. Stack depth is 3.5 µm. **e-g**, The same region and depth as in **c**,**d**, showing the IHC channels for the three connexin proteins. **h**, Quantification of overlap between connexin images and RGC contact region masks. Values are similar before and after a 90 degree rotation of the connexin image. Points mark the overlap of the single F-mini-ON RGC with each F-mini-OFF RGC in the image.

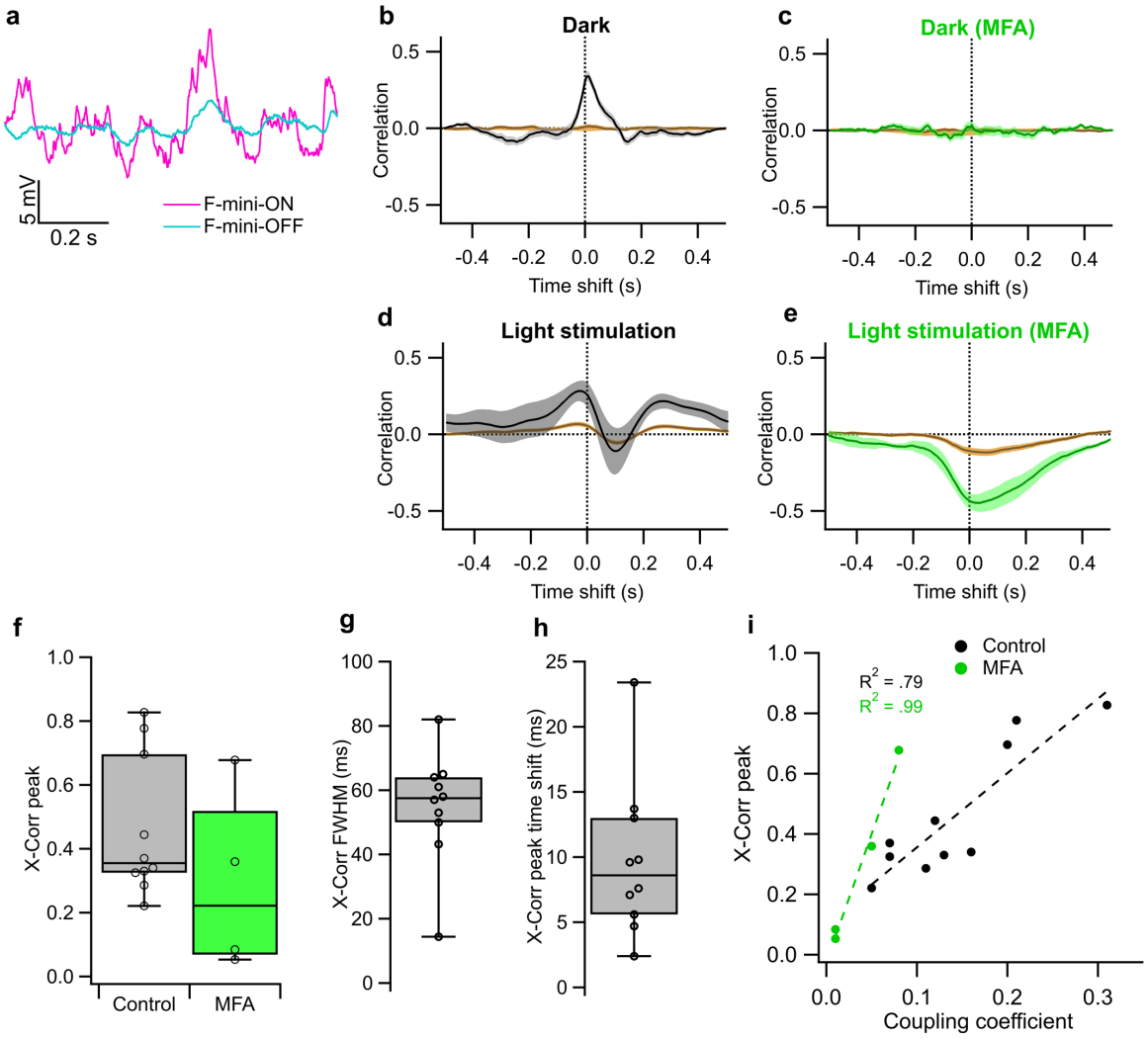

Extended Data Fig. 5 | Noise correlations between F-mini-ON and F-mini-OFF RGCs. a, Traces from a simultaneously recorded pair of F-mini-ON (magenta) and F-mini-OFF (cyan) RGCs in current clamp in darkness (no stimulus). **b-e**. Example cross correlation of the simultaneous voltage from the cells in **a**. Brown trace is for shuffled trials. Shaded regions are SEM across trials. Time shift is F-mini-ON - F-mini-OFF (positive values are F-mini-ON earlier). **b**, Results in darkness. **c**, Results in darkness in the presence of MFA. **d**, Results under randomly moving object light stimulation. **e**, Results under the same light stimulation in the presence of MFA. **f**, Population data showing peak cross-correlation in control and in MFA. Values in MFA are significantly lower than corresponding values in control ($n = 4$ cell pairs, $p = 0.0068$, paired-sample one-tailed t-test). **g**, Full width at half max and **h**, time shift (right) of cross correlation peak in control conditions. Error bars in **f-h** are SEM across cell pairs and points are each cell pair. **i**, Relationship between cross-correlation peak and coupling coefficient in darkness measured from current injections as in Fig. 2e-h. Box plots in **f**,**g**,**h** show maximum, 75th percentile, median, 25th percentile, and minimum.

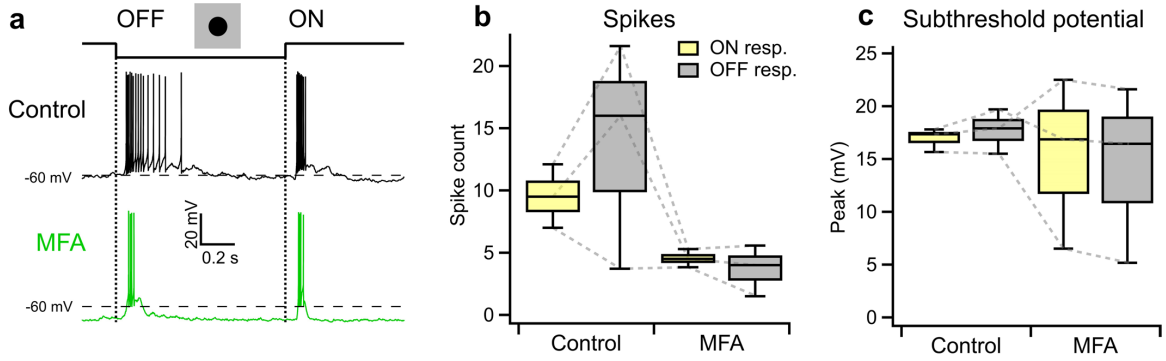

Extended Data Fig. 6 | MFA does not selectively eliminate OFF responses in non-F-mini RGCs. a, Example of an ON-OFF direction selective RGC responding to the onset and offset of a dark spot from a mean luminance of 2000 R*/rod/s in control conditions (black) and in MFA (green). **b**, Population data of spike counts and **c**, subthreshold potential responses to an OFF light step as in **a** for 3 ON-OFF DS RGCS. Baseline voltage level shift mean in control RGCs was −59.9 to −61.8 mV ($n = 3$ cells). Box plots in **b,c** show maximum, 75th percentile, median, 25th percentile, and minimum.

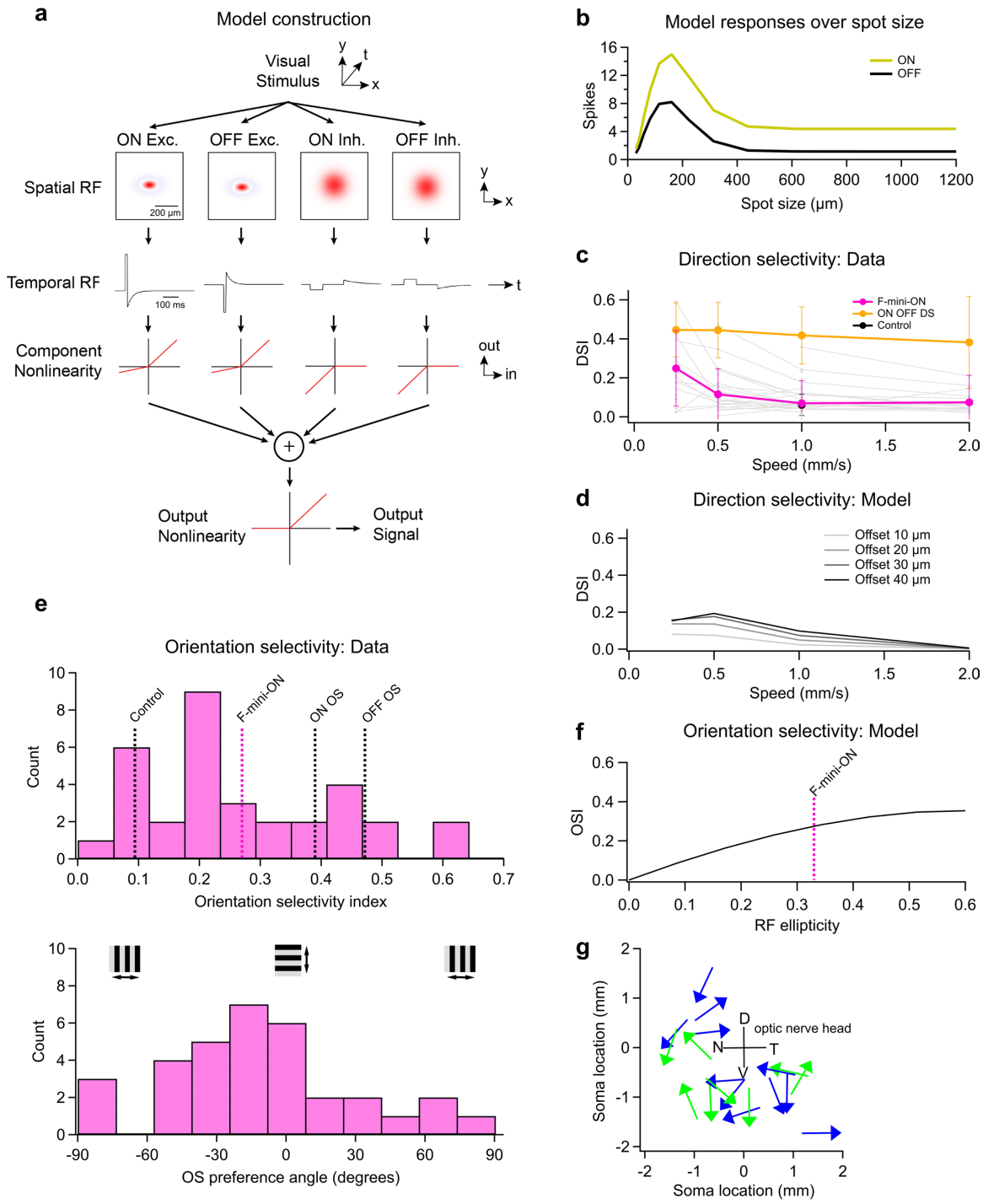

Extended Data Fig. 7 | See next page for caption.

Extended Data Fig. 7 | A single cell model generates responses similar to those observed in F-mini-ON RGCs. a, Diagram of single cell receptive field offset model showing the parameters for each of four RGC input component pathways. **b**, Responses of the model to flashed spots of varying sizes showing a qualitative match of surround properties to F-mini-ON RGCs as seen in Extended Data Fig. 2a. **c**, Measured direction selectivity mean in F-mini-ON and ON-OFF DS RGCs, varying over speed (error bars are SD). Individual F-mini-ON RGCs are shown in gray ($n = 103$ F-mini-ON and $n = 279$ ON-OFF DS). **d**, Model response DSI over object speed showing similar DSI magnitude and low-speed preference properties to measured responses. **e**, (upper) Orientation selectivity of the population of F-mini-ON RGCs. Dashed lines are published means for OS and control RGCs[28,29]. (lower) Distribution of OS preference angle. **g**, Moving bar DS preference angle distribution across retina space of F-mini-ON RGCs. Blue = left eye, green = right eye. D,V,N,T denote dorsal, ventral, nasal, and temporal, respectively.

Appendix B:

A Survey of the Retinal Ganglion Cell Types of the W3 Mouse Line

A Survey of the Retinal Ganglion Cell Types of the W3 Mouse Line

Sam Cooler, Gregory Schwartz

Abstract

We survey the retinal ganglion cell (RGC) types found in the W3 mouse line. We find nine types of RGCs labeled, matched to the Schwartz Lab and Eyewire typology datasets. Although we see a correspondence between RGC type and soma brightness, we find no evidence of a bimodal intensity distribution, contrary to earlier reports. These results may require a reevaluation of previous work on the W3B cell type, especially where the W3 mouse line was not used.

Introduction

The mouse retina is composed of many repeating microcircuits made of discrete types of cells (Sanes and Masland 2015). A genetically modified mouse line in which a subset of retinal neurons is fluorescently labeled can be used to identify cells for experimentation. Several genetic lines have been used for cell type identification. In lines where all labeled neurons are of the same type, this yields straightforward results. However, many mouse lines have several types of cells labeled similarly, so discriminating among them remains an experimental task.

The W3 mouse line is such a line. Fluorescent labeling is generated by the expression of yellow fluorescent protein (YFP) under the direction of the neuron-specific Thy1 gene promoter (I.-J. Kim et al. 2010). Labeled cells appear as fluorescent somas in the ganglion cell layer. Cell dye fills show that they all have axons extending toward the optic nerve, marking them as retinal ganglion cells (RGCs). They are notable as a class for their dendritic stratification near the middle of the inner plexiform layer. Clear differences in the light response behaviors of these RGCs shows that they are multiple types. Several works have made partial or complete descriptions of the labeled RGCs and their input cell types, summarized in the Discussion. However, none of these results provide confidence in the full set of unique RGC types that can be referenced to broadly available datasets. We aim to resolve this situation by providing a clear typology of these labeled RGCs.

Results

The W3 mouse line labels an inhomogeneous set of RGCs, containing several unique types. With light response electrophysiology, confocal microscopy morphology, and simple soma properties, we have identified nine types of RGCs. Light responses were matched to typology

datasets available at RGCTypes.org. Morphology stratification density was matched to Eyewire Museum datasets for typology confirmation. The resulting types and their properties are shown in Table 1.

Type name	EW	Labeling intensity	Soma size	N	Light response characteristics	References
F-mini-ON	63	bright	small	32	ON trans. + OFF trans.	(Cooler and Schwartz 2020; Rousso et al. 2016)
UltraHighDef	5ti	bright	small	29	ON trans. + OFF trans.	(Jacoby and Schwartz 2017)
HighDef 2	5so	bright	small	15	ON trans. + OFF trans.	(Jacoby and Schwartz 2017)
OFF trans. small	4on	dim	small	12	OFF trans.	RGCTypes.org
ON trans. small	6sn	dim	small	8	ON trans.	RGCTypes.org
ON trans. med.	6sw	dim	small	5	ON trans.	RGCTypes.org
OFF trans. alpha	4ow	dim	large	5	OFF trans.	(Pang, Gao, and Wu 2003; Krieger et al. 2017; Münch et al. 2009)
OFF sus. alpha	1wt	dim	large	3	OFF sus.	(Krieger et al. 2017; Pang, Gao, and Wu 2003)
ON alpha	8w	dim	large	3	ON sus.	(Krieger et al. 2017; Pang, Gao, and Wu 2003; Schwartz et al. 2012; Estevez et al. 2012)

Table 1: Types of RGCs found in the W3 mouse line

Results from the classification of *n* = 112 RGCs in *n* = XX mice. EW is the Eyewire Museum anatomical type name. Labeling intensity, soma size, and light response characteristics are qualitative measures.

Other RGC types may be present but did not rise to our typology confidence count threshold of three examples, with at least one having an image for morphology verification. We used a biased cell selection method to sample less dense types sufficiently. We observed an inverse relationship between dendritic area and cell count, which would be expected if all cells of a labeled type are labeled.

Initial typology to split W3 RGCs from each other was done using spike counts of responses to positive contrast spots of multiple sizes (SMS), qualitative spiking properties observed by eye such as spike waveforms, and soma size and brightness. These measurements were then matched to the RGCTypes.org dataset to determine cell types. This data is shown in Figure 1.

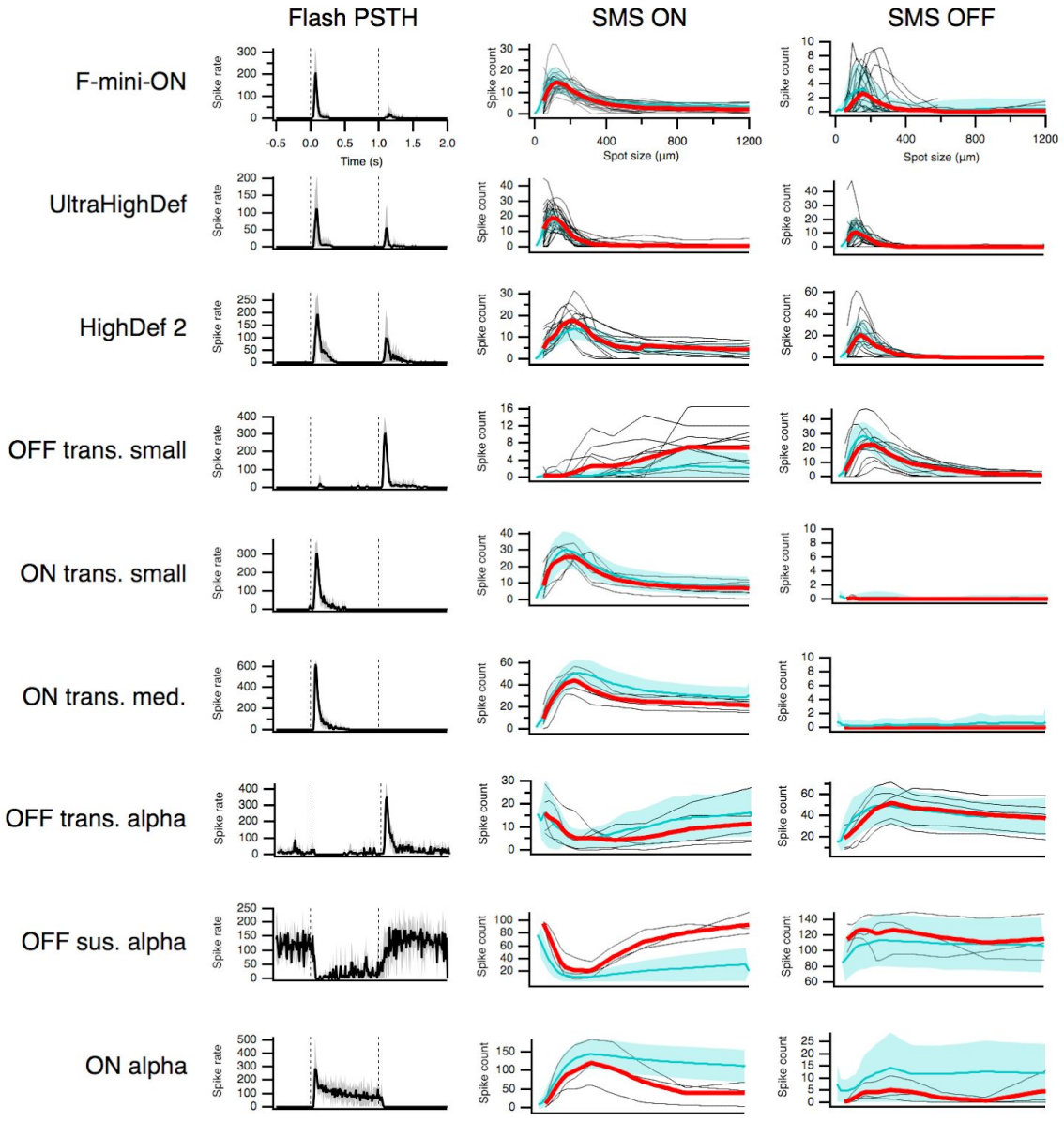

Figure 1: Cells match known unique electrophysiological types in Schwartz Lab dataset

Left column: Peri-stimulus time histograms (PSTH) showing light response mean spike rate for the population of each type of RGC in response to a 214 µm diameter spot of positive contrast lasting 1.0 sec. Most responses are transient with low latency following contrast change (at dashed lines). Center and right columns: Light response spike count to ON (center) and OFF (right) steps of a positive contrast spot, plotted by spot diameter. Mean ± s.d. of identified RGCs in cyan, RGC Types Atlas mean in red.

We validated the RGC types we observed by measuring the morphology of the labeled RGCs using light microscopy. Examples of each type were filled with Neurobiotin for dendrite tracing. Immunohistochemistry was performed to label Choline Acetyltransferase (ChAT), which is present only in starburst amacrine cells, which enabled computational flattening of the images (see Methods). Retinas were imaged by confocal microscopy (Fig 2, left column), and the resulting stratification density profiles were matched to those in the Eyewire Museum dataset, with good results (Fig 2, right column). Refer to these types at RGCTypes.org for more details and evidence of uniqueness.

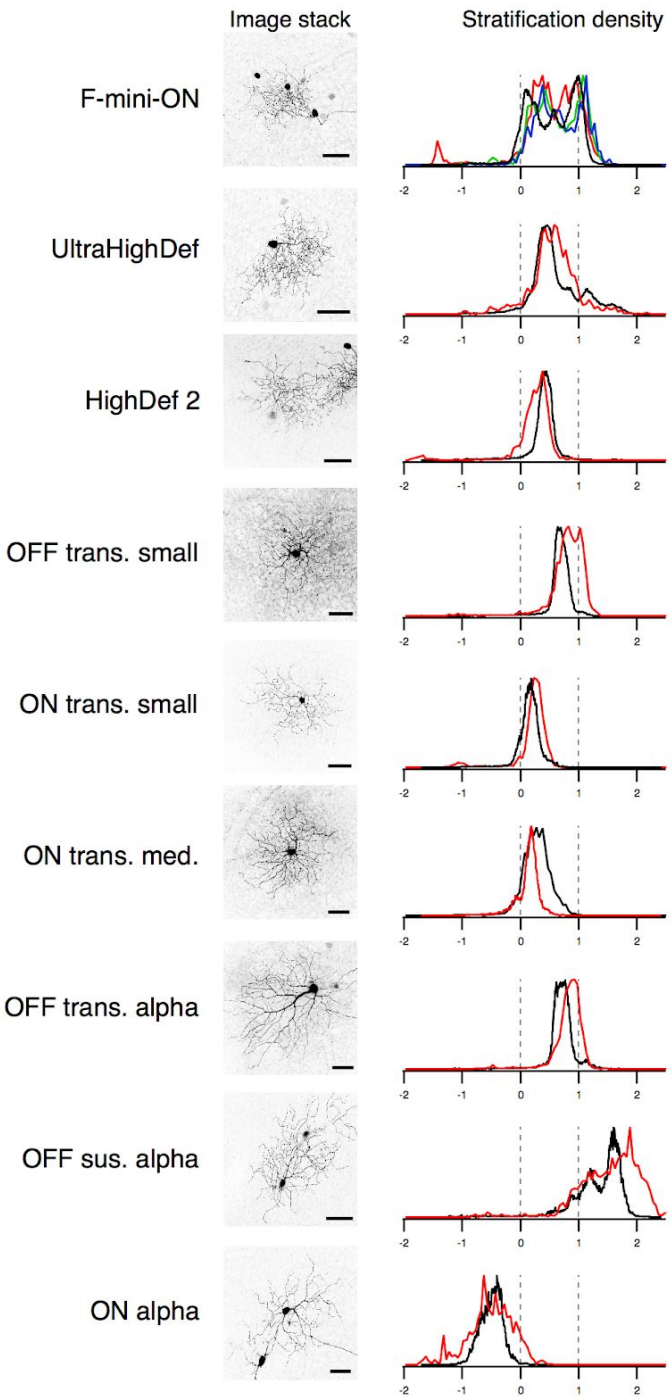

Figure 2: Typology is confirmed by matches to Eyewire Museum stratification density profiles

Left column: Examples of en-face maximum projections of confocal images of dye-filled RGCs, which were used for visual morphological analysis and measurement of stratification density for Eyewire comparison. The characteristic morphologies of the cell types are

apparent. In images showing two cells, the central cell is the target example. Intensity is inverted for display; scale bar is 50 µm. Right column: stratification density profiles from confocal images (colored), Eyewire Museum type mean density profiles (black). Data from the two experimental techniques are expected to have differing distortions, so visual comparisons are qualitative. 3D images were computationally flattened before density analysis; see Methods.

Several reports on the W3 line have used the labeling intensities of the somas as a guide to classifying the RGCs. This strategy was founded on the observation that the brightness distribution is bimodal, and the assertion that the bright RGCs were a single unique type. We found that brightly labeled RGCs fall into three distinct RGC types: F-mini-ON, UltraHighDef, and HighDef 2. We measured the overall distributions of the labeling intensity and soma area in wide-field imaging of fixed W3 retinas, shown in Fig. 3. The resulting distribution is not clearly multi-modal, Fig 3B, and does not have an apparent variation in mean across the horizontal (nasal-temporal) or vertical (dorsal-ventral) axes (Fig 3E,F).

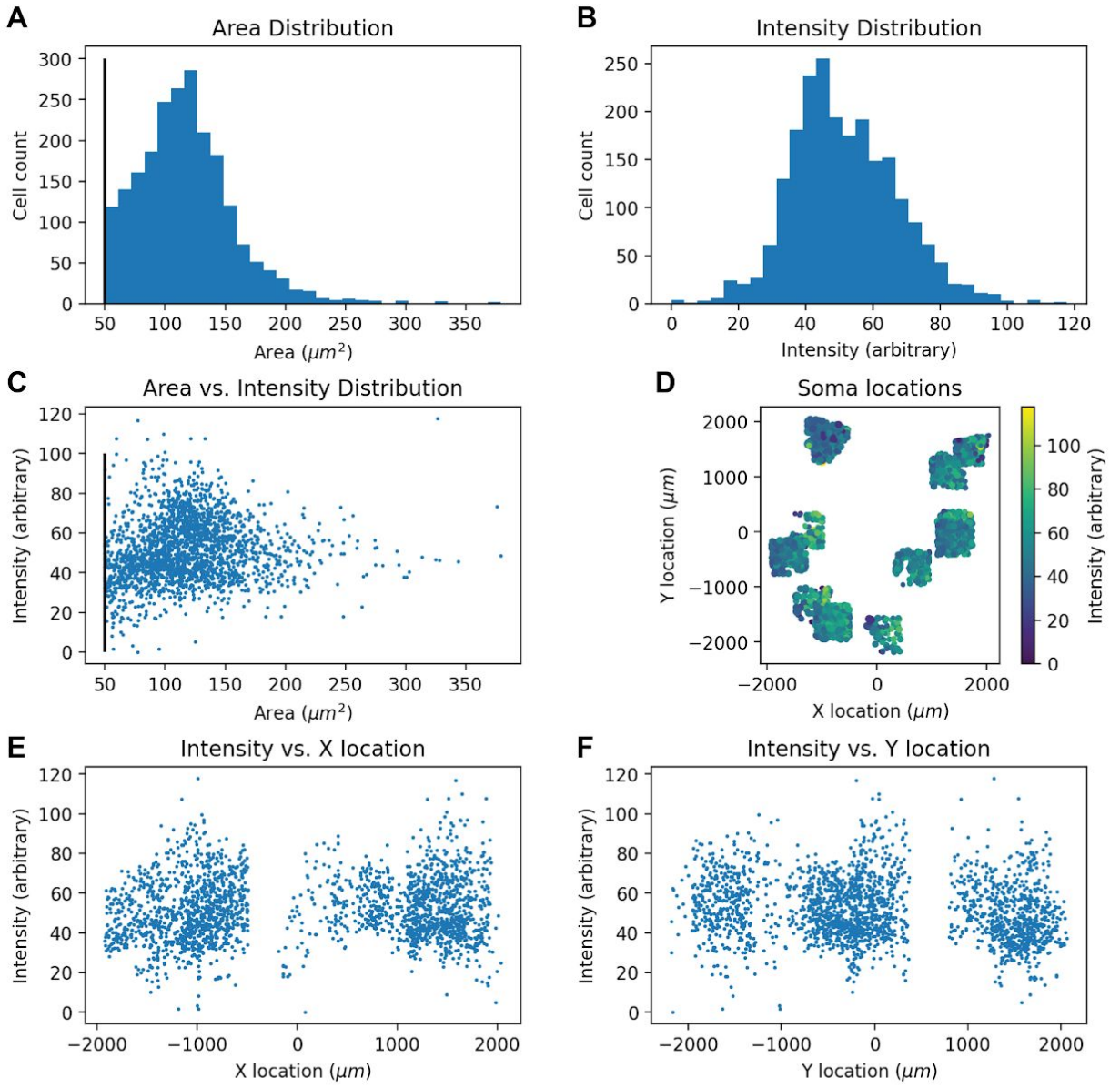

Figure 3: Labeling intensity and soma area distributions show no clear separation

A. Distribution of the area of labeled somas. **B.** Distribution of fluorescent labeling intensity of somas, showing no apparent bimodality. **C.** Scatter plot of soma area and labeling intensity. **D.** Somas plotted at their retinal location by area (dot size) and labeling intensity (dot color). **E, F.** Soma labeling intensity plotted across X location (nasal-temporal) and Y location (dorsal-ventral) on the retina. Somas, *n* = 2882, are from *n* = 2 retinas, from 2 mice.

Discussion

We have identified nine unique types of retinal ganglion cells in the W3 mouse line. These types are matched to those found in the Eyewire Museum and RGCTypes.org datasets. The morphology, light response electrophysiology, and development of neurons labeled in the W3 line have been studied previously by several groups with varying results.

A transcriptomic classification of the W3 line found seven or more RGC types, which was aligned to an overall RGC dataset (Tran et al. 2019). They find Sidekick 2 in a subset of the W3 line, which they align to the W3B, denoting it cluster 6. They additionally found cluster 3 (F-mini-ON), cluster 4 (F-mini-OFF), cluster 2, cluster 23 (OFF trans. alpha), cluster 21, and cluster 30. This typology aligns well with the findings here. Validation using FOXP2 labeling confirms the presence of at least one type of F-mini RGC. The OFF trans. small described here may be a mix of F-mini-OFF and the true OFF trans. small.

An updated version of that dataset aligns these clusters to [add here once atlas paper is finalized].

The W3 “Bright” Type

The RGC somas labeled in the W3 line have varying fluorescent label intensity, which appears to correlate with cell type (Table 1). Several works have measured an apparent bimodality in that distribution (Y. Zhang et al. 2012; I.-J. Kim et al. 2010). Researchers have relied on the unique identification of the W3B, the brighter subset of the cells, as a single cell type. Some evidence has shown that this is the case: the density recovery profile matches what would be expected from a single cell type (Yifeng Zhang et al. 2012) and the presence of Sidekick 2 may mark a single RGC type (Krishnaswamy et al. 2015).

In an inhomogeneously labeled genetic line containing multiple types, there is no guarantee that cell types can be split cleanly by labeling intensity. The intensity distribution we measured in wide-field imaging does not show clear peaks of multimodality, which contrasts with previous findings that the distribution is well fit by two Gaussians (Y. Zhang et al. 2012). If it is the case that each of the nine RGC types has its own distribution of brightnesses, then it is likely that the overlap is such that they cannot be separated from intensity data alone. Furthermore, we find that there is more than one RGC type within the brightly labeled subset.

The W3B RGC type has been found to have input from several amacrine cell types. The VG3 amacrine cell makes glutamatergic input to the W3B; this was found in three labs: The Zhou Lab found connectivity without the use of the W3 mouse line or validation of the RGC typology (Lee et al. 2014). The Sanes Lab subsequently made a similar finding, using the W3 mouse line (Krishnaswamy et al. 2015). The Kerschensteiner Lab made this finding without using the W3 mouse line (T. Kim et al. 2020). The VIP amacrine cell makes GABAergic input to the W3B; this was found by the Demb Lab and measured in a triple transgenic W3 mouse line (Park et al. 2015). The TH2 amacrine cell makes GABAergic input to the W3B; this was found by the

Kerschensteiner Lab without the use of the W3 mouse line. The typology was done by matching light responses to the LED type, which was hypothesized by the Schwartz Lab to be the W3B, but which was not found in this survey.

Although these results appear broadly coherent, a subset of them were done without the use of the W3 mouse line. Because the typology of the W3B type has not been confidently aligned to a complete dataset of types, these results may be incorrect. Unclear typology involving RGCs described as W3B reduces the accuracy of circuit analysis results and the replicability of the experiments for the field. In particular, W3B should not be used to describe a cell type that is more accurately described as the LED or HD2 (T. Kim et al. 2020; Tahnbee Kim and Kerschensteiner 2017) or as a small ON-OFF RGC of unknown type (Lee et al. 2014).

To measure this type-based labeling intensity property accurately, a particular experiment will be necessary: record individual cells for their cell type by light responses, record their locations without the use of fluorescent dyes, then perform wide-field imaging of the cell populations as described here in Figure 3.

Other W3 RGCs

No prior works have presented physiological measurements of the dimly labeled W3 RGCs. We find that these are a heterogeneous population of approximately six RGC types, varying in light response polarity preference, soma size, and RF preference size. Their dendrites have a shared central-IPL stratification pattern, which may reflect a connection between the fluorescent label insertion site and a protein used in the dendritic stratification development process. Although these RGC types have varying properties, commonalities among them may make them worth exploring as a group, in investigations of dendritic development, cellular wiring, or specific properties of ON and OFF transient responses.

Conclusions

Incorrect cell type identification leads to conflicting results in the scientific field, which muddies conclusions and delays progress. The use of the term W3B to denote a single cell type should be restricted to studies using the W3 mouse line, and in general future work on specific cell types in the mouse retina should be aligned to the type-complete Eyewire Museum, Sanes Atlases, and Schwartz Lab/RGCTypes.org datasets [add ref to atlas].

Methods

Mouse line: The Jackson Laboratory, B6.Cg-Tg(Thy1-YFP)W3Jrs/J, Stock No: 033114. Mice of both sexes were used, ages above P30. The mice were dark adapted overnight and euthanized by cervical dislocation in accordance with all animal care standards provided by Northwestern

University's Institutional Animal Care and Use Committee. Animal protocols were done as described previously (Cooler and Schwartz 2020)

Electrophysiology was done as described previously (Jacoby and Schwartz 2017). Stimuli and typology as described in Atlas paper or RGCTypes.org. Stratification analysis including computational flattening using ChAT labeling was performed as described previously (Cooler and Schwartz 2020).

Imaging parameters for soma brightness: Nikon AR1 confocal microscope, galvo mode, single scan, dwell 6.2 ms, 1024x1024 resolution, 0.618 µm per pixel (632.8 µm image width), 16-bit depth, 4X repeat line averaging. Lens: Plan Apo VC 20x DIC N2, laser: 514.5 nm, YFP config, Z step: 0.9 µm each step centered on Z value with highest overall soma intensity, 25 frames depth or 15 frames depth, which captured the entire soma depth in the imaging field. All fields were imaged with the same microscope, laser, optics, and scan configurations.

To identify somas in wide-field confocal microscopy images the CellPose software package was used (Stringer et al., n.d.). This uses a trained convolutional neural network to identify cell somas automatically. Images were masked by hand to ignore areas of retinal damage or folding. The results were post-processed in Python, which is available online. Soma size is thresholded at 50 μm^2 to reject incorrectly identified somas. Label intensity was normalized across all fields for each retina.

References

Cooler, Sam, and Gregory W. Schwartz. 2020. "An Offset ON–OFF Receptive Field Is Created by Gap Junctions between Distinct Types of Retinal Ganglion Cells." *Nature Neuroscience*. https://doi.org/10.1038/s41593-020-00747-8.

Estevez, Maureen E., P. Michelle Fogerson, Marissa C. Ilardi, Bart G. Borghuis, Eric Chan, Shijun Weng, Olivia N. Auferkorte, Jonathan B. Demb, and David M. Berson. 2012. "Form and Function of the M4 Cell, an Intrinsically Photosensitive Retinal Ganglion Cell Type Contributing to Geniculocortical Vision." *The Journal of Neuroscience: The Official Journal of the Society for Neuroscience* 32 (39): 13608–20.

Jacoby, Jason, and Gregory W. Schwartz. 2017. "Three Small-Receptive-Field Ganglion Cells in the Mouse Retina Are Distinctly Tuned to Size, Speed, and Object Motion." *The Journal of Neuroscience: The Official Journal of the Society for Neuroscience* 37 (3): 610–25.

Kim, In-Jung, Yifeng Zhang, Markus Meister, and Joshua R. Sanes. 2010. "Laminar Restriction of Retinal Ganglion Cell Dendrites and Axons: Subtype-Specific Developmental Patterns Revealed with Transgenic Markers." *The Journal of Neuroscience: The Official Journal of the Society for Neuroscience* 30 (4): 1452–62.

Kim, Tahnbee, and Daniel Kerschensteiner. 2017. "Inhibitory Control of Feature Selectivity in an Object Motion Sensitive Circuit of the Retina." *Cell Reports* 19 (7): 1343–50.

Kim, T., N. Shen, J-C Hsiang, K. P. Johnson, and D. Kerschensteiner. 2020. "Dendritic and Parallel Processing of Visual Threats in the Retina Control Defensive Responses." *Science*

Advances 6 (47). https://doi.org/10.1126/sciadv.abc9920.

Krieger, Brenna, Mu Qiao, David L. Rousso, Joshua R. Sanes, and Markus Meister. 2017. "Four Alpha Ganglion Cell Types in Mouse Retina: Function, Structure, and Molecular Signatures." *PloS One* 12 (7): e0180091.

Krishnaswamy, Arjun, Masahito Yamagata, Xin Duan, Y. Kate Hong, and Joshua R. Sanes. 2015. "Sidekick 2 Directs Formation of a Retinal Circuit That Detects Differential Motion." *Nature* 524 (7566): 466–70.

Lee, Seunghoon, Lujing Chen, Minggang Chen, Meijun Ye, Rebecca P. Seal, and Z. Jimmy Zhou. 2014. "An Unconventional Glutamatergic Circuit in the Retina Formed by vGluT3 Amacrine Cells." *Neuron*. https://doi.org/10.1016/j.neuron.2014.10.021.

Münch, Thomas A., Rava Azeredo da Silveira, Sandra Siegert, Tim James Viney, Gautam B. Awatramani, and Botond Roska. 2009. "Approach Sensitivity in the Retina Processed by a Multifunctional Neural Circuit." *Nature Neuroscience* 12 (10): 1308–16.

Pang, Ji-Jie, Fan Gao, and Samuel M. Wu. 2003. "Light-Evoked Excitatory and Inhibitory Synaptic Inputs to ON and OFF Alpha Ganglion Cells in the Mouse Retina." *The Journal of Neuroscience: The Official Journal of the Society for Neuroscience* 23 (14): 6063–73.

Park, S. J. H., B. G. Borghuis, P. Rahmani, Q. Zeng, I-J Kim, and J. B. Demb. 2015. "Function and Circuitry of VIP Interneurons in the Mouse Retina." *Journal of Neuroscience*. https://doi.org/10.1523/jneurosci.0222-15.2015.

Rousso, David L., Mu Qiao, Ruth D. Kagan, Masahito Yamagata, Richard D. Palmiter, and Joshua R. Sanes. 2016. "Two Pairs of ON and OFF Retinal Ganglion Cells Are Defined by Intersectional Patterns of Transcription Factor Expression." *Cell Reports* 15 (9): 1930–44.

Sanes, Joshua R., and Richard H. Masland. 2015. "The Types of Retinal Ganglion Cells: Current Status and Implications for Neuronal Classification." *Annual Review of Neuroscience* 38 (July): 221–46.

Schwartz, Gregory W., Haruhisa Okawa, Felice A. Dunn, Josh L. Morgan, Daniel Kerschensteiner, Rachel O. Wong, and Fred Rieke. 2012. "The Spatial Structure of a Nonlinear Receptive Field." *Nature Neuroscience* 15 (11): 1572–80.

Stringer, Carsen, Tim Wang, Michalis Michaelos, and Marius Pachitariu. n.d. "Cellpose: A Generalist Algorithm for Cellular Segmentation." https://doi.org/10.1101/2020.02.02.931238.

Tran, Nicholas M., Karthik Shekhar, Irene E. Whitney, Anne Jacobi, Inbal Benhar, Guosong Hong, Wenjun Yan, et al. 2019. "Single-Cell Profiles of Retinal Ganglion Cells Differing in Resilience to Injury Reveal Neuroprotective Genes." *Neuron* 104 (6): 1039–55.e12.

Zhang, Yifeng, In-Jung Kim, Joshua R. Sanes, and Markus Meister. 2012. "The Most Numerous Ganglion Cell Type of the Mouse Retina Is a Selective Feature Detector." *Proceedings of the National Academy of Sciences of the United States of America* 109 (36): E2391–98.

Zhang, Y., I-J Kim, J. R. Sanes, and M. Meister. 2012. "The Most Numerous Ganglion Cell Type of the Mouse Retina Is a Selective Feature Detector." *Proceedings of the National Academy of Sciences*. https://doi.org/10.1073/pnas.1211547109.